(2)

AD-A226 057

ARI-RR-789

DEVELOPMENT OF LASER SPECTROSCOPIC DIAGNOSTICS TO SUPPORT ADVANCED COMPOUND SEMICONDUCTOR DEPOSITION TECHNIQUES

Prepared by

J.C. Wormhoudt
Aerodyne Research, Inc.
45 Manning Road
Billerica, MA 01821

Prepared for

Directorate of Physical and Geophysical Sciences
Air Force Office of Scientific Research
Bolling Air Force Base
Washington, DC 20322

Final Report
Contract No. F49620-87-C-0052

July 1990

Unclassified

SECURITY CLASSIFICATION OF THIS PAGE

REPORT DOCUMENTATION PAGE

1a. REPORT SECURITY CLASSIFICATION Unclassified	1b. RESTRICTIVE MARKINGS
2a. SECURITY CLASSIFICATION AUTHORITY	3 DISTRIBUTION / AVAILABILITY OF REPORT Approved for public release; Distribution unlimited
2b. DECLASSIFICATION / DOWNGRADING SCHEDULE	
4 PERFORMING ORGANIZATION REPORT NUMBER(S)	5. MONITORING ORGANIZATION REPORT NUMBER(S) AFOSR-TR- 90 0865
6a. NAME OF PERFORMING ORGANIZATION Aerodyne Research, Inc. — 6b. OFFICE SYMBOL (If applicable)	7a. NAME OF MONITORING ORGANIZATION Air Force Office of Scientific Research
6c. ADDRESS (City, State, and ZIP Code) 45 Manning Road Billerica, MA 01821	7b. ADDRESS (City, State, and ZIP Code) Bolling Air Force Base DC 20332-6448
8a. NAME OF FUNDING / SPONSORING ORGANIZATION AFOSR — 8b. OFFICE SYMBOL (If applicable) NP	9. PROCUREMENT INSTRUMENT IDENTIFICATION NUMBER F49620-87-C-0052
8c. ADDRESS (City, State, and ZIP Code) Bldg 410 Bolling AFB DC 20332-6448	10. SOURCE OF FUNDING NUMBERS PROGRAM ELEMENT NO. 61102F — PROJECT NO. 2301 — TASK NO. A4 — WORK UNIT ACCESSION NO

11. TITLE (Include Security Classification)
Development of Laser Spectroscopic Diagnostics to Support Advanced Compound Semiconductor Deposition Techniques

12. PERSONAL AUTHOR(S)
Wormhoudt, Joda C.

13a. TYPE OF REPORT	13b. TIME COVERED	14. DATE OF REPORT (Year, Month, Day)	15. PAGE COUNT
Final Technical	FROM 870601 TO 900601	900730	111

16. SUPPLEMENTARY NOTATION

17 COSATI CODES			18. SUBJECT TERMS (Continue on reverse if necessary and identify by block number)
FIELD	GROUP	SUB-GROUP	Diagnostic Instrumentation, Electronic Materials, Infrared Absorption, Lasers, Microelectronic Fabrication, Semiconductor Processing, Spectroscopy
		20.08	

19. ABSTRACT (Continue on reverse if necessary and identify by block number)

This program constructed and demonstrated an apparatus for the development of laser diagnostics for the gas phase molecules involved in semiconductor fabrication techniques, particularly the organometallic chemical vapor deposition of compound semiconductors like gallium arsenide. Work in this apparatus, a flow tube with mirrors for long path tunable infrared diode laser absorption and electrodes for a radio frequency glow discharge, culminated in observations designed to assess the importance of arsenic hydride radicals in the decomposition of organoarsenic compounds. Preliminary observations of fluorocarbon and methane plasmas produced observations of several species which could be compared with models and other observations and which added to knowledge of these systems with their important applications in silicon etching and diamond deposition. The program also resulted in band strength measurements for the methyl and difluorocarbene radicals, using tunable diode laser, dye laser, and fast flow reactor techniques.

RR 1-91

20. DISTRIBUTION / AVAILABILITY OF ABSTRACT	21 ABSTRACT SECURITY CLASSIFICATION
☒ UNCLASSIFIED/UNLIMITED ☒ SAME AS RPT ☐ DTIC USERS	Unclassified
22a. NAME OF RESPONSIBLE INDIVIDUAL Dr. Ralph Kelley	22b. TELEPHONE (Include Area Code) (202) 767-4908 — 22c. OFFICE SYMBOL AFOSR/NP

DD FORM 1473, 84 MAR — 83 APR edition may be used until exhausted. All other editions are obsolete.

SECURITY CLASSIFICATION OF THIS PAGE
Unclassified

TABLE OF CONTENTS

Table of Contents (Continued)

LIST OF ILLUSTRATIONS

List of Illustrations (Continued)

1.0 RESEARCH OBJECTIVES

1.1 Introduction

This is the final report for Contract F49620-87-C-0052, "Development of Laser Spectroscopic Diagnostics to Support Advanced Compound Semiconductor Deposition Techniques." Work under the contract was performed in two areas, laboratory measurement of quantitative spectroscopic parameters and development and demonstration of spectroscopic diagnostics. The program goal was investigation of plasma and thermal decomposition of deposition feed gases by laser spectroscopic detection of their decomposition products. These studies were carried out in a long path plasma reactor capable of simulating the gas phase environments of a wide range of semiconductor processing systems.

The focus systems for this work were the gallium arsenide and diamond deposition systems. Gallium arsenide is already important in commercial semiconductor devices including optoelectronic, microwave, and high-speed circuits, and its use promises to expand tremendously as soon as larger high quality wafers are available. Diamond and hard carbon deposition has attracted widespread attention only in the last few years, but the research effort is now very intense and has yielded a few investigations of electronic devices, as well as substantial progress in other applications such as tribological coatings. The chemical species involved in diamond deposition from hydrocarbons are a subset of those involved in organometallic vapor deposition. These C_xH_y species may be among the most important in MOCVD as well.

Research into both techniques is therefore an extremely active field, with most of it being empirical in nature, searching for incremental improvement in existing deposition techniques. Increased basic knowledge may

allow more rapid progress towards improved deposition techniques. Our assessment was that the systems described above would provide the richest context of accumulated observations, into which any mechanism studies could be integrated.

At the beginning of the contract, we submitted an interim report giving a prioritized list of candidate molecular species. As we began experiments in the plasma reactor, the methyl radical led the list, due to wide presumptions of its importance in both deposition systems and its easy detectability using tunable diode laser absorption. We succeeded in making observations of its concentration in methane plasmas, along with observations of CH_4, C_2H_2, and C_2H_4. Next in order were the AsH_x family of radicals, expanded to include the arsine molecule and the arsenic atom and diatomic molecule. In the final year of the contract, after the apparatus had been fully checked out using a series of less hazardous gases, we made observations of infrared absorption by the AsH radical during plasma decomposition of two organoarsine compounds.

Initial checkout work with the plasma reactor focused on the CF_4 plasma commonly used for etching of semiconductor silicon. The species detected included the CF_2 radical for which we previously made band strength determinations, as well as the CF_4 and C_2F_6 stable molecules. Since we already had well-characterized diodes in these spectral regions, we felt we could combine initial system check-out with a set of observations which could lead to substantial mechanism understanding from relatively modest efforts. These results gave us confidence that we could interpret observations in the methane and organoarsine systems.

1.2 Statement of Work

The statement of work for the program included the following task descriptions. The construction of the plasma reactor was completed in its scheduled first year of the program, and was followed by testing and diagnostic demonstration. Work under the basic measurement task was performed

during the first year while the plasma apparatus was under construction, while the interaction task was ongoing throughout the project. In detail, the tasks are:

- To use chemical, laser photolysis, and discharge radical sources and tunable diode and dye lasers to obtain required quantitative spectroscopic data for gas phase molecules in compound semiconductor deposition systems.

- To construct a model deposition reactor for compound semiconductor systems, including plasma enhancement capability and optical access for laser absorption and resonance fluorescence diagnostic techniques.

- To perform infrared, visible, and ultraviolet laser spectroscopic studies of gas-phase species resulting from plasma and thermal decomposition of deposition feed gases, with the object of quantifying those species which take part in semiconductor fabrication processes.

- To interact with the semiconductor fabrication research community through visits to and technology exchange with leading academic, government and industrial deposition research programs.

2.0 STATUS OF THE RESEARCH EFFORT

2.1 Introduction

During the first year of the program, the major effort was the construction of the long path plasma apparatus. We began generating plasmas in July 1988, performing check-out experiments involving plasmas of CF_4 and CH_4 with various dilution and additive gases until November of 1989. A second construction period, involving modifications to the plumbing and exhaust systems needed for operation with arsenic compounds, lasted until May 1990. A series of observations of plasma decomposition of organoarsine compounds completed the program.

After describing the plasma apparatus, we will discuss each area of experimental investigation. Two laboratory measurements were completed during the first year, yielding infrared band strength values for the CH_3 and CF_2 molecules. Each of these experiments has been documented in detail in a paper published in Chemical Physics Letters.[1,2] These papers are included here as Appendices A and B, so in this section we simply present a brief review of each effort, commenting on their contributions towards achievement of the research objectives, and updating comparisons with theory and other experiments. We conclude with sections on each of the three plasma systems studied. Additional details on the experimental results will be found in papers published in the Journal of Vacuum Science and Technology,[3] and to be published in meeting proceedings by the Society of Photo-Optical Instrumentation Engineers,[4] the Materials Research Society,[5] and the Electrochemical Society.[6] These papers are also reproduced here as Appendices C through F. (An earlier Materials Research Society paper[7] has been superseded by the above papers and is not reproduced here.) Following this

section on research results are short sections listing publications, research personnel, and interactions associated with the program.

2.2 Long Path Plasma Reactor

2.2.1 Design Considerations

The laser spectroscopic diagnostic technique we chose as our focus was tunable diode laser infrared absorption. It has a number of advantages, including wide applicability and quantitative capability, but its sensitivity is such that great effort is often required to detect radical species at the column densities to be expected in real semiconductor processing systems. Especially when searching for absorption spectra about which little is known, the chances of success are raised substantially by the use of a long absorption path. We set ourselves the goal of placing a 1 meter long volume of plasma between the mirrors of a multipass cell which would allow at least the effective limit of about 60 passes set by typical mirror reflectivities. The design of the apparatus involved a number of considerations.

To protect the mirrors from attack and deposition due to the active gases, it was necessary to separate them by a substantial volume into which purge gas is admitted at flow rates similar to the total flow rate through the active region. We therefore chose a mirror separation of about 2 meters. As this distance grows, the sizes of the infrared spots on the mirrors and therefore the required mirror diameters also grow. A 2 m separation was the largest which could be accommodated by 15 cm diameter mirrors, and these in turn were the largest which could fit inside a ten inch diameter outer vacuum jacket, considering the requirements of fitting electrodes between the vacuum wall and the plasma volume.

The requirements on the outer vacuum jacket included the possibility in the future that we might try to deposit semiconductor films in the apparatus. Although a vacuum system to study gas phase chemistry need in many instances only be leak-tight enough that chemical reaction with air does not affect the

concentrations of the species of interest, the vacuum requirements for reproducible production of films with good electrical properties are more stringent, and are best met by a UHV system. Considering the added advantage that many features of UHV design are more reliable and durable than quartz outer jackets and O-ring seals, we constructed our vacuum system out of stainless steel pipe and con-flat flanges. However, vacuum seals were made with rubber gaskets rather than the much more expensive copper.

A metal vacuum jacket means that the RF electrodes must be inside the vacuum and must not contact the vacuum wall. This means separating them with a dielectric material. To maintain the UHV capability, we used quartz, rather than a more easily worked material like Teflon. Any volume not substantially filled with dielectric will instead support a plasma, which is undesirable as it draws power away from the observation region and may cause deposition or chemical attack in undesirable places. In particular, it was necessary to repack regions around the electrode feedthroughs with refractory fiber products in order to suppress discharges which had resulted in pinhole leaks in cooling lines. The minimum spacing which will support a plasma drops as the pressure increases. We found that discharges in the feedthrough regions were still a problem at pressures much above 1 Torr, thus limiting the useful pressure range of the apparatus as presently constructed.

To protect the electrodes from attack and deposition, we also wanted an inner liner. We began with a quartz liner, but in the fluorocarbon plasma work etching of the quartz and liberation of oxygen-containing species was enough of a problem that we switched to a Teflon liner, and did not switch back for the duration of the program. The desire to be able to easily remove the liner as plasma systems change or for cleaning was one of several motivations for designing the apparatus as a series of concentric cylinders-vacuum wall, dielectric, electrodes (two half-cylinders), and inner liner.

The multipass cell is an off-axis resonator design, differing from those used in Aerodyne flow tubes and field measurements apparatus only by its large

size (and the fact that both front and back mirrors are curved, doubling the spacing for the same focal length). The other components of the initial system, including gas manifold, flowmeters, pressure gauge, gate valve and mechanical pump, were standard items. Special features for working with arsenic compounds, such as a temperature bath for organometallic compounds, and an exhaust treatment system (primarily relying on thermal decomposition) were added after a series of initial experiments involving hydrocarbon plasmas and other relatively benign active gases, and will be discussed in a following subsection.

2.2.2 Plasma Reactor Construction

Figure 1 is a schematic drawing of the long path plasma apparatus. The active volume is contained inside a 1 m long inner liner with a 15 cm inner diameter. For almost all the studies to date this liner has been the Teflon tube indicated, although a quartz tube is also available. The electrodes which surround the inner liner are copper half-tubes, with water cooling provided by one line of copper tubing set into the electrode surface in a loop near the outer edge. They are separated from the outer stainless steel vacuum wall by an outer quartz dielectric tube.

The feed gas, together with any carrier or additive gases, enters the tube through a ring injector just before the upstream end of the electrodes. Argon purge gas is introduced behind each mirror, and small flows are also put into each of the cross ports which are presently used for visual observation and emission spectroscopy. (Initially, a flow of purge gas was directed onto the face of the upstream mirror, but this apparently helped to carry reactive radicals out of the active volume and onto the mirror. After the center of the mirror was etched away, we changed the purge plumbing so all gas flows originate behind the mirrors.) Bubblers containing organoarsine compounds were kept in an ice bath and connected to a measured flow and pressure of carrier gas.

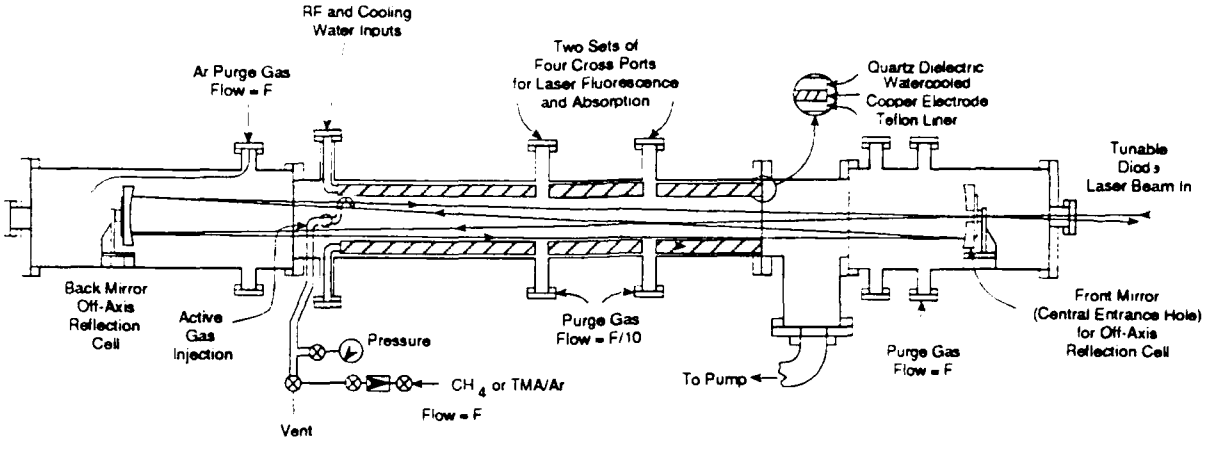

Figure 1. Long Path Plasma Absorption Apparatus

The mirrors used for multi-pass infrared absorption have 15 cm diameters and are separated by approximately 2 meters. They form an off-axis resonator, in which the laser beam enters and exits through the same central hole in the downstream mirror, and forms a spot pattern on both mirrors which can be circular or (as we now use it) which can be flattened into an ellipse whose major axis is still almost the full 15 cm but with a minor axis of a little over 1 cm.

With a 30 cfm mechanical pump and 3 inch diameter pumping line, pressures in the 0.1 to 1.0 Torr range are achieved with total flows in the 15 to 400 sccm range. These translate into gas velocities of from 6 to 150 cm/s, or residence times in the active region of from 17 to 0.7 seconds. We concluded from studies in which the residence time was varied while the pressure remained constant that the plasmas studied have reached a steady state, with their composition not strongly affected by residence time.

The RF power is standard 13.56 MHz, from a supply with 1000 W capability. If all the power went into the plasma, power densities up to 0.1 W/cm^3 would be achieved, within the range of values used in commercial etching and deposition reactors. The fraction actually dissipated in the plasma is difficult to measure or estimate, but it is very likely to be less than half. On the other hand, we have operated the system with only one 0.5 m section of

the electrodes connected, thus potentially doubling the power density (detailed studies of this mode of operation were not made).

2.2.3 Arsenic Compound Exhaust Treatment System

After discussions with several workers in the field, including D. Speckman and J. Wendt of The Aerospace Corporation and members of the groups of Profs. R. Reif and K. Jensen of MIT, we developed a set of modifications to the plasma apparatus intended to allow safe operation using organoarsine compounds in the feed gas stream. In this subsection we describe these modifications.

A first important set of changes resulted in the isolation of the apparatus in its own separately exhausted enclosure. This was done by building a framework around the table supporting the plasma apparatus and covering it with Lexan panels. Seams around the top were sealed with duct tape but bottom seams were left open and some holes were drilled in the panels to allow air to be drawn in at floor level. A separate, powerful (1200 cfm at 1 inch static pressure, driven by a 3 hp electric motor) exhaust blower was mounted on the roof and connected to the top of the apparatus enclosure with a new line of 8-inch diameter ductwork. Proper blower operation was monitored by a Photohelic gauge whose readout was mounted on the apparatus enclosure.

Passage of the organoarsine compounds through the plasma discharge might under some circumstances completely dissociate them and result in the deposition of all input arsenic in solid form on the walls of the plasma reactor. However, in general we must assume that some fraction of the input compounds leaves the reactor still in the gas phase, either as organometallic compounds or as arsine and other arsenic hydrides. We wanted a system which would ensure that no arsenic was emitted from the exhaust, and which minimized contamination of the vacuum pump as well. The additions to the vacuum line which achieve this are shown in the scale drawing in Figure 2.

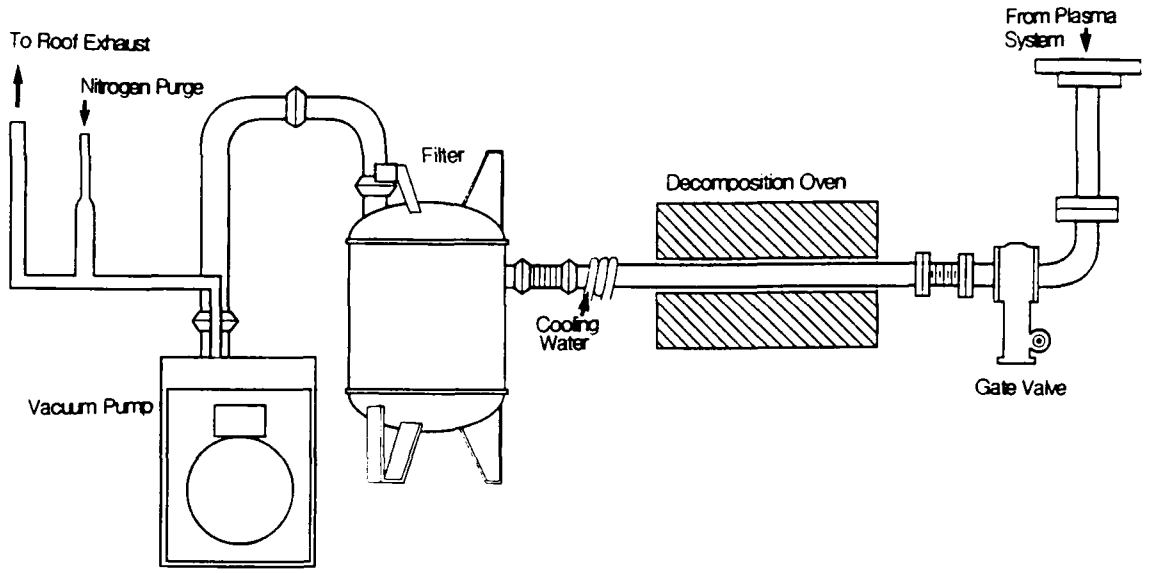

Figure 2. Plasma Apparatus Exhaust Treatment System

The principle is that arsenic compounds in the flow will be thermally decomposed and deposit arsenic on downstream surfaces of the pumping system. To do this, a tube furnace was placed around a section of 2 inch diameter stainless steel tubing, separated from the rest of the pumping line by metal bellows at each end. The oven is operated at 900°C, as measured by a fine wire thermocouple wired to the outside of the tube in the center of the oven. Downstream of the oven is an MV Multi-Trap, which contains two stages of removable cartridge filters, whose high surface area results in negligible loss of pumping speed while giving elemental arsenic every chance to deposit out on cold surfaces. Because the vacuum seal to the trap is made with rubber o-rings, a small water cooling coil is wrapped around the downstream end of the oven tube. Thermocouples attached to the pumping line upstream and downstream of the oven show that the thermal conductivity of the stainless steel tube is such that all points remain at safe temperatures.

Even these precautions for overheating the pumping line would have been unnecessary if we had been able to follow precisely the systems we were taking as models by using a quartz tube in the decomposition oven. This would have had the added advantage that deposition on downstream walls could have been monitored without taking apart the apparatus. However, it turned out that the length of a quartz tube and the quartz-to-glass-to-metal seals needed for permanent connections could not be accommodated inside the apparatus enclosure. We had already conducted proof-of-principle experiments using silane (with a higher decomposition temperature than arsine) and quartz tubes sealed with Cajon fittings, and so felt confident that an all-metal permanent system would work. These experiments used two tubes and two ovens, the one shown upstream of the pump and a second, one inch diameter tube on the pump exhaust, where the flow is so slow that we could be confident that all remaining silane would be decomposed and deposit on the tube. In fact, no significant deposition was observed on the second tube, and we concluded that a single decomposition oven upstream of the pump would be adequate. This will be checked when we analyze the pump oil for arsenic and take wipe samples at various points along the exhaust system.

The last point to be noted in Figure 2 is the nitrogen injection port in the pump exhaust line. We wanted to be able to use the hydrogen carrier gas typical in both MOCVD and diamond deposition systems, and nitrogen injection is used to bring the hydrogen concentration in the exhaust to well below the flammability limit.

The pump exhaust line is brought up through the apparatus table and extends several feet into the blower exhaust duct at the top of the enclosure. The final set of exhaust treatment devices, on the roof upstream of the blower, must guard against two eventualities: the passage of small amounts of arsenic compounds through the pump from the plasma apparatus, and a leak or other accidental release of the organoarsine compound within the apparatus enclosure. Two such devices were installed: a carbon trap (Ventsorb, Calgon

Carbon Corporation) filled with 230 lbs of granular activated carbon) and a biological grade HEPA filter (Flanders Filters, with 4 inch thick glass fiber packing and a 24 inch square cross section). When we smoke tested the apparatus enclosure, the smoke cleared in a few seconds, yet an observer on the roof saw no smoke emitted from the blower, indicating that the trap and filter together had removed all particles from the exhaust.

These tests gave us enough confidence in the integrity of the apparatus enclosure that we decided against purchasing an arsine leak detector, whose sensitivity is in any case considerably reduced when dealing with the organoarsine compounds we used. However, we did purchase a Matheson 8057 hazardous gas leak detector, which is a general detector of combustible gases including arsine, organoarsine compounds, and hydrogen. Although its detection thresholds for arsine and hydrogen are at best only 0.3 and 5.0 ppm respectively, these compare well with the lethal concentration for arsine (less than 50 ppm) which we did not plan to use as a feed gas, and even better with the values for the arsenic precursors we did use, tertiarybutylarsine (70 ppm) and trimethylarsenic (20,000 ppm). The detector has a small pump and a flexible nozzle which is inserted into the apparatus enclosure- the detector can also be removed to track down hydrogen leaks and so forth outside the enclosure.

2.3 CH_3 Infrared Band Strength Measurement

The methyl radical was of great interest in both of our focus systems, thought to be the cause of the carbon contamination which is among the greatest concerns in high quality compound semiconductor deposition, and put forward as a major growth species in diamond systems. It has the further advantage that the dilute methane in hydrogen used in the latter area is relatively easier to work with than arsenic containing compounds. Therefore, CH_3 was our first choice as a species for investigation in the plasma apparatus.

This required characterization of a laser diode, a task best done using the lines of the actual species to be detected as well as those of reference gas lines. It also required a knowledge of the infrared band strength, and although one value was available in the literature,[8] enough questions surrounded it that a second measurement was indicated. Thus we had two motivations to generate methyl radicals in a flow tube in such a way that their observation using a tunable diode laser would lead to a measurement of the infrared band strength.

A description of the experiment is contained in the paper in Appendix A. The results were quite satisfying. The authors of Ref. 8, Yamada and Hirota, are at the very top of the craft of diode laser spectroscopy, so that it comes as no surprise that our analysis indicates no conflict between our infrared observations. The band strength we report is only 30 percent higher than the value in their paper, well within the combined error limits. However, there is strong evidence that they made an incorrect choice of the methyl radical recombination rate coefficient which is used to estimate CH_3 concentration, and that use of a better value could increase the disagreement to the factor of two level. The advantage of our experiment over that of Yamada and Hirota is that both the temperature and the third body efficiency of the bulk gas are more easily quantified in the flow tube.

2.4 CF_2 Infrared Band Strength Measurement

As detailed in our first annual report,[9] we also carried out a band strength measurement for the CF_2 radical (see Appendix B for details). In addition to its usefulness in analyzing observations in our subsequent plasma system checkout studies using CF_4, this experiment had the added motivation of demonstrating the use of a fiber optic system to transmit 248 nm KrF excimer laser light. Its absorption was detected after crossing the CF_2 flow at the same point in the fast flow tube as the multiple passes of the infrared tunable diode laser beam. A recent measurement of the CF_2

ultraviolet absorption cross section[10] allowed us to quantify CF_2 concentrations and convert diode laser absorption measurements into a band strength.

In this case too, before our analysis was complete, another measurement of a line strength was reported.[11] On the other hand, a conversion error marred their original report of a band strength. We pointed this out, and their erratum appeared[12] with a value which agreed with ours to within the fairly large estimates of experimental error.

Our band strength measurement and that of Orlando et al.[11,12] were both of the ν_1 band, but in a CF_4 plasma this band would be badly overlapped by a strong CF_4 absorption band. The ν_3 band, on the other hand, should be relatively free of interferences and suitable for diagnostic work in CF_4 plasmas. Therefore, we delayed publication of our paper to complete collaboration with Jim Burkholder of NOAA/CIRES, in which his FTIR observations of both bands[28] were used to generate a band strength ratio and hence a ν_1 band strength.

Prior to this, the only estimates of CF_2 band strengths were the theoretical values of Newton and Person, which were higher than ours by more than 50 percent in each case. Discussions with Prof. Person resulting in his finding no reason to re-evaluate his predictions. In our paper we compared our values to his and to a more recent ab initio calculation,[14] which was in even greater disagreement with the experiments. Furthermore, after our result was published, we received word of two other ab initio calculations,[15,16] in both cases assigned a very high degree of confidence by the groups who performed them, and bearing the same (much larger) relationship to the experimental values.

Finally, a very recent paper by Suto and Steinfeld[17] reported the first direct measurement of the ν_3 band strength. As can be seen in Table 1 which summarizes all band strength values to date, this value agrees well with the

Table 1 - Infrared Band Strengths (km mol^{-1}) for CF_2

Band	ν_1	ν_2	ν_3
Frequency, cm^{-1}	1220	668	1102
Experiments	ν_1	ν_2	ν_3
Wormhoudt et al.[2]	65 ±25		160 ±80
Orlando et al.[11,12]	90 ±25		
Suto and Steinfeld[17]			170
Theory	ν_1	ν_2	ν_3
Newton and Person[13]	105 ±25	4 ±3	270 ±180
Schaefer et al.[14]	400	8.7	200
Botschwina[15]	123	3.0	
Peterson and Woods[16]	98	2.9	390

value we published. The question of agreement between theory and experiment remains unresolved, except to say that the error limits on all three experiments are fairly large, and that it may be that theoretical methods which have produced excellent results for stable molecules may have problems with radicals.

2.5 Observations in CF_4 Plasmas

The first systems observed were plasmas of CF_4 and argon (with Ar introduced only through the purge lines). They were chosen because we expected to make long runs as part of our initial check-out, and wanted a system which would be less destructive to the apparatus than deposition plasmas. In fact, although these plasmas are used in semiconductor etching and contain high concentrations of fluorine atoms, we were able to make

observations over a period of over four months before moving on to the next system (at which point the mirror etching mentioned above was discovered).

Most observations were made in the spectral region indicated by the arrow in Figure 3. The 1090-1120 cm^{-1} region contains the strongest lines of the CF_2 radical. At the upper end of this range they are overlapped by strong sharp features of the C_2F_6 molecule, while at the lower end C_2F_6 features are not detectable. Thus, we were able to take spectra from which we could deduce concentrations of both molecules, or spectra in which we were confident that the CF_2 spectra were free from interferences. Finally, some measurements of CF_4 dissociation were made in the weak band at around 1060 cm^{-1}, while others were made in the fundamental band in the 620-625 cm^{-1} region.

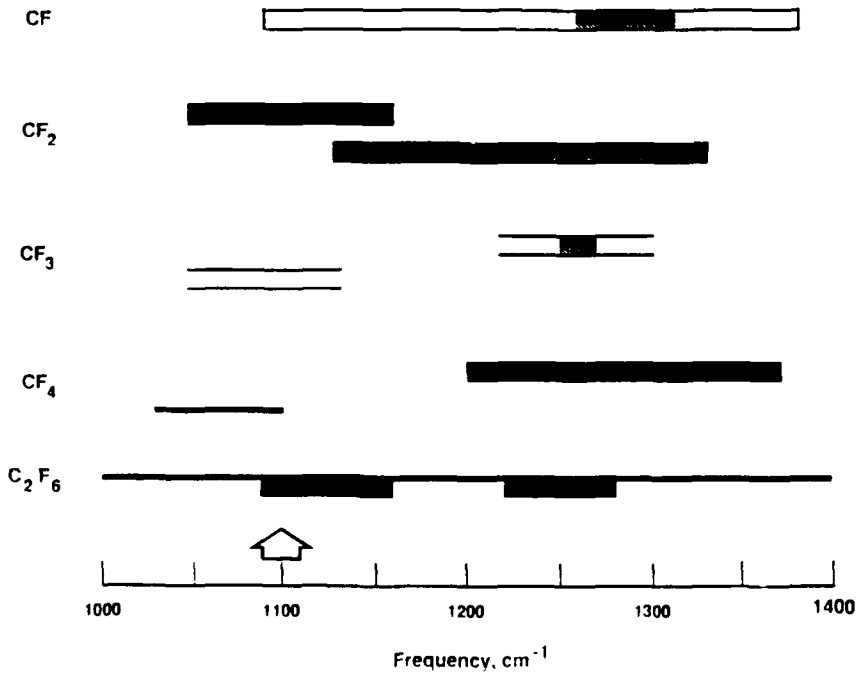

Figure 3. Infrared Absorption Bands of CF_x Molecules

2.5.1 Concentration Measurements with RF Power

As examples of the absolute concentration data obtained from analysis of infrared absorption features, we first consider Figure 4, beginning with the straight-line growth of CF_2 as the applied RF power is increased. This behavior seems plausible enough, but it must be pointed out that the dependence of any molecular concentration on a system parameter involves a balance of production and destruction rates. A linear dependence is by no means guaranteed, although the qualitative behavior of higher radical concentrations at higher powers is perfectly reasonable.

The behavior of the decomposition product C_2F_6 is seen to be in sharp contrast, being essentially constant and probably slightly decreasing with increasing power. It will be seen below that the fraction of CF_4 dissociated is increasing with increasing power, so the fraction converted into C_2F_6 is clearly decreasing with increasing power. In this case, then, the balance between production and destruction has different results, with C_2F_6 possibly more vulnerable to electron-impact fragmentation than is CF_2. C_2F_6 appears to

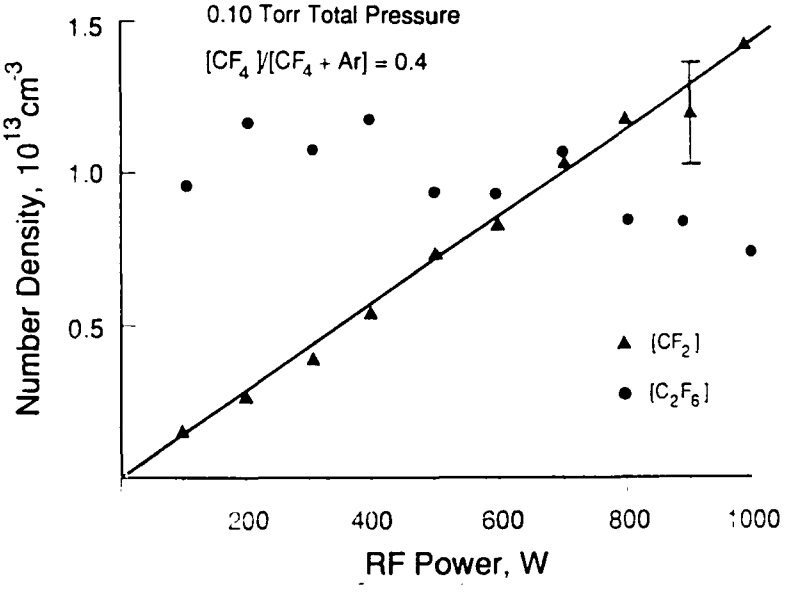

Figure 4. CF_2 and C_2F_6 Number Densities with RF Power

be an intermediate which reaches a steady-state concentration which happens to have about the same value even as the CF_4 concentration is decreasing and the concentrations of other decomposition and recombination products are increasing.

As discussed in our second annual report,[18] the observations in Figure 4 were made when the reactor had the following characteristics: a pure argon discharge had no observable CF_2 in it for an initial period, of the order of a few minutes, but thereafter CF_2 concentrations were seen of the same order as those observed with CF_4 addition. We concluded this was due to release of fluorcarbon species from the Teflon liner, and that this was consistent with higher CF_2 levels observed when the liner was new. Nevertheless, we also concluded that the data in Figure 3 are at least more representative of gas phase chemistry than the earlier, higher values.

Furthermore, we shall see below that CF_2 is a small fraction of the total products of CF_4 dissociation and is part of a complex plasma chemistry including many molecular species. On the other hand, argon ion bombardment of Teflon (molecular formula $(CF_2)_x$) may well produce CF_2 as its primary product, resulting in a plasma whose CF_2 concentration is (coincidentally) similar to that from CF_4 dissociation, but whose total fluorocarbon concentration is only a small fraction of that present when CF_4 is a feed gas. In other words, when CF_4 is a feed gas, the CF_2 from the walls may in fact be only a slight perturbation on the concentration of CF_2 (or other species) in the gas phase. Processes occurring on the walls, particularly radical reactions forming larger molecules, could still have a very important effect on observed concentrations. As we remarked on our previous discussion, how observations would change with other wall materials, such as stainless steel, would depend on whether a polymer layer was deposited and on recombination rates on the surface.

These wall effects may be the cause of the differences between our observations and the most detailed computer model of the chemistry of the CF_4

plasma, that of Plumb and Ryan.[21] Ian Plumb very kindly carried out a few calculations using this model for the conditions of our reactor.[22] (These conditions are very different from those of Smolinsky and Flamm,[23] the observations used previously by Plumb and Ryan and earlier modelers to calibrate their models.) We will discuss the major difference below, and at this point only present a comparison of CF_2 and C_2F_6 concentrations.

Figure 5 repeats the observed points of Figure 4, and adds two predicted points (open symbols) for each molecule. (This plot assumes that half the RF power is actually deposited in the plasma.) Though the differences appear

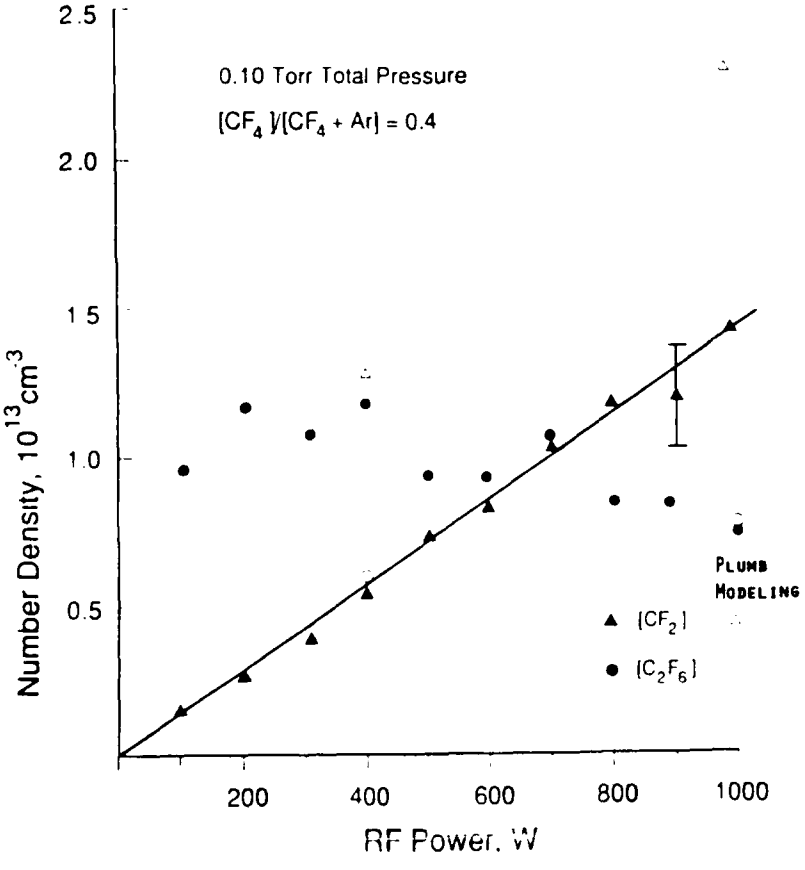

Figure 5. CF_2 and C_2F_6 Number Densities from Figure 4, with Model Predicted Points (Open Symbols) by Ian Plumb[22]

large when plotted on a linear scale, the agreement is in fact quite satisfying - both CF_2 predictions are less than a factor of two above the observations, perfectly respectable for a radical species, and while the low power C_2F_6 prediction is a factor of two below the prediction, the high power point is right on.

2.5.2 Observations of CF_2 Concentration with Oxygen Fraction

Molecular oxygen is a standard additive to CF_4 etching plasmas, being known to substantially increase the etch rate.[24] Oxygen atoms are known to react readily with CF_2 to form COF which eventually forms the stable species COF_2 and CO_2.[25]

We made one set of observations of CF_2 number densities as a function of added oxygen, shown in Figure 6. Here, the interpretation is straightforward, as is the comparison with the existing work shown in the right side of Figure 6. Comparing the predictions of Ryan and Plumb for a pure CF_2 plasma (at 0.5 Torr) of a CF_2 steady state number density of around 4×10^{14} cm^{-3} to those of Plumb and Ryan[26] for a 75% CF_4/25% O_2 plasma in which the CF_2 number density has dropped to 2×10^{13} cm^{-3} after about a 50 msec residence time and is continuing to drop, we expect oxygen addition to have a substantial effect.

The effect observed in Figure 6 is somewhat less dramatic, involving a drop of about a factor of six at the 20% oxygen level. The emission data given beside it show a slightly larger fractional drop. Like the Smolinsky and Flamm study, this experiment[27] was done in a small alumina tube with a high power density, here as high as 4 W/cm^{-3}, with a pressure of 1 Torr.

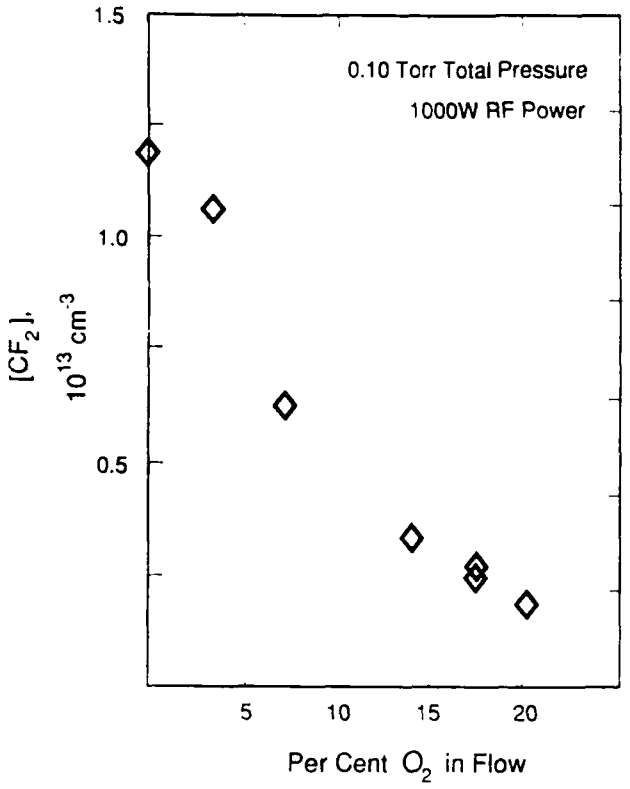

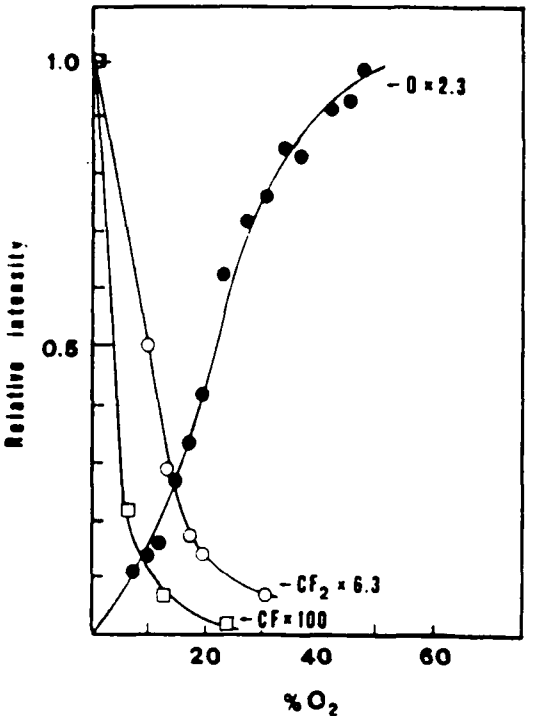

Figure 6. (a) CF_2 Number Density with Percent O_2 in Flow. (b) Normalized Electronic Emission Intensities of CF_2, CF, and O as a Function of O_2 Percent in Feed, from Ref. 27.

2.5.3 Temperature Measurements of CF_4 Plasmas

We have already noted above that the observed CF_2 concentrations are a small fraction of the input CF_4. The question of what fraction they are of the CF_4 actually dissociated can be addressed by the CF_4 absorption experiments mentioned in the introduction. However, before a change in a CF_4 line absorption intensity can be converted into a fractional dissociation, we must have a measurement of the temperature of the gas when the discharge is on, since otherwise a change in the total gas density would be mistaken for a change in the CF_4 partial pressure.

Since we desired a translational temperature, the ideal measurement was the temperature derived from the Doppler width of the infrared absorption line, as was done in our Cl atom work.[19] However, this was not possible, as all lasers used in studying CF_4 plasmas had laser linewidths (jitter widths)

of the same order as the Doppler width. On the other hand, rotational degrees of freedom are expected to be in equilibrium with translation in these plasmas, so a search was undertaken for CF_2 lines with sufficiently differing lower state energies that a rotational temperature could be measured. We were aided in our search by a complete high resolution (FTIR) spectrum of CF_2 taken by Burkholder and Howard,[28] and a matching theoretical prediction of line positions and intensities using the asymmetric rotor program developed by Carter and Halonen.[29] These and other developments in CF_2 spectroscopy are reviewed in our CF_2 band strength paper (Ref. 2 and Appendix B).

After several attempts it became obvious that lines originating on levels separated by a few hundred wavenumbers would not give adequate sensitivity. Whether the problems were overlapping lines of CF_2 or other molecules, or peak height variations induced by perturbation of the diode current tuning rate by the RF or some combination was not determined, but no reasonable temperatures were derived until spectral scans were examined which included two small lines at 1091.65 and 1091.835 cm^{-1}. The lower state energies for these lines are 1715.8 and 1692.3 cm^{-1}, respectively. An example of a temperature determination using these two lines and a number of lines from the same spectral scan with smaller lower state energies is given in Figure 7.

The slope of the plotted quantity, ln(od/S), is -1/RT. The temperature given in the example, 425K, is close to the 500K reported in Ref. 27 at 1 Torr and a much higher power density, as determined by optical emission from CO and N_2. Remarkably, observations like those in Figure 7 made at powers from 100 to 1000 W yielded no significant variation in the derived temperature. On the other hand, measurements at a total pressure of 0.10 Torr yielded a somewhat higher temperature, 465K with a standard deviation of about 50K.

We observed essential independence of bulk plasma temperature with applied power in our earlier chlorine atom work,[19] and ascribed it to the generation of larger concentrations of electronically and vibrationally excited molecules at higher powers. These excited species are much better

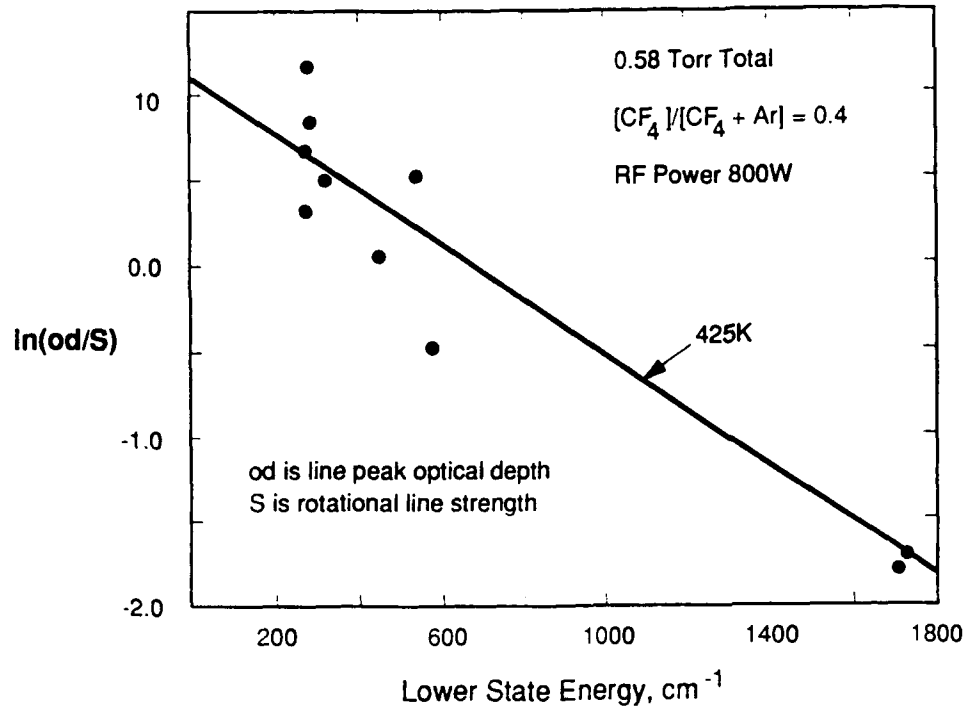

Figure 7. Example of Rotational Temperature Measurement Using CF_2 Absorption Line Intensities

conductors of heat to the walls than molecules with only rotational and translational energy, and as their concentration increases the heat flux to the apparatus increases roughly proportionally to the input power while the temperature can remain almost constant. It is certainly plausible that the same thing is going on in these CF_4 plasmas.

One other point of comparison is the laser induced fluorescence experiment of Hancock and co-workers, in which LIF of the CF molecule yielded a rotational temperature.[30] They were observing a commercial parallel plate plasma etching reactor with a volume of about 1200 cm^3, with applied 13.56 MHz power in the range of 50 to 200 W, giving power densities at the upper end of our range. Their pressure of 0.05 Torr is somewhat below our lowest value, while their residence time of about 0.1 s is two orders of magnitude shorter than ours at the same pressure. Whether these differences affect the heat transfer and temperature is not easy to guess, but their observations do

differ from ours, being lower and showing more dependence on applied power (ranging from 324 ±15 K at 50 W to 443 ±30 K at 200 W).

On the other hand, both our observations and the other data for CF_4 discharges agree on the qualitative point that discharge temperatures are fairly low, in the 300 to 500 K range and therefore affecting the density by less than a factor of two, where our chlorine plasma measurements[19] yielded temperatures as high as 800 K (not surprising in light of the lower thermal conductivity of chlorine).

This conclusion was further bolstered by a set of measurements we did on static charges of argon or Ar/CF_4 mixtures, observing the pressure rise when the discharge was turned on. Times for the pressure to reach a roughly steady value were of the order of the typical residence time in the flowing system, but it is clear that these experiments will never be perfectly comparable to the system with flows. On the other hand, it is reassuring that the temperatures derived from these measurements are in roughly the same (400 to 600 K) range, have the same behavior of decreasing with increasing pressure, and are roughly constant with applied power.

2.5.4 Observations of CF_4 Dissociation Fraction

Having convinced ourselves that we could approximately correct for temperature changes in analyzing CF_4 absorption observations, and that a large change in CF_4 absorption would in fact be due in part to CF_4 dissociation, we were ready to analyze observations of CF_4 absorption line intensities. One other correction should be noted, one due to the fact that the CF_4 is introduced slightly upstream of the discharge region. In the analysis leading to the data presented here, we assumed that if all CF_4 were immediately dissociated in the discharge, a peak absorption of 0.08 of the discharge-off value would still be observed.

Figure 8 shows the results of CF_4 dissociation measurements as a function of RF power. It can be seen that except for low powers, the fraction dissociated was always quite large. Figure 9 shows observations as a function of total pressure, for three different power settings. Presumably owing to inaccuracies in the corrections described above, there is substantial scatter in these curves, as well as disagreement from one day's observation to the next, but the qualitative conclusion stands that over most of the parameter range we covered, over half the CF_4 has been dissociated.

The apparent drop-off in dissociation fraction at the very highest pressures will receive some additional comment in the following section on CF_2 number density variation with pressure. For now, we can remark that we have made visual and photographic observations of these plasmas as a function of pressure and power, and observe that while at the lowest pressures a fairly

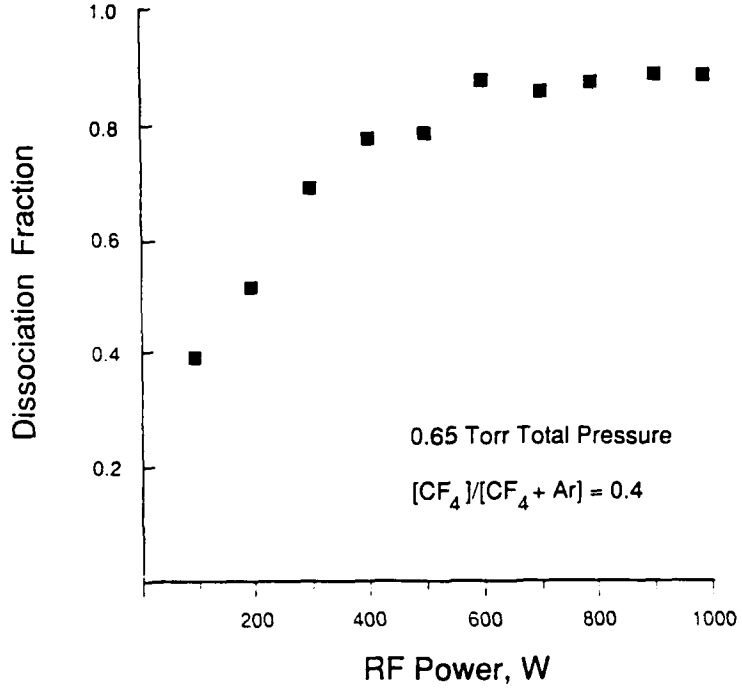

Figure 8. Fraction of CF_4 Dissociated with RF Power

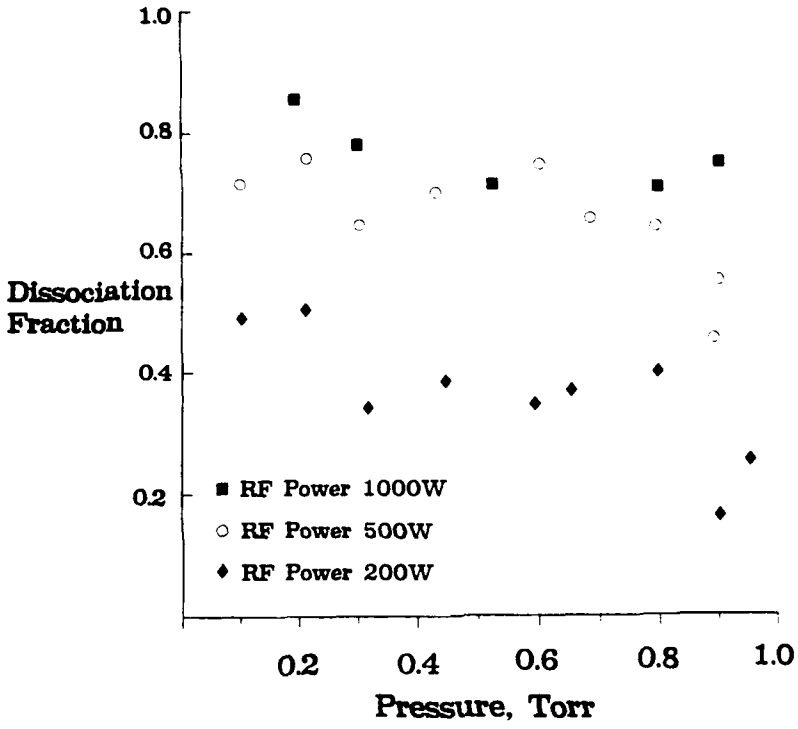

Figure 9. Fraction of CF_4 Dissociated with Total Pressure

uniform glow fills the tube, at higher pressures the glow retreats towards the walls, so that less and less of the elliptical spot pattern is passing through a brightly glowing region.

2.5.5 Observations of Concentration Variation with Total Pressure

Now we turn to Figure 10, which shows absolute CF_2 and C_2F_6 number densities as a function of total pressure, for a constant mixing ratio. The remarkable features of the CF_2 curve are a sharp increase with decreasing pressure below 0.15 Torr, and an essentially constant behavior at higher pressures. The C_2F_6 concentration mirrors this behavior to a lesser extent, but may show a peak at 0.2 Torr and may also be increasing as the pressure increases to 1.0 Torr.

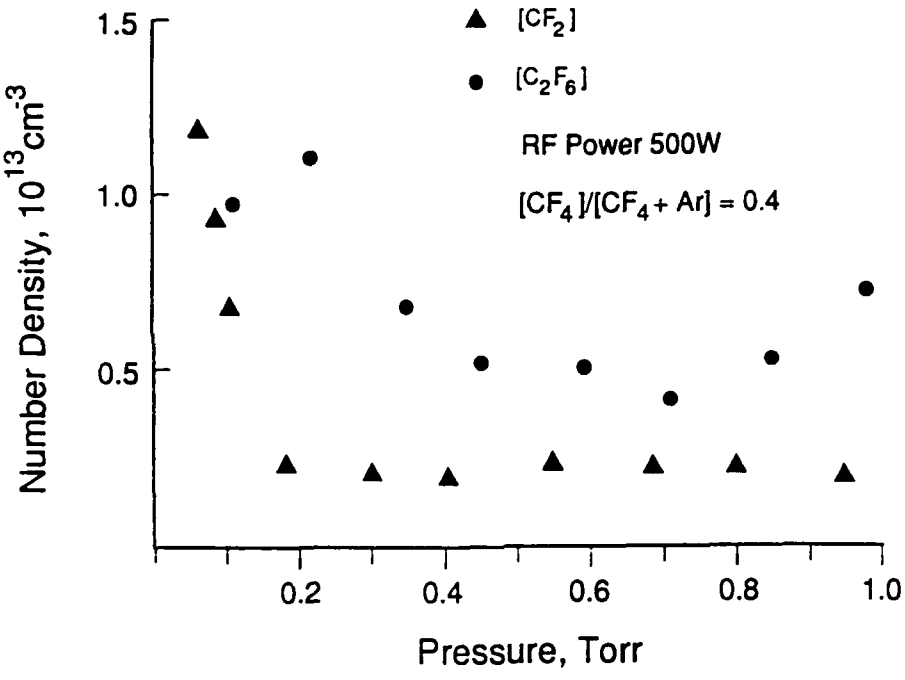

Figure 10. CF_2 and C_2F_6 Number Density with Total Pressure

The apparently discontinuous behavior of CF_2 between 0.1 and 0.2 Torr is questionable enough that we immediately turn to another way of presenting the same data. In Figure 11 we have divided the absolute CF_2 concentrations by the amount of CF_4 dissociated at each pressure to produce an effective branching ratio for the dissociation of CF_4 and the resulting chemistry leading to CF_2. Now, the points at 0.1 Torr and below extrapolate neatly to the 0.2 Torr point, and a relatively smooth curve can be fit through the entire data set.

In preceding sections we have already discussed why the behavior seen in Figure 11 is plausible, based on bulk gas-phase chemistry. Higher pressures could favor gas-phase recombination reactions, shifting the steady state away from CF_2 and towards larger molecules. Of course, at even lower pressures the CF_2 concentration would eventually decrease with decreasing pressure.

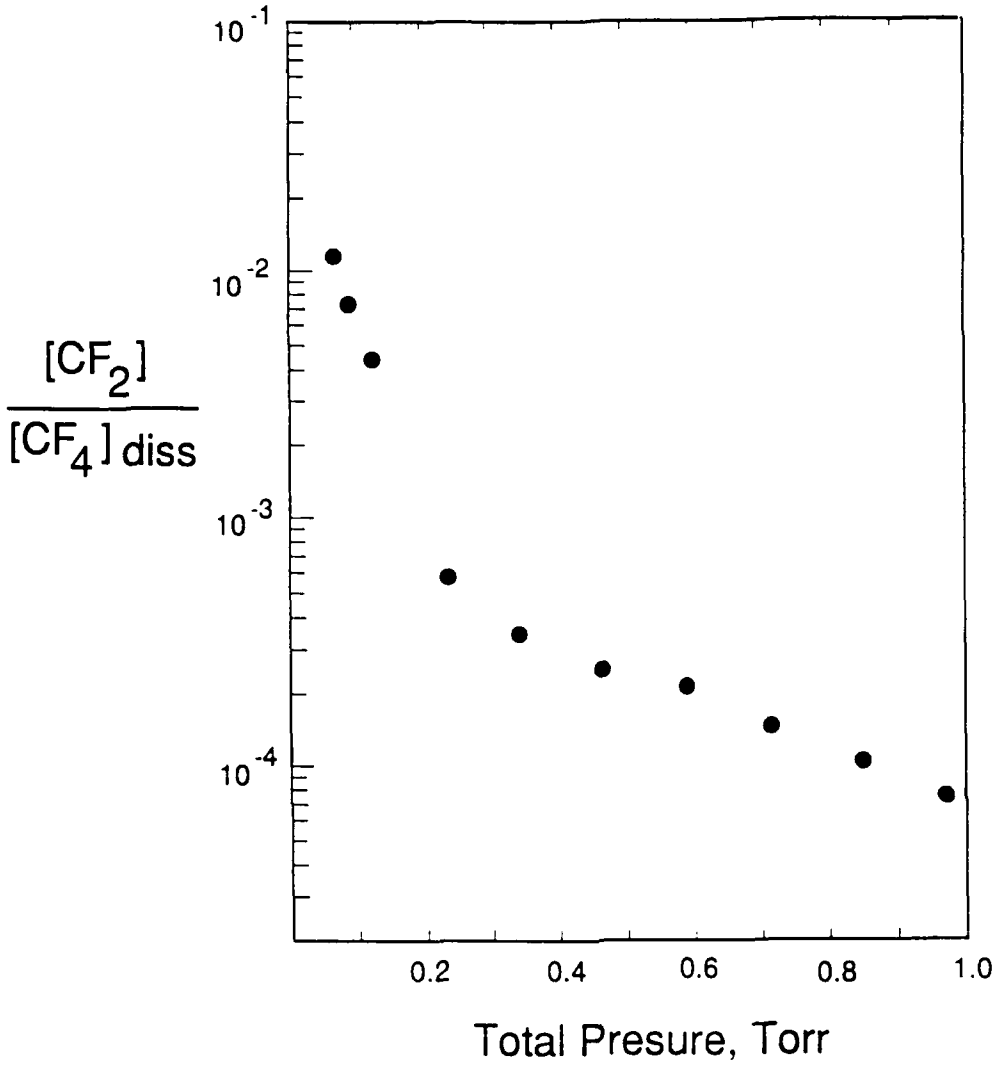

Figure 11. Fraction of Dissociated CF_4 Converted to CF_2

However, the surface source in our system might not decrease linearly with pressure, if higher ion energies produced more desorption per ion as the total (and ion) densities decreased. Still, we expect a peak in CF_2 concentration at some total pressure below 0.05 Torr. The possibilities that C_2F_6 peaks above this, and that it increases as the pressure goes past 1 Torr, are both consistent with it being a product of radical recombination and reaction whose rates are faster at higher total pressures.

However, these bulk gas considerations may not be the major mechanism behind the concentration variations with pressure. One phenomenon which must be considered, the lowering of the average energy of the electron distribution with increasing pressure as observed by Tachibana et al.[41] in methane plasmas, may only be important in reactors with shorter residence time than ours. An enhanced efficiency of CF_x species removal from the Teflon liner by bombardment by higher energy ions at lower pressures could play a role, but if our hypothesis that this flux of surface-generated species is primarily CF_2 and is small compared to the gaseous CF_4 input, this contribution to the observed pressure effect may also be small. Instead, the increasing spatial nonuniformity with higher pressure, with the glow and presumably the source of radicals moving more towards the electrodes, may play a major role.

Figure 12 presents a recent laser induced fluorescence study of CF_2 profiles in a parallel-plate reactor.[31] They interpret their results in terms of a diffusion length L which in fact is an e-folding length for CF_2 chemical reaction, primarily with fluorine atoms. Looking at the power variation in Figure 12, we see that at the lowest concentration of CF_2 (and other reactive radicals, including F atoms) this length is the size of the electrode spacing and the CF_2 concentration is uniform throughout the reactor volume. Only a doubling of power and radical densities is required to establish a noticeable gradient. Of course, the effect of pressure on the discharge is first of all a result of changing electron and ion kinetics, but the concept of a chemical diffusion length must then be applied to assess how far from a glow or source region radicals can travel before being consumed. We expect that the source region is moving away from the laser spot pattern as the total pressure is raised, and that the chemical diffusion length is if anything decreasing as well, and that both effects may be contributing to the decrease in CF_2 column density observed.

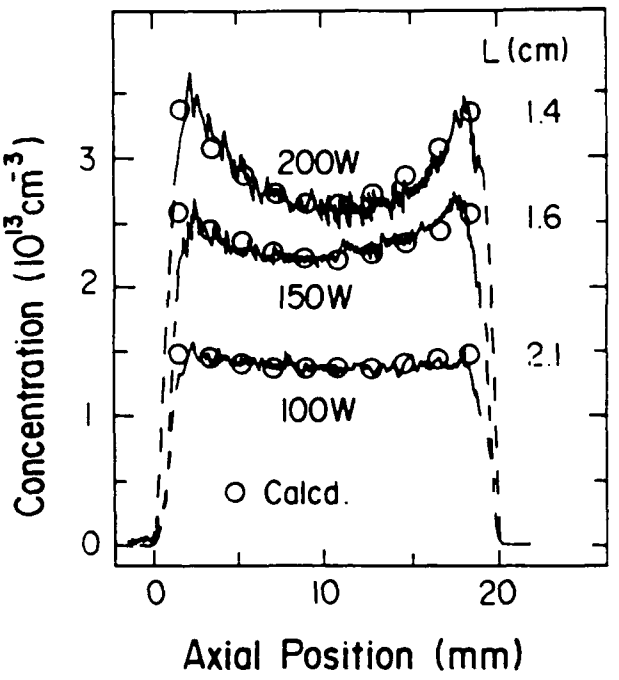

Figure 12. Axial Profiles of CF_2 By Laser Induced Fluorescence with RF Power, from Ref. 31. L is the chemical diffusion length, used to calculate the curves indicated by circles.

On the other hand, C_2F_6 is a stable molecule, and if at higher pressures there is indeed a widening volume in the center of the tube with low electron, ion, and radical concentrations, C_2F_6 should have no trouble filling the tube uniformly at pressures of 1 Torr and below. Therefore, the lower C_2F_6 concentrations observed at higher pressures in Figure 11 would seem to reflect a change in the gas phase chemistry averaged over the reactor volume.

Finally, we address the question of the drop in observed CF_4 dissociation at the highest pressures, keeping in mind that these data have enough uncertainty that the effect may not be real. A nonuniform plasma could result in an essentially constant fractional dissociation until the distance over which radical recombination to form CF_4 takes place becomes shorter than the distance between the laser beam pattern and the effective source of dissociation near the electrodes.

2.6 Observations in CH_4 Plasmas

Species observed in CH_4 plasmas include the methyl radical, CH_3, ethylene, C_2H_4, and acetylene, C_2H_2. Observations of CH_4 dissociation and rotational temperature were also made. Studies in one spectral region where CH_2 lines were expected resulted in the observation of several discharge-produced absorption lines which do not match with the known CH_2 spectrum. We suspect C_2H_4 or C_2H_6, also plausible decomposition products, but have not been able to make a positive assignment.

2.6.1 CH_3 and C_2H_2 Concentration Measurements

The work on methane plasmas was simply directed to determining which species could be detected for later coordinated parametric studies. However, having located good absorption lines, we did perform a few parametric variations. We present examples here, beginning with Figure 13 which shows CH_3 number density variation with RF power. It will be noted, first, that the

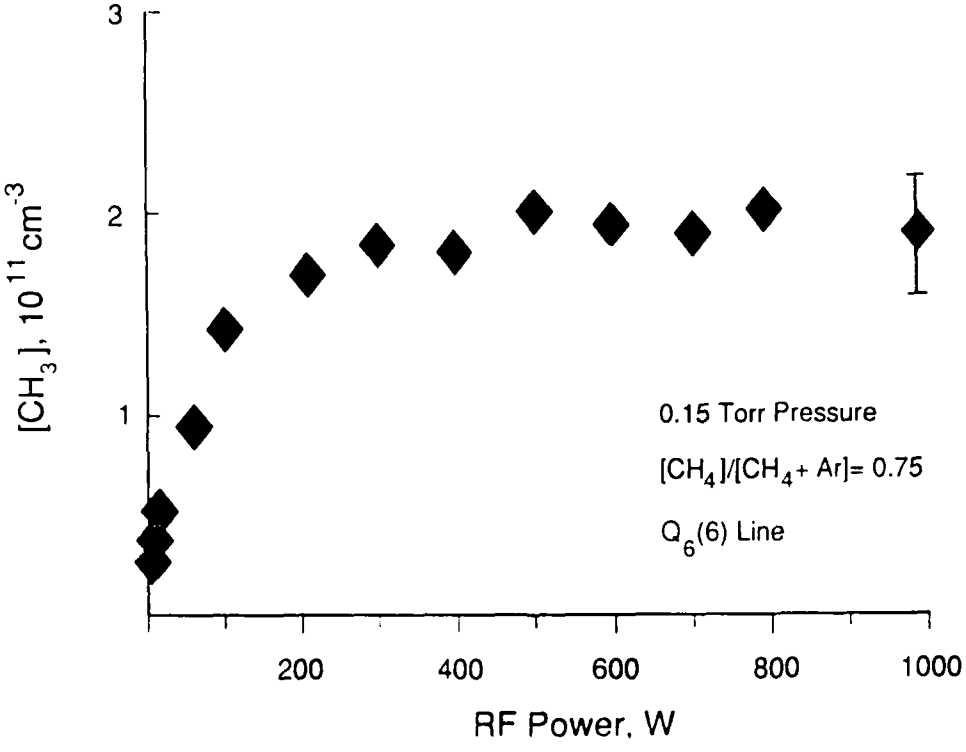

Figure 13. CH_3 Number Density with RF Power

methyl radical concentration is two orders of magnitude smaller than the CF_2 concentration in an otherwise similar CF_4 plasma. It is also seen that its concentration rapidly plateaus out at a limiting steady state value. Both observations are consistent with concentrations determined by gas phase chemistry, considering that the CH_3 radical is much more reactive than the CF_2 radical.

Figure 14 shows the CH_3 radical concentration variation with total pressure. Once again, the absolute number density decreases as the total pressure (and the CH_4 number density) increases. The decrease is more gradual when compared to the steep drop in CF_2 concentration between 0.1 and 0.2 Torr. We can speculate that

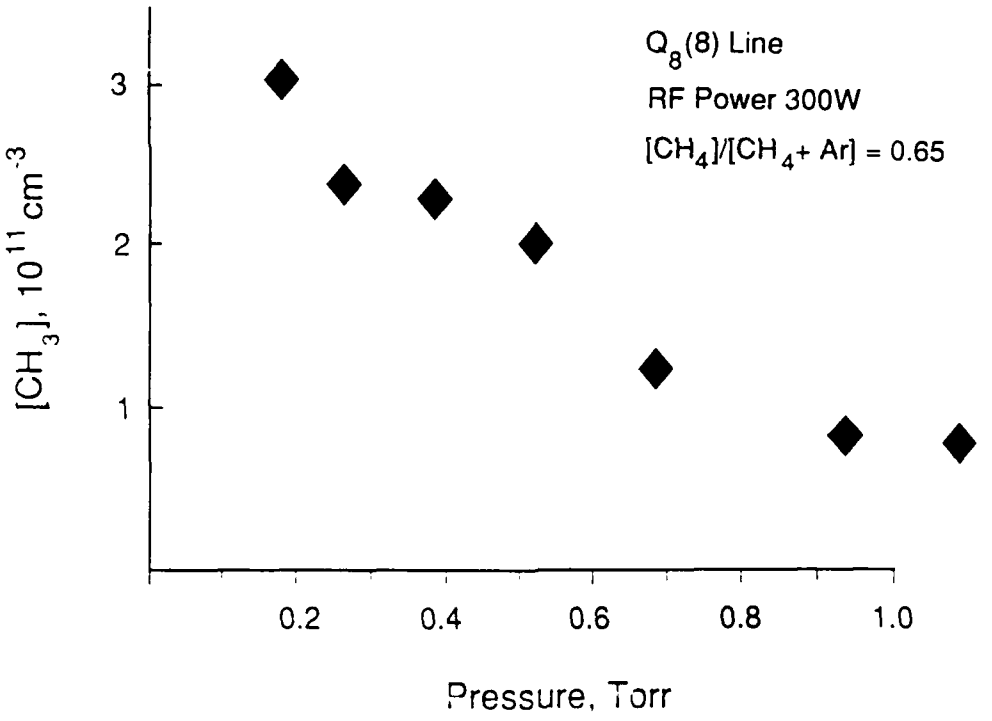

Figure 14. CH_3 Number Density with Total Pressure

because of the high reactivity of CH_3, if there is a region where the balance between production and destruction changes to produce a dramatic increase in number density, it occurs at lower pressures than for CF_2.

Finally, Figure 15 shows C_2H_2 number density over the same total pressure range. Although C_2H_2 is present in much larger concentrations than the radicals we have studied, it still is under 10 percent of the input methane. Since the line used in Figure 15 is a hot band line (originating in the first vibrational excited state rather than the ground state) it will be more sensitive to temperature than the neighboring ground state line. Analysis of such pairs can yield a vibrational temperature, which will in general be out of equilibrium (higher) with the translational/rotational temperature. Our

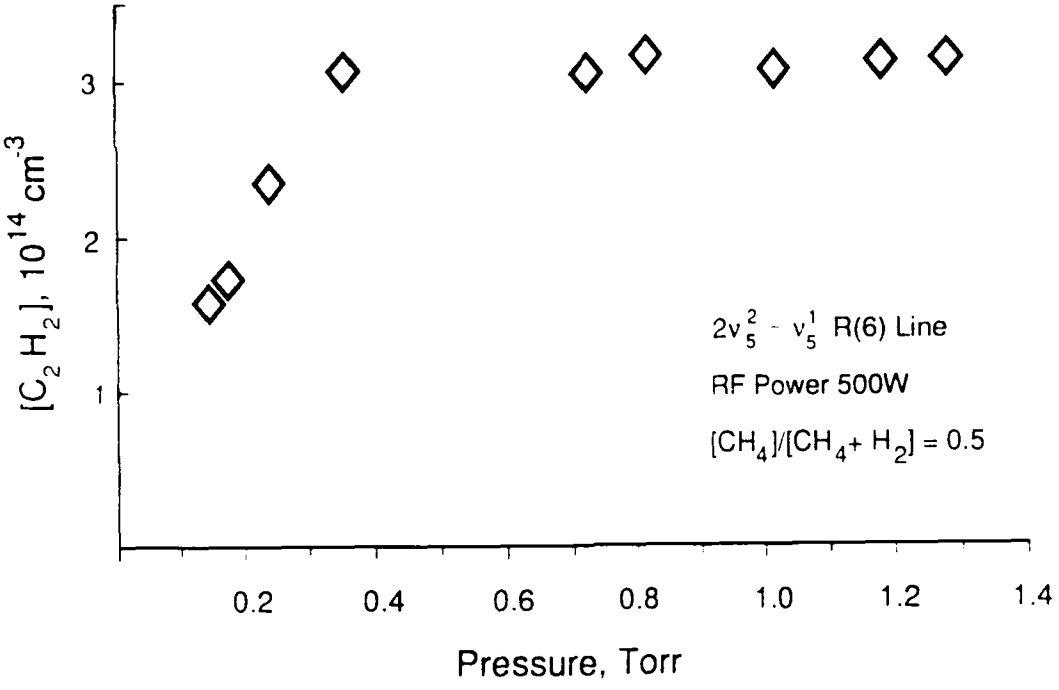

Figure 15. C_2H_2 Number Density with Total Pressure

analysis suggested that even the vibrational temperature in these plasmas is not too high, and that the 500 K temperature we assumed in order to analyze the data of Figure 15 is not too greatly in error. In the following subsection, we will see the rotational temperature we measured later is lower still.

2.6.2 CH_4 Dissociation and Temperature Observations

The above observations raised at least two questions which can now be given tentative answers based on additional results presented here. First, does C_2H_2 account for the majority of dissociated CH_4 which would imply a low (order of 0.12) fractional dissociation, or are there more dissociation product species not yet detected?

The second question concerns the drop in fractions of both C_2H_2 and CH_3 with increasing pressure. It is observed that at low pressures the glow discharge fills the flow tube, while at higher pressures (approaching 1 Torr) the center of the tube is darker and the glow is concentrated near the electrodes. Does this smaller volume of glow (in which most of the electron impact dissociation occurs) result in lower average dissociation of CH_4 at higher pressures, and is this in turn the reason for lower fractions of dissociation products? Or, does the plasma chemistry change with total pressure, changing the distribution of products?

Both of these questions call for a measurement of the CH_4 dissociation fraction. However, this in turn requires an accurate knowledge of the plasma temperature, since an observed decrease in adsorption line intensity can be due to dissociation or simply to a change in density due to gas heating, or a combination of both effects. We were fortunate to find a region of the CH_4 absorption spectrum (shown in Figure 16) which provided both concentration and temperature information in a single diode scan. The strong line on the right hand side is seen to have a low energy ground state and to decrease in intensity both due to dissociation and heating, while the intensities of the

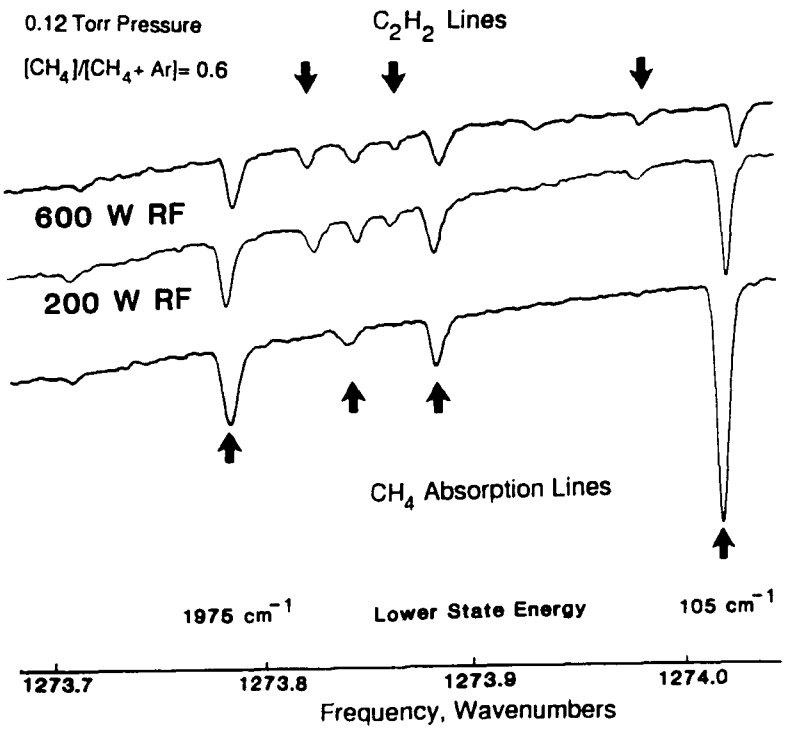

Figure 16. Infrared Spectral Region Used in CH_4 Dissociation Fraction and Temperature Measurement (Lower Trace, Plasma Off, Upper Traces, Plasma On)

lines on the left remain almost unchanged as dissociation is almost counterbalanced by increases in relative intensity due to gas heating.

Plasma temperatures were obtained using the ratio of CH_4 line intensities. The lines used were the set of lines with high rotational energies (high J) at 1273.7822, 1273.7843 and 1273.7859 cm^{-1}, and the low-J ^{13}C line at 1274.0176 cm^{-1}. As an example of the variation of plasma temperature with applied power we show in Figure 17 observations for a total pressure of 0.12 Torr and a CH_4 fraction in the tube of 0.63 of the total of CH_4 and Ar purge gas. The plasma temperature rises to about 325 K with only 50 W applied power, and continues to rise in a roughly linear fashion to arrive at about 400 K in the region of 1000 W of applied power.

Figure 18 shows a set of measurements of the CH_4 dissociation fraction, measured using the same ^{13}C line used in the temperature measurement described

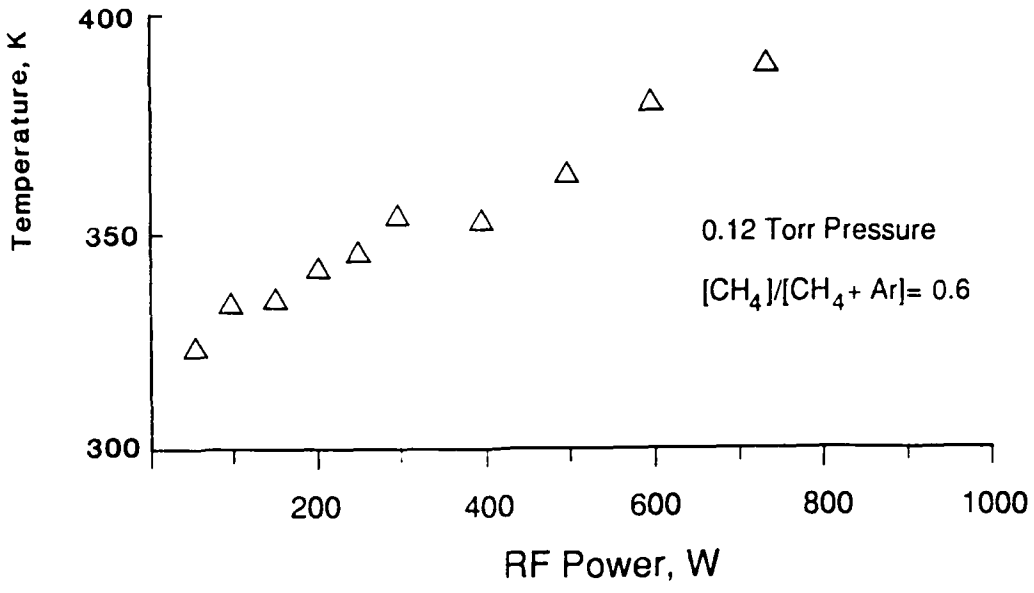

Figure 17. Methane Plasma Temperature Obtained from CH_4 Rotational Line Intensities

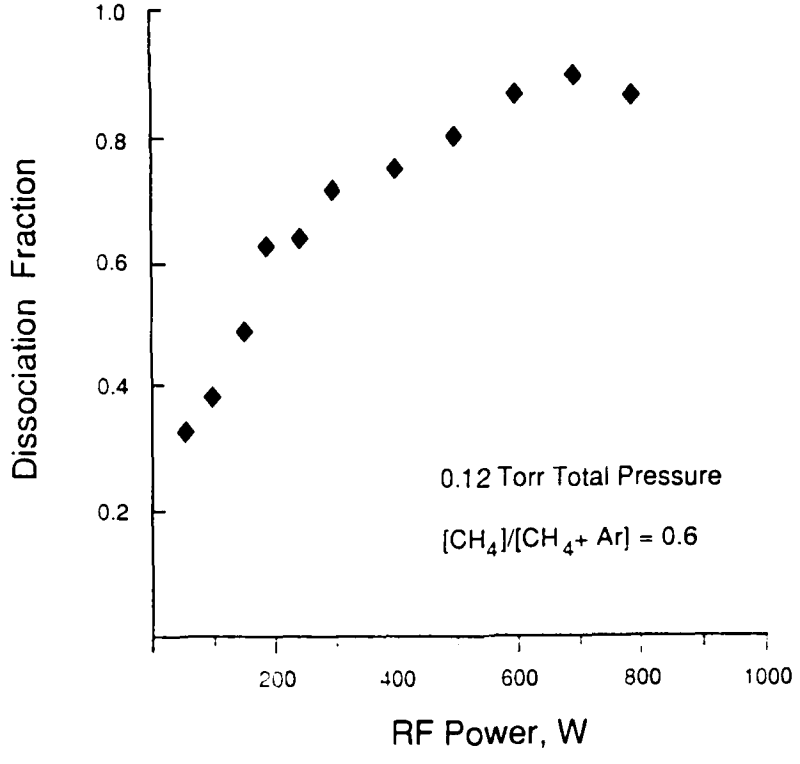

Figure 18. CH_4 Dissociation Fraction Measured by Infrared Absorption Line Intensities

above. The observed peak optical depths must be corrected to values which are representative of the CH_4 concentration in the active plasma region by subtracting out the optical depth appropriate to a small region between the ring injector and the electrodes, where it is assumed that no dissociation occurs. This region is estimated to be about 5 cm long, compared to an effective single pass absorption length (calculated from the tabulated line strength, the observed line width and discharge-off optical depth, and an average CH_4 concentration in the tube) of about 125 cm.

The fraction of CH_4 which remains is related to the ratio of these corrected optical depths. However, before it is subtracted from one to yield a dissociation fraction, this ratio is corrected by multiplying it by the ratio of discharge-on and discharge-off temperatures to correct for the change in density, and by the ratio of Boltzmann factors (discharge-off to discharge-on) to correct for the change in line strength as the gas is heated (if a change in line width had been observed, a correction for this would also have been included). In this way, the observed column densities are converted into a fraction of the total CH_4 which is dissociated, which represents an average over the line of sight down the tube. It can be seen that except at very low powers the majority of the CH_4 has been dissociated, and that the dissociation fraction approaches 0.9 at high powers.

We can also see in Figure 16 that additional absorption lines appear when the discharge is on. These turn out to be C_2H_2 lines. We found no information on this band in the spectroscopic literature, but simply identified it, and quantified the line strengths at room temperature, by taking spectra of a static sample of C_2H_2 in the flow tube. The fact that we do not know lower state energies and hence temperature dependences for these lines introduces an uncertainty into absolute concentration measurements made using them. However, since the temperature rise in the plasma is small, we expect the error to be small, most likely much less than a factor of two. In fact, the C_2H_2 concentrations shown in Figure 19, obtained assuming no

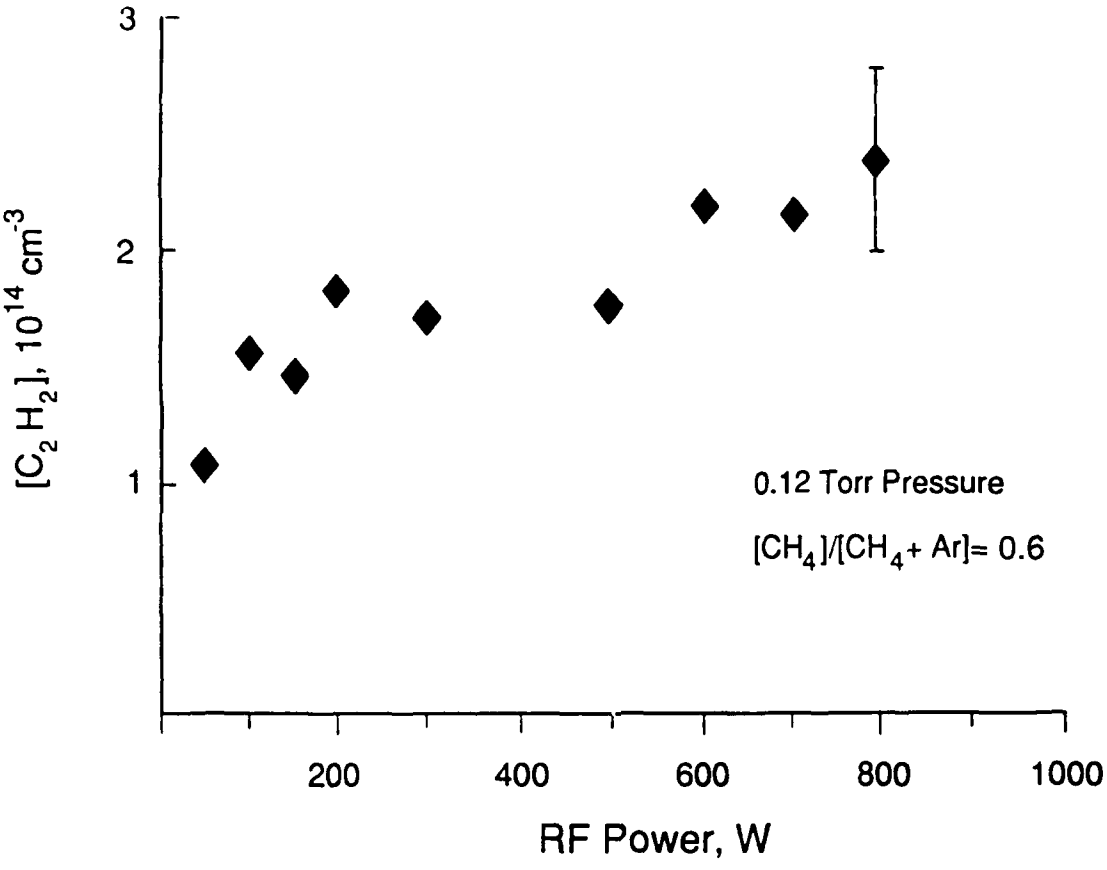

Figure 19. C_2H_2 Concentrations Obtained from Absorption Lines in Figure 16

significant change in line strength, agree with our earlier[5] observations using known lines, when those observations are corrected from an assumed temperature to the observed temperatures reported here.

2.6.3 AsH_x Species in Organoarsine Decomposition

From its inception in 1986, our research program has had as its ultimate goal the development and demonstration of laser diagnostics to support deposition mechanism studies for compound semiconductors, with gallium arsenide chosen as being representative and having the largest base of phenomenological observations and modeling studies with which our investigations could connect. We chose as a particular focus a hypothesis

connecting suppression of carbon incorporation into the growing film with the action of AsH_x radicals in carrying reactive hydrogen to the surface. Considering that in the MOCVD of GaAs from arsine and trimethyl gallium, most of the gallium is thought to arrive at the surface with at least one CH_3 group still attached, it is in one sense remarkable that only a tiny fraction of the incoming carbon is in fact incorporated. Even a tiny fraction, however, has tremendous effects on the electrical properties of the film.

An understanding of carbon incorporation mechanisms has become even more important as the industry has moved away from arsine as the arsenic source to organoarsine compounds which are safer but which themselves carry carbon to the growth surface. It is observed that compounds such as trimethylarsenic (TMAs) which have no As-H bonds give rise to very high levels of carbon incorporation, while compounds which could directly dissociate to AsH or AsH_2 radicals give much lower carbon. The above hypothesis is now regularly invoked in explaining these observations.[32-36]

Clearly, measurements of absolute AsH, AsH_2, and AsH_3 concentrations in organoarsine decomposition systems would add much to our understanding. AsH_2 has never been observed by direct infrared absorption, although one infrared band position is known through analysis of its electronic spectra. The AsH radical has received one preliminary study using tunable diode lasers.[37] We chose it as the first AsH_x radical to attempt to observe. However, before beginning AsH observations we made a search of a region of containing known AsH_3 lines, in a plasma containing TMAs.

Determination of AsH_3 concentrations is a useful preliminary to looking for AsH, since the AsH band overlaps an AsH_3 band. In addition, recent investigations into afterglow decomposition of organometallics including TMAs in a deposition chamber[38,39] and into microwave plasma generation of AsH_3 from TMAs[40] have reported AsH_3 as a decomposition product. We noted that, using present thermodynamic data for arsenic containing species, the only energetically favored gas phase reactions which can lead to AsH_3 are those

which add hydrogen atoms to AsH_x radicals, and that these three-body recombination reactions will be extremely slow at the reduced pressures of plasma discharges. Therefore, our observations of decomposition of a 2:1 mixture of Ar and TMAs at a total pressure of 0.44 Torr and an input RF power of 400 W were made under conditions in which AsH_3 observation would have been surprising.

In the event, we observed no AsH_3, down to a sensitivity level conservatively estimated to be 10^{11} cm^{-3}. In other words, the fraction of TMAs converted into AsH_3 under these conditions is much less than 10^{-4}. This is not necessarily in conflict with observations of AsH_3 formation in other plasma sources,[38-40] since plasma sputtering of hyrogenated arsenic films in those systems could give rise to AsH_x species which are unable to form in gas phase reactions. Our studies (to be discussed below) of a region containing AsH lines were more extensive, including: the use of tertiarybutylarsine as the arsenic-containing species (one which is capable of direct dissociation into AsH_2); use of hydrogen as a carrier gas; observation of discharges of argon and hydrogen or hydrocarbons alone; and improvement of our detection sensitivity using computer averaging of laser scans. These studies showed that some AsH could be driven off the walls of the reactor by a pure argon discharge, and that more appeared when hydrogen containing compounds were added to the flow. However, we did not return to the AsH_3 region to see if it could be formed in measurable quantities from wall deposits using argon/hydrogen discharges.

2.6.4 C_2H_4 in TMAs and CH_4 Decomposition

On the other hand, our observations in the 1076-1078 cm^{-1} region did show a set of absorption lines whose appearance was associated with the plasma decomposition of TMAs. We soon determined that the same lines appeared upon decomposition of CH_4, and that they were due to C_2H_4. Estimates of C_2H_4 concentrations based on room temperature line strengths (again, no line identifications were available) gave the result that in both CH_4 and TMAs

systems the conversion to C_2H_4 was of the same order, with perhaps 5 percent or less the input carbon being converted to C_2H_4.

With this observation and the CH_4 dissociation study reported above, we can return to the questions we posed at the beginning of this discussion. We now know that the fractional dissociation of CH_4 is high, so that its conversion fraction into C_2H_4, C_2H_2 and other species not yet identified must be large. We have not made a systematic study of CH_4 dissociation fraction as a function of total pressure. However, our extensive observations of CH_4 dissociation and of CF_4 dissociation fraction taken at the same pressure precisely overlay each other (see Figures 9 and 18). At higher pressures, our observations are that the CF_4 dissociation fraction decreases somewhat, but only by 10 or 20 per cent from 0.1 to 1.0 Torr. We also made some studies of dissociation using C_2H_4 as a feed gas, and found its dissociation was essentially complete throughout our pressure range. If this is true for CH_4 as well, then lower dissociation of the feed gas is clearly not the reason for a drop in CH_3 fraction by a factor of 20. We conclude that a major reason for the drop in fractions of particular dissociation products is that higher pressures facilitate chemical reactions which shift the molecular species distributions to larger and less reactive molecules.

2.7 AsH in Organoarsine Compound Decomposition

In our observations of AsH radicals in the plasma decomposition of tertiarybutylarsine (TBA) and trimethylarsenic we had several goals. At the diagnostic development level, we wanted to see if AsH absorption lines could be detected without interference from other AsH species or from hydrocarbon compounds. Plasma decomposition presumably yields a wider variety of products and is therefore a greater challenge than thermal decomposition. We found that AsH lines were indeed detectable without substantial interference, even against a background of hydrocarbon species lines.

At the mechanism definition level, we had three practical systems which our plasma system could in some degree be thought to resemble. As discussed

in subsection 2.6.3, these systems are the dominant film deposition method of decomposition over a hot substrate, afterglow decomposition of organometallics[38,39] and microwave plasma generation of arsine from TMAs.[40] The afterglow decomposition studies have not involved putting the organometallic compounds directly into the plasma, and have not reported observations any more basic than film quality, and for both reasons it is difficult to make direct connections between this work and ours at the present time. The microwave arsine generation system is closest to ours in principle, although differences in the nature of the wall coatings and the energies of electrons and ions in the two plasmas could make the results quite different.

Finally, there is the question of what connection, if any, can be made between observations in our plasma system and the processes occurring in thermal decomposition above a hot substrate. In particular, we wanted to switch back and forth between TMAs and TBA feed gases and observe a difference in the AsH concentration. It is already clear that the differences between the plasma and thermal decomposition systems are substantial. For one, we expect the major arsenic-containing thermal decomposition product of TBA to be the dihydride, with little or no initial AsH. For another, we do observe substantial AsH formation in pure argon plasmas, presumably from arsenic deposited on the walls of the reactor, and from hydrogen either incorporated in this film or from water adsorbed on all reactor surfaces. That the hydrogen, whatever its source, is the limiting factor is seen in the observation that only a few minutes of running of a pure argon plasma reduces the AsH absorption by a large fraction, but addition of hydrogen or a hydrocarbon to the gas flow brings the AsH level back up.

There is indeed one additional factor which complicates the interpretation of observations of plasma decomposition of organoarsine compounds. These compounds form very stable negative ions, and the high degree of electron attachment results in a plasma with very low electron energies. We had not known this when we originally planned our experiments,

but were warned of the possibility a few months before we began work with arsenic compounds by Vince Donnelly of AT&T Bell Laboratories, who had worked with phosphorous analogs and expected the same effects with arsenic compounds. His remarks saved us from repeating what he described as a day of panic when he began his experiments, since the result of adding these compounds to a brightly glowing argon or hydrogen discharge is that the glow almost completely disappears (since almost all electrons capable of exciting visibly emitting states have been attached), a condition usually associated with an arc in a feedthrough or other invisible region of the apparatus. Indeed, we observe that adding even small amounts of organoarsine compound to the discharge reduces light emission to a faint purple glow only visible with all the room lights off.

The result of this is that the concentration of decomposition products has a maximum as a function of organoarsine compound concentration in the feed gas. At low concentrations (on the order of 10 per cent in argon, with a total pressure in the 0.2 to 0.3 Torr range), we seem to observe a slight increase in AsH concentration over that seen in discharges containing only argon and hydrogen. At only somewhat higher concentrations, however, the AsH concentration is lower,as is the glow intensity. From our observations to date, it is difficult to tell what fraction of the AsH at any organoarsine concentration comes from gas phase decomposition and what from the walls. However, as we have discussed in the fluorocarbon and methane systems, it is very possible that AsH is a large fraction of the total flux of arsenic compounds from the wall but a small fraction of the arsenic compounds generated by gas phase decomposition. This could mean that the AsH concentrations observed with organoarsine feeding are very close to what they would be if there were no wall source, even though they are only 10 to 50 per cent higher than AsH concentrations using an argon/hydrogen discharge. The other limit is that only the difference between organoarsine and no organoarsine flows is the AsH due to gas phase decomposition. The lowering of electron energy with added organoarsine compound will result in lower AsH production whether the source is the gas phase or the wall.

With all of these caveats in mind, we can now turn to Figures 20 and 21 which give examples of our observations of plasmas containing TMAs and TBA, respectively. The strong, broad absorption lines in the center of each scan are from an external cell of NO, used in case the RF affected the diode scan. In addition to the two AsH lines indicated, there are several lines from an unidentified radical species, probably originating from the fluorocarbon liner (since their intensities are larger in a pure argon discharge). The TBA spectrum differs from the TMAs spectrum chiefly in that the AsH intensities are larger, though only on the order of 40 per cent larger. We repeatedly switched back and forth between the two source gases and found this difference to be reproducible.

In discharge spectra using larger feed gas concentrations, we had observed a second difference, that TBA decomposition also gives rise to several stable hydrocarbon products with absorption lines in this region, while no such lines are observed in TMAs decomposition. A few lines match with ethylene, but most are unidentified. Although there seems to be an overlap between the left hand AsH line and one of the smaller of these hydrocarbon lines, the right hand AsH line seems to be free from interference (except for a small fluorocarbon radical line). In feed gas mixtures containing 50 percent TBA, the fractional absorption of these hydrocarbon lines (whose positions are indicated by the upper set of arrows) had been 10 percent and more. Therefore, it is surprising to see how much weaker they are in Figures 20 and 21, and even more surprising to find they now appear with both TBA and TMAs. It is possible to put forward various explanations, including additional chemistry (gas phase or surface) which consumes small concentrations of the hydrocarbon products during the tube residence time, and either the presence of these hydrocarbons in the film deposited on the reactor wall or possibility that the organoarsine feed lines were never adequately purged of one compound before observations on the other began. However, we are not now in a position to prove or disprove any of these hypotheses.

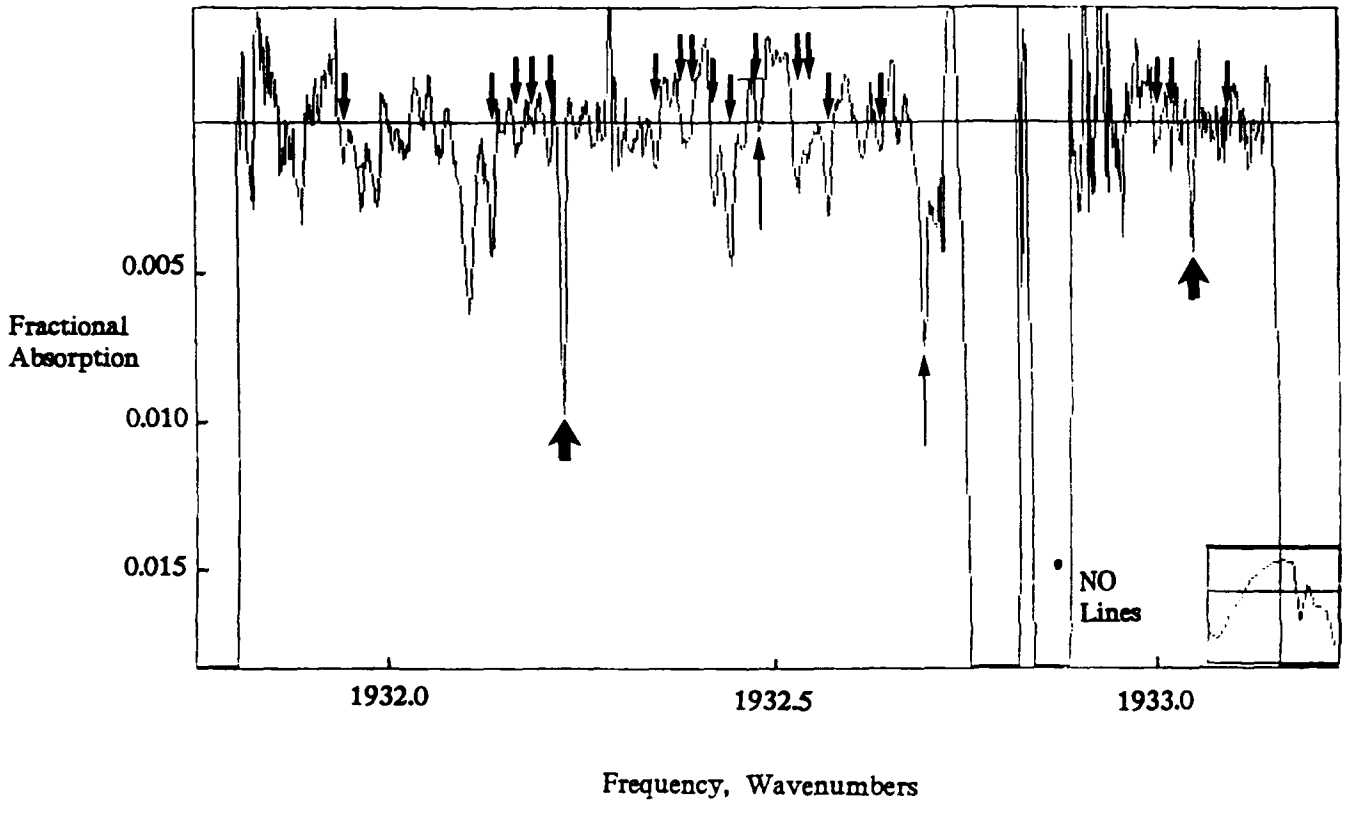

Figure 20. Infrared Absorption Spectrum of AsH Line Region for 500 W Discharge of Approximately 20 Percent Mixture of TMAs in Argon. The Upper Set of Arrows Denote Hydrocarbon Decomposition Product Line Positions Derived from Spectra of High Concentrations of TBA. Large Lower Arrows Indicate AsH Line Positions, while Light Arrows Denote Lines which Increase in Intensity in Pure Argon Discharges, and are Presumed to be a Fluorocarbon Radical Species.

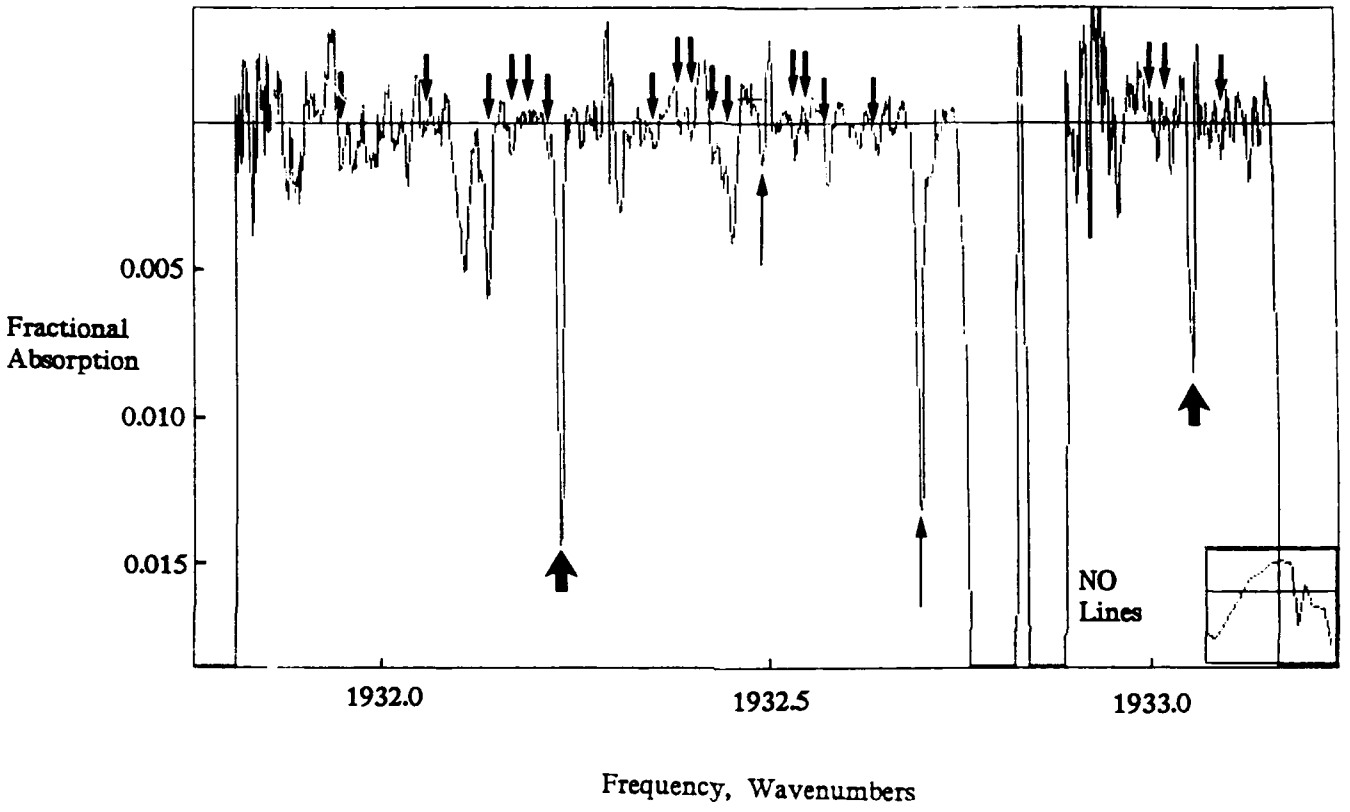

Figure 21. Infrared Absorption Spectrum of AsH Line Region for 500 W Discharge of Approximately 10 Percent Mixture of TBA in Argon. The Upper Set of Arrows Denote Hydrocarbon Decomposition Product Line Positions Derived from Spectra of Higher Concentrations of TBA. Large Lower Arrows Indicate AsH Line Positions, while Light Arrows Denote Lines which Increase in Intensity in Pure Argon Discharges, and are Presumed to be a Fluorocarbon Radical Species.

The observation of even somewhat more AsH from TBA than from TMAs is suggestive of the role of arsenic hydride species in thermal decomposition, and is not all that surprising if the major source of AsH is gas phase decomposition of the feed gases. However, we must emphasize again that we cannot assume this and that this system has enough complications that easy interpretation is not possible at this time. For one, although the absolute concentrations of TMAs and TBA in the feed gas have considerable uncertainties, the vapor pressure expressions we have indicate a factor of two higher concentration for TMAs for a 273 K bubbler temperature (our present estimates of feed gas concentrations for TMAs and TBA are 20 and 15 per cent of the total flow, repectively). We also observe that the AsH concentration goes down when we double the TBA concentration in the feed gas. Therefore, we cannot be sure whether the differences in AsH concentration seen in comparing Figures 20 and 21 are really connected to differences in gas phase decomposition processes, or are in fact only related to a difference in the peak concentration for each compound resulting from the competition between increasing arsenic concentration and decreasing electron energy. The only thing we can be sure of is that additional measurements of AsH concentrations as well as hydrocarbon decomposition species concentrations as a function of parameters such as total and partial pressures could shed additional light on the mechanisms involved in a very complex chemical system.

2.8 Conclusions

Infrared tunable diode laser absorption spectroscopy is a very useful diagnostic of RF plasmas, capable of detection of a wide variety of the radicals and stable molecules found in the CF_4, CH_4, and organoarsine systems. Although our long path system resulted in strong absorption levels, allowing us to use simple direct detection using a slow laser scan rate and a simple detection system, standard techniques for high sensitivity detection would allow measurements of all the species measured to be made over the 10 cm paths typical of plasma processing equipment. A high degree of feed gas

dissociation was observed, with only a small fraction going into the steady-state concentration of the reactive radicals such as CF_2, CH_3 and AsH. While C_2H_4 and C_2H_2 are clearly major decomposition products in hydrocarbon systems, there may well be other important species as well. We have no doubt that with its ability to make quantitative, sensitive measurements of both stable and transient species, tunable diode laser absorption will be applied to not only the systems and molecules studied in this report, but many others as well, and contribute substantial understanding of the complex chemical mechanisms involved in semiconductor processing systems.

2.9 References

1. J. Wormhoudt and K.E. McCurdy, Chem. Phys. Lett. 156, 47 (1989).

2. J. Wormhoudt, K.E. McCurdy, and J.B. Burkholder, Chem. Phys. Lett. 158, 480 (1989).

3. J. Wormhoudt, J. Vac. Sci. Technol. A8, 1722 (1990).

4. J. Wormhoudt, to appear in Proc. SPIE 1185, (1990).

5. J. Wormhoudt, to appear in Materials Research Society Symposium Proceedings Vol. 165, Characterization of Plasma-Enhanced CVD Processes, ed. D.E. Ibbotson, G. Lucovsky and D.W. Hess, (1990).

6. J. Wormhoudt, to appear in Proceeding of the Symposium on Plasma Processing, 177th Meeting of the Electrochemical Society, ed. G.S. Mathad and D.W. Hess, (1990).

7. J. Wormhoudt, in Materials Research Society Symposium Proceedings Vol. 117, Process Diagnostics: Materials, Combustion, Fusion, ed. A.K. Hays, A.C. Eckbreth, and G.A. Campbell, (1988), p. 73.

8. C. Yamada and E. Hirota, J. Chem. Phys. 78, 669 (1983).

9. J.C. Wormhoudt, "Development of Laser Spectroscopic Diagnostics to Support Advanced Compound Semiconductor Deposition Techniques," First Annual Report for AFOSR Contract No. F49620-87-C-0052, ARI-TR-661, June 1988.

10. S. Sharpe, B. Hartnett, H.S. Sethi, and D.S. Sethi, J. Photochem. 38, 1 (1987).

11. J.J. Orlando, J. Reid, and D.R. Smith, Chem. Phys. Lett. 141, 423 (1987).

12. J.J. Orlando, J. Reid, and D.R. Smith, Chem. Phys. Lett. 147, 300 (1988).

13. J.H. Newton and W.B. Person, J. Chem. Phys. 68, 2799 (1978).

14. Y. Yamaguchi, M.J. Frisch, T.J. Lee, H.F. Schaefer III, and J.S. Binkley, Theoret. Chim. Acta 69, 337 (1986).

15. P. Botschwina, private communication, July 1989.

16. K. Peterson and R.C. Woods, private communication, August 1989.

17. O. Suto and J.I. Steinfeld, Chem. Phys. Lett. 168, 181 (1990).

18. J.C. Wormhoudt, "Development of Laser Spectroscopic Diagnostics to Support Advanced Compound Semiconductor Deposition Techniques," Second Annual Report for AFOSR Contract No. F49620-87-C-0052, ARI-TR-715, June 1989.

19. J. Wormhoudt, A.C. Stanton, A.D. Richards, and H.H. Sawin, J. Appl. Phys. 61, 142 (1987).

20. A.D. Richards and H.H. Sawin, J. Appl. Phys. 62, 799 (1987).

21. K.R. Ryan and I.C. Plumb, Plasma Chem. Plasma Process. 6, 231 (1986).

22. I.C. Plumb, private communication, August 1989.

23. G. Smolinsky and D.L. Flamm, J. Appl. Phys. 50, 4982 (1979).

24. C.J. Mogab, A.C. Adams and D.L. Flamm, J. Appl. Phys. 49, 3796 (1978).

25. K.R. Ryan and I.C. Plumb, Plasma Chem. Plasma Process. 4, 271 (1984).

26. I.C. Plumb and K.R. Ryan, Plasma Chem. Plasma Process. 6 205 (1986).

27. R. d'Agostino, F. Cramarossa, S. DeBenedictis, and G. Ferraro, J. Appl. Phys. 52, 1259 (1981).

28. J.B. Burkholder, C.J. Howard and P.A. Hamilton, J. Mol. Spectry. 127, 362 (1988).

29. S. Carter and L.O. Halonen, Program ASYMVIB, Spectrochim. Acta 41A (9) (1985), software survey section.

30. J.P. Booth, G. Hancock, and N.D. Perry, Appl. Phys. Lett. 50, 318 (1987).

31. M. Kitamura, H. Akiya, and T. Urisu, J. Vac. Sci. Technol. B7, 14 (1989)

32. T.F. Kuech, G.J. Scilla and F. Cardone, J. Crystal Growth 93, 550 (1988).

33. R.M. Lum, J.K. Lingert, D.W. Kisker, S.M. Abys, and F.A. Stevie, J Crystal Growth 93, 120 (1988).

34. C.A. Larsen, N.I. Buchan, S.H. Li, and G.B. Stringfellow, J. Crystal Growth 93, 15 (1988).

35. D.M. Speckman and J.P. Wendt, J. Crystal Growth 93, 29 (1988).

36. T.F. Kuech, M.A. Tischler, P.J. Wang, G. Scilla, R. Potemski, and F. Cardone, Appl. Phys. Lett. 53, 1317 (1988).

37. J.R. Anacona, P.B. Davies and S.A. Johnson, Mol. Phys. 56, 989 (1985).

38. T. Sheng, B. Pihlstrom, Z. Yu and G.J. Collins, Appl. Phys. Lett. 55, 2411 (1989).

39. B. Pihlstrom, T. Sheng, Z. Yu and G.J. Collins, to appear in Materials Research Society Symposium Proceedings Vol. 165, Characterization of Plasma-Enhanced CVD Processes, ed. D.E. Ibbotson, G. Lucovsky and D.W. Hess.

40. T.R. Omstead, D.G. Coronell and K.F. Jensen, abstracts of Fourth Biennial Workshop on Organometallic Vapor Phase Epitaxy, Monterey, CA, October 8-11, 1989, The Minerals, Metals and Materials Society, Warrendale, PA.

41. K. Tachibana, M. Nishida, H. Harima, and Y. Urano, J. Phys. D: Appl. Phys. 17, 1727 (1984).

3.0 PUBLICATIONS

J. Wormhoudt, in Materials Research Society Sumposium Proceedings, Vol. 117, Process Diagnostics: Materials, Combustion, Fusion, ed. A.K. Hays, A.C. Eckbreth, and G.A. Campbell (1988) p. 73.

J. Wormhoudt and K.E. McCurdy, Chem. Phys. Lett., 156 47 (1989).

J. Wormhoudt, K.E. McCurdy, and J.B. Burkholder, Chem. Phys. Lett. 158, 480 (1989).

J. Wormhoudt, J. Vac. Sci. Technol. A8, 1722 (1990).

J. Wormhoudt, to appear in Proc. SPIE 1185 (1990).

J. Wormhoudt, to appear in Materials Research Society Symposium Proceedings Vol. 165, Characterization of Plasma-Enhanced CVD Processes, ed. D.E. Ibbotson, G. Lucovsky and D.W. Hess.

J. Wormhoudt, to appear in Proceeding of the Symposium on Plasma Processing, 177th Meeting of the Electrochemical Society, ed. G.S. Mathad and D.W. Hess (1990).

4.0 PERSONNEL

Dr. Joda Wormhoudt, the Principal Investigator, designed the plasma apparatus and analyzed the band strength measurements. Mr. Warren Goodwin constructed, maintained, and operated the plasma reactor and Mr. Keith McCurdy carried out the band strength experiments. Drs. Doug Worsnop and Andrew Freedman made valuable contributions in computer data acquisition and apparatus operation, respectively. Dr. Steven Coy of Harvard and MIT consulted at several points on questions of spectroscopy.

5.0 INTERACTIONS

Presentations were made at the following meetings:

40th Annual Gaseous Electronics Conference, Atlanta GA, October 13-16, 1987.

Materials Research Society Spring Meeting, Symposium on Process Diagnostics, Reno NV, April 5-9, 1988.

Symposium on Molecular Spectroscopy, Columbus OH, June 13-17, 1988.

Gordon Research Conference on Plasma Chemistry, Tilton, NH, August 15-19, 1988.

41st Annual Gaseous Electronics Conference, Minneapolis, MN, October 18-21, 1988.

16th IEEE International Conference on Plasma Science, Buffalo, NY, May 24, 1989.

ARO Workshop on Hydrocarbon Plasma Discharge Diagnostics, Madison, WI, June 7-8, 1989.

SPIE Symposium on Microelectronic Integrated Processing, Technical Conference on Dry Processing for Submicrometer Lithography, Santa Clara, CA, October 12-13, 1989.

42nd Annual Gaseous Electronics Conference, Palo Alto, CA, October 17-20, 1989.

Optical Society of America, Annual Meeting, Orlando, FL, October 15-20, 1989.

American Vacuum Society, Annual Meeting, Boston, MA, October 23-27, 1989.

Materials Research Society Fall Meeting, Boston, MA, November 27-December 2, 1989.

Electrochemical Society, Spring Meeting, Montreal, Canada, May 6-11, 1990.

APPENDIX A

A MEASUREMENT OF THE STRENGTH OF THE ν_2 BAND OF CH_3

J. WORMHOUDT and K.E. McCURDY [1]

Center for Chemical and Environmental Physics, Aerodyne Research Inc., 45 Manning Road, Billerica, MA 01821, USA

Received 14 November 1988

The infrared band strength of the ν_2 band of the methyl radical has been measured using tunable diode laser absorption by the $Q_8(8)$ line at 608.3 cm^{-1}. Experiments were performed in a discharge-flow apparatus, using the homogeneous recombination decay to quantify CH_3 concentrations. The measured line strength at 300 K is $(3.2 \pm 1.0) \times 10^{-19}$ cm^{-1} (molecule/cm^2)$^{-1}$, resulting in a band strength of $(2.5 \pm 0.8) \times 10^{-17}$ cm^{-1} (molecule/cm^2)$^{-1}$. This agrees with an earlier value to within the combined error limits.

1. Introduction

The methyl radical is an important intermediate in a number of reactive systems. Measurements of its concentration would contribute greatly to the understanding of chemical vapor deposition or combustion systems, to name two examples. Quantitative infrared absorption measurements have been performed in MOCVD and diamond deposition systems [1,2] using a tunable diode laser. These measurements of absolute concentration depend on a knowledge of the strength of the absorption line used. One measurement of this quantity has been reported [3], but its interpretation required assumptions with considerable uncertainties. A measurement under somewhat different conditions was therefore undertaken, and is reported here.

2. Experimental

Methyl radicals are produced in the discharge-flow apparatus shown schematically in fig. 1, using the reaction of fluorine atoms with a large excess of methane. Fluorine atoms are produced in a microwave discharge of a 10% F_2 in He mixture. The discharge tube is alumina with a 1 cm inner diameter. F_2 mixture flows were varied in the range 0.25–2.15 STP cm^3 s^{-1}, while a diluting flow of He through the discharge of 12 STP cm^3 s^{-1} served to minimize F atom losses on the wall of the discharge tube.

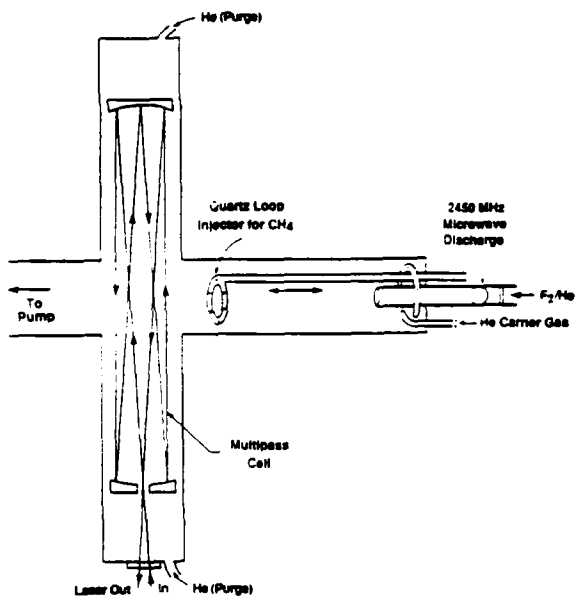

Fig. 1. Discharge-flow apparatus with multiple-pass absorption cell.

The flow tube is a 6 cm inner diameter stainless steel tube coated with halocarbon wax. Helium carrier gas is added through a loop injector at the back of the flow tube. The carrier gas flow used in the set

[1] Present address: Questek, Inc., 44 Manning Road, Billerica, MA 01821, USA.

0 009-2614/89/$ 03.50

of measurements reported here was about 27 STP $cm^3 s^{-1}$. Total flow rates into the flow tube resulted in an average gas velocity of 1950 cm s^{-1}. The measurements reported here were performed at 0.57 Torr and 295 K.

Methane (1.6 STP $cm^3 s^{-1}$) is added to the flow through a movable injector downstream of the F atom injection point. In the present experiments, the discharge tube is fixed just downstream of the carrier gas injection loop. Helium purge gas flows are added through the transverse tubes of the observation region which contain the mirrors for the multipass absorption cell. The flow tube pressure is measured with a capacitance manometer (MKS) and the flow rates are measured with thermal conductivity-type flowmeters (Tylan), calibrated by measuring the change of pressure with time in a known volume.

The beam of a tunable diode laser was collected using an off-axis paraboloidal mirror and passed through a 0.25 m monochromator for mode selection before being focused into the absorption cell. The absorption path is contained in an off-axis resonator cell [4] transverse to the flow. It is composed of a 5 cm diameter, 50 cm focal length back mirror and a 5 cm diameter plane front mirror with a central 0.5 cm diameter entrance/exit hole. The mirror spacing is about 30 cm, giving 32 passes of the laser beam through the flow before exiting to be focused onto a HgCdTe detector.

The absorption path length is determined by introducing a measured flow of N_2O through the injector used for CH_4 (keeping the helium flows constant) and recording the absorption of a line whose strength is known [5]. The flow tube N_2O concentrations are calculated from the relative flow rates and the flow tube pressure. The total effective path length for the conditions of the measurements reported here was determined to be 225 ± 20 cm. This corresponds to 7 cm per pass, which is reasonable for a flow exiting a 6 cm diameter tube and partially confined by purge flows. This effective path length was not sensitive to the N_2O injection point over the range of positions later used for CH_4 injection, indicating fast mixing within the flow tube.

Second derivative detection was used, in which a sawtooth modulation was imposed on the laser diode current, and a lock-in amplifier was used at twice the modulation frequency to detect changes in signal due to absorption lines. In addition, a variant of sweep integration was used, in which a computerized data acquisition system accumulated sequential second derivative scans. The diode laser current scan was swept across the absorption line at 2.9 Hz while the output of the lock-in amplifier was sampled by an analog to digital converter. The time constant of the lock-in amplifier was 4 ms, and about 200 scans of the CH_3 line were averaged for each fluorine flow and injector position.

Background subtraction was performed using a discharge-off scan. Interference fringes from various pairs of surfaces in the optical train were present at levels of up to 20% of the smallest peak absorption signals. Calibration of both the second derivative detection efficiency and the computer data acquisition system was done by measuring a strong CH_3 line in direct absorption using a slow scan, and comparing the chart recorded traces with the computer-generated second derivative scans.

3. Results

The data set upon which we base the line strength determination is shown in fig. 2. The inverse of the CH_3 line peak optical depth has been plotted as a function of CH_4 injector position, where the zero point is closest to the absorption region (about 5 cm upstream of the center of the infrared beam pattern). Optical depth is defined as $\alpha = \ln(I_0/I)$, where I and I_0 are laser intensities with and without absorption.

Since the CH_3 formation reaction between F atoms and CH_4 is rapid, changing the distance between the injection and the observation region changes the time during which the CH_3 concentration decays before being observed. If homogeneous recombination were the only process affecting CH_3, a plot of inverse optical depth with reaction distance would show a linear dependence, since the CH_3 concentration follows the expression

$$\frac{1}{[CH_3]} = \frac{1}{[CH_3]_0} + 2k\Delta t\,. \qquad (1)$$

where k is the (two-body) recombination rate coefficient. This can be rearranged to give

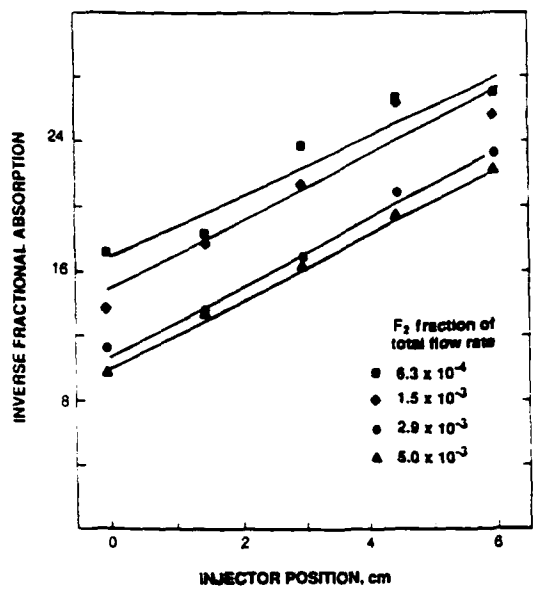

Fig. 2. Second-order plot of inverse CH_3 line peak optical depth with injector position. The average flow velocity is 1950 cm/s, the temperature and pressure are 295 K and 0.57 Torr, and the path length is 225 cm.

$$[CH_3]_0 = \frac{1}{2k\Delta t}\left(\frac{[CH_3]_0}{[CH_3]} - 1\right) \qquad (2)$$

so that the ratio of two concentrations separated by a time Δt can be replaced by the ratio of observed optical depths at two injector points.

Therefore, we first obtain $[CH_3]_0$ at the zero (furthest downstream) injector position from the slopes of the lines in fig. 2. Then, eq. (1) can be used to extrapolate to obtain the CH_3 concentration in the center of the observation region. The extrapolation distance is obtained by using fig. 2 to find the distance to the point where the observed CH_3 optical depths are in the same ratio as the measured F_2 flow rates [6]. The best value for this distance is 4.5 cm downstream from the injector "zero" point.

Losses of CH_3 to the walls of the flow tube could also contribute to the observed change in CH_3 optical depth. Wall losses of CH_3 were not measured directly, although wall losses of F atoms were measured and found to be negligible. However, the linearity of the second-order plots in fig. 2 indicates that first-order losses are negligible compared to the second-order recombination.

With homogeneous recombination established as the dominant loss mechanism, eq. (1) can be used to convert least-squares fits of the data in fig. 2 into CH_3 concentrations, if the recombination rate constant k is known. Methyl radical recombination kinetics have been extensively studied. From a review of the literature [7–11], we chose a value of 3.85×10^{-11} cm^3 molecule^{-1} s^{-1} for our carrier gas, temperature and pressure.

An independent value of k can be obtained from the data in fig. 2, if the CH_3 concentrations can be obtained from the measured F_2 flow rates. Assuming a 1.32 to 1 conversion of F_2 to CH_3 [6], the slopes of the lines in fig. 2 may be converted to recombination coefficients. The precision of the data is not adequate to produce an estimate of the rate constant of greater accuracy than can be obtained from the literature – a least-squares analysis yields about $(2\pm1.5)\times10^{-11}$ cm^3 molecule^{-1} s^{-1}, which is in fair agreement with the value quoted above.

Having obtained a CH_3 concentration, the line strength can be obtained from

$$S = 2.13\Delta\nu\,\alpha_0/l[CH_3]\,. \qquad (3)$$

In this equation, α_0 is the line peak optical depth, l is the absorption path length, $\Delta\nu$ is the linewidth (half width at half maximum), and the factor $2.13 = (\ln 2/\pi)^{-1/2}$ is only appropriate if the lineshape is Gaussian. For many lasers, frequency jitter adds a substantial component to the linewidth, so that the lineshape is no longer Gaussian and the product of $2.13\Delta\nu$ and α_0 should be replaced by the integral over the lineshape. However, in this case the analysis of the N_2O lines used in determining the path length showed the instrumental broadening to be very small, so that use of the product of height and width involves no loss of accuracy.

The values obtained from fig. 2 for the line strength of the $Q_8(8)$ line of the ν_2 band are 3.03×10^{-19}, 2.93×10^{-19}, 3.40×10^{-19}, and 3.42×10^{-19} cm^{-1} (molecule/cm^2)$^{-1}$ in order of increasing initial CH_3 concentration. We weight the smallest CH_3 value less heavily than the others (due to its smaller signal to noise ratio), and report a line strength of $(3.2\pm1.0)\times10^{-19}$ cm^{-1} (molecule/cm^2)$^{-1}$. The error estimate takes into account 20% limits on systematic and random errors in the slopes of lines in fig. 2, 20% in the recombination rate coefficient, and

10% errors in both the contact time and absorption path length.

4. Discussion

Yamada and Hirota [3] have used a flash photolysis–diode laser absorption technique to obtain a band strength for the ν_2 band based on absorption measurements using the $Q_4(4)$ line at 600 K. To compare their value with ours, we convert our line strength to a band strength by dividing by the fraction of the intensity in a single line.

$$A_{NK} g_I g_N \exp[-E(N, K)/kT]/Q_{NS} Q_R Q_v . \quad (4)$$

In this expression, $A_{NK}=K^2/N(N+1)$ is the Hönl–London factor [12], g_I is the nuclear spin weight (4 for $K=3$, 6, 9, and so on, and 2 for all other lower levels including those for both lines considered here), $g_N=2N+1$ is the rotational degeneracy, $E(N, K)$ is the rotational energy (computed using constants from ref. [13]), Q_{NS} is the nuclear spin partition function (8 for CH_3), Q_R is the rotational partition function divided by the symmetry number (6 for CH_3), and Q_v is the vibration partition function. Applying this conversion factor, our value for the strength of the ν_2 band of CH_3 is $(2.5\pm0.8)\times10^{-17}$ cm^{-1} (molecule/cm^3)$^{-1}$. This is somewhat larger than the value obtained from ref. [3] of $(1.9\pm0.6)\times10^{-17}$, although the two values agree within the combined error limits.

The two measurements may disagree more than it might first appear. Eqs. (1) and (2) show that the line strength determination in both studies is directly proportional to the choice of recombination rate coefficient. A review of the pertinent CH_3 recombination literature [7–11], much of it published after ref. [3] appeared, suggests that the analysis of the Yamada and Hirota data should have used a substantially smaller value of the recombination rate coefficient. They used a value of 4.7×10^{-11} cm^3 molecule^{-1} s^{-1} from Laguna and Baughcum [7], who measured it at 300 K in 2–20 Torr of Ar and He and found no measurable pressure or third-body dependence. Under the conditions of the Yamada and Hirota study, which used di-tert-butyl peroxide (DTBP) as a third body and was done at a temperature of 600 K, the appropriate recombination rate coefficient could be smaller by as much as a factor of two [9,10].

A smaller value for the rate coefficient results in a smaller value for the line strength. The actual value for rate constant applicable to the Yamada and Hirota study is difficult to determine since there are no measurements of the third-body collision efficiency in DTBP. The advantage of the discharge-flow technique used in this study is that the temperature is well defined and third-body efficiency in argon has been well characterized.

Acknowledgement

Helpful discussions with S. Anderson, M. Zahniser, D. Worsnop, and S. Coy are gratefully acknowledged. Research sponsored by the Air Force Office of Scientific Research (AFSC), under Contract F49620-87-C-0052.

References

[1] J.E. Butler, N. Bottka, R.S. Sillmon and D.K. Gaskill, J. Cryst. Growth 77 (1986) 163.
[2] F.G. Celii, P.E. Pehrsson, H.-T. Wang and J.E. Butler, Appl. Phys. Letters 52 (1988) 2043.
[3] C. Yamada and E. Hirota, J. Chem. Phys. 78 (1983) 669.
[4] D.R. Herriot, H. Kogelnik and R. Kompfner, Appl. Opt. 3 (1964) 523.
[5] L.S. Rothman, R.R. Gamache, A. Goldman, L.R. Brown, R.A. Toth, H.M. Pickett, R.L. Poynter, J.-M. Flaud, C. Camy-Peyret, A. Barbe, N. Husson, C.P. Rinsland and M.A.H. Smith, Appl. Opt. 26 (1987) 4058.
[6] M.S. Zahniser and A.C. Stanton, J. Chem. Phys. 80 (1984) 4951.
[7] G.A. Laguna and S.L. Baughcum, Chem. Phys. Letters 88 (1982) 568.
[8] M.L. [illegible]en, L. Leinonen, H. Lemmetyinen and J. Koskikallio, Finn. Chem. Letters (1974) 207.
[9] M.T. MacPherson, M.J. Pilling and M.J.C. Smith, Chem. Phys. Letters 94 (1983) 430.
[10] W. Tsang and R.F. Hampson, J. Phys. Chem. Ref. Data 15 (1986) 1087.
[11] I.R. Slagle, D. Gutman, J.W. Davies and M.J. Pilling, J. Phys. Chem. 92 (1988) 2455.
[12] H. Herzberg, Molecular spectra and molecular structure, Vol. 2, Infrared and Raman spectra of polyatomic molecules (Van Nostrand, Princeton, 1945).
[13] C. Yamada, E. Hirota and K. Kawaguchi, J. Chem. Phys. 75 (1981) 5256.

APPENDIX B

MEASUREMENTS OF THE STRENGTHS OF INFRARED BANDS OF CF_2

J. WORMHOUDT, K.E. McCURDY [1]
Center for Chemical and Environmental Physics, Aerodyne Research Inc., 45 Manning Road, Billerica, MA 01821, USA

and

J.B. BURKHOLDER
NOAA Aeronomy Laboratory, R/E/AL2, 325 Broadway, Boulder, CO 80303, USA
and CIRES, University of Colorado, Boulder, CO 80309, USA

Received 21 February 1989; in final form 17 May 1989

The ν_1 infrared band strength of the CF_2 radical has been measured using tunable diode laser absorption by the $^PR_1(20)$ line at 1240.50 cm^{-1}. Experiments were performed in a flow apparatus in which CF_2 was generated by thermal dissociation of CF_2HCl. Simultaneous single pass absorption of UV light from a KrF excimer laser was used with a literature value of the UV absorption cross section to quantify CF_2 concentrations. The measured line strength at 360 K is $(1.4 \pm 0.4) \times 10^{20}$ cm^{-1} (molecule/cm^2)$^{-1}$. This results in a band strength of $(1.1 \pm 0.4) \times 10^{-17}$ cm^{-1} (molecule/cm^2)$^{-1}$, in good agreement with a measurement using a different technique. Analysis of FTIR spectra of the ν_1 and ν_3 bands indicates that the ν_3 band strength is larger by a factor of 2.4.

1. Introduction

The CF_2 radical is an important molecular species in such semiconductor processing systems as etching plasmas. As such, a number of investigations have used it as a basis for spectroscopic diagnostics, including laser-induced fluorescence [1–7] and electronic emission [8,9]. Chemical kinetics modeling studies for CF_4 plasma [10] predict CF_2 to be a major species, with concentrations approaching that of the fluorine atoms which are the primary etchant species. Measurements of absolute CF_2 concentrations in etching plasmas are important in evaluating the chemical kinetic and electron collision mechanisms involved in these predictions. Such a measurement is possible if the strength of the absorption line used is known. We therefore undertook a measurement of the ν_1 band strength, using a flow system and a tunable diode laser.

[1] Present address: Questek, Inc., 44 Manning Road, Billerica, MA 01821, USA.

2. Experimental

CF_2 radicals are produced in the flow apparatus shown schematically in fig. 1 by thermal decomposition of CF_2HCl in a tube oven inserted into the back of the flow tube. The flow tube is a 6 cm inner diameter stainless steel tube with an observation region formed from a six-armed cross. Two arms of the cross carry the gas flow, and two arms contain a multipass absorption cell for the infrared laser beam. The other two perpendicular arms (not shown) are not used in this experiment, but two smaller diameter (2.2 cm) arms at a 45° angle to the flow and multipass arms are used for a single pass UV absorption measurement using a KrF excimer laser.

The entire flow of CF_2HCl and argon carrier gas passing down the flow tube was injected through the oven. The oven is constructed of stainless steel, with a 0.4 cm inner diameter pipe surrounded by a 30 cm long wrapped resistance heater and an outer water jacket to prevent heating of the flow tube. Total flow into the oven was 12 STP cm^3 s^{-1}, with a CF_2HCl flow of about 1 STP cm^3 s^{-1}. The oven was operated

0 009-2614/89/$ 03.50

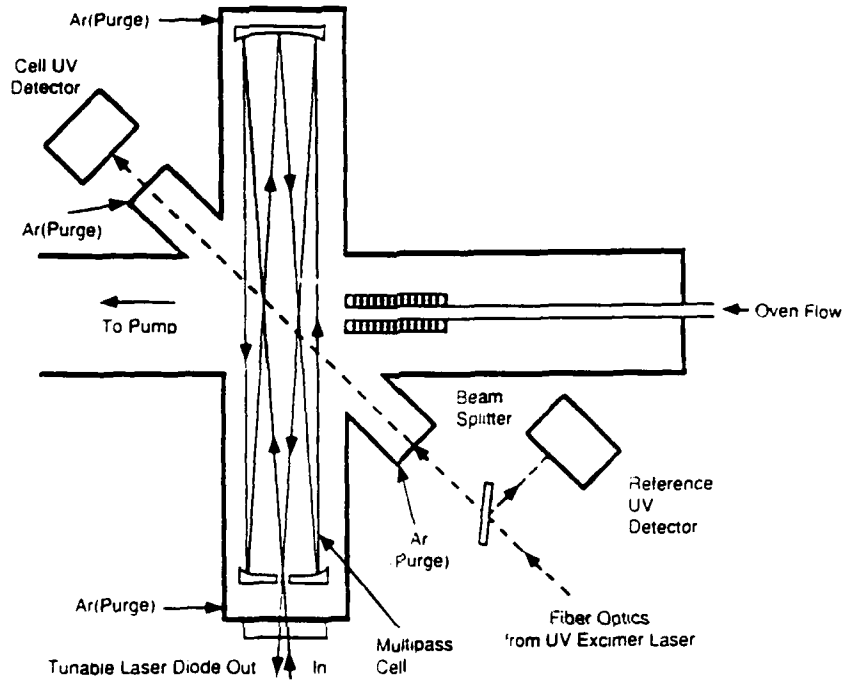

Fig. 1. Flow apparatus for CF_2 band strength measurement, including oven for CF_2HCl thermal dissociation, infrared multipass cell, and double beam ultraviolet excimer laser absorption setup.

at a temperature of 1100 K, measured by a thermocouple welded to the inner pipe. The flow tube pressure was about 0.7 Torr, so that the flow velocity in the flow tube was 550 cm s^{-1}.

Argon purge gas was added to the four transverse 6 cm diameter arms at flow rates which roughly matched the flow into the flow tube. Smaller purge flows were also added to the two UV absorption arms. These flow rates were set by reducing them until they no longer affected the observed CF_2 absorption line intensities. The gas flow rates were measured with thermal conductivity-type flowmeters (Tylan), and the flow tube pressure was measured with a capacitance manometer (MKS).

The infrared absorption path is contained in an off-axis resonator cell [11] composed of two 5 cm diameter mirrors. The plane front mirror has a central 0.5 cm diameter entrance/exit hole, while the back mirror is curved, with a 50 cm focal length. The mirror spacing of about 30 cm gives 32 passes of the laser beam through the flow. Tunable diode laser radiation is collected using an off-axis paraboloidal mirror and passed through a mode-selecting 0.25 m monochromator before being focused into the multipass cell. After exiting the cell, the laser beam is focused onto a HgCdTe detector. Second derivative detection of the absorption signal is used, by sawtooth modulation of the diode frequency (through its injection current) and lock-in detection at twice the modulation frequency. The second derivative signal is calibrated by observing reference gas lines in both second derivative and direct absorption modes. The frequency scale is calibrated using well known [12] N_2O lines as a reference.

The KrF laser beam is brought to the experiment through an ultraviolet transmitting fiber cable (NRC). The beam from the fiber is then collimated and split into flow tube and reference beams. Each beam is detected by focusing it onto a white card placed in front of a silicon photodiode. Direct detection of the ultraviolet is also possible, but the signal from the visible fluorescence from the card is less affected by laser beam wander. The linearity of the white card fluorescence is assured by two observations: the absolute intensities of the beams falling on the two detectors differ by about an order of mag-

nitude, and the ratio of intensities remains constant over an order of magnitude variation in laser power.

The laser pulses are amplified and broadened using an operational amplifier with a 20 ms RC decay time constant. The two output signals are then sampled by a personal computer interfaced through an A/D converter. The computer averages a specified number of laser pulses, then reports a sample-to-reference beam intensity ratio. Averaging over 200 laser pulses produced standard deviations in these ratios which were typically 0.05% or less.

3. Results

Examples of the infrared and ultraviolet data are shown in fig. 2. The bottom trace shows an N_2O reference gas spectrum taken in direct intensity mode which sets the frequency scale. Direct intensity traces were also taken periodically through the experiment to monitor the diode laser absolute intensity, which is required to convert second derivative signal sizes to absolute absorptions. In the second panel of fig. 2 are two second derivative traces of the CF_2 $^PR_1(20)$ line used in this study, corresponding to fractional absorptions of about 0.04. The first is at the correct position in relation to the N_2O reference lines (1240.50 cm^{-1}), while the second (displaced) trace is taken a few minutes later. As shown, the peak-to-valley distances are measured, then converted to absolute absorptions using the second derivative calibration factor and the measured direct intensity. At the top of the figure, on a time axis which includes the two observations of the infrared line, is a record

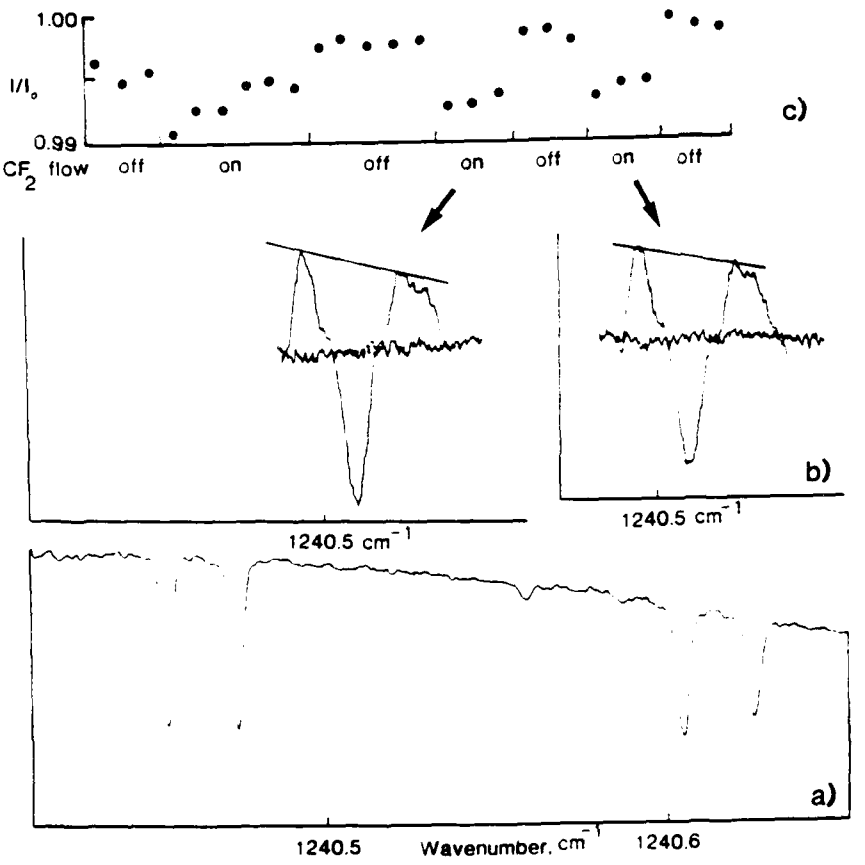

Fig. 2. Example absorption data. (a) N_2O reference gas trace, in direct infrared absorption. (b) CF_2 infrared absorption traces, using second derivative detection. (c) CF_2 ultraviolet absorption. Points indicate values of ratios of flow tube and reference beam intensities averaged over 200 laser pulses, while arrows indicate when infrared scans were made.

of ratios of ultraviolet intensity at flow tube and reference detectors, which can then be converted into absolute absorptions. Each point represents the average of 200 laser pulses.

From the ultraviolet absorption record and traces of the infrared absorption line we obtained values of the ratio of infrared absorption to ultraviolet absorption, α_{IR}/α_{UV}. The average of these values was 8.9, with a 10% standard deviation.

The UV absorption cross section was obtained from a study by Sharpe et al. [13] which used a deuterium lamp and a 0.5 m monochromator with a variety of slit widths (bandwidths from 0.040 to 0.200 nm) to record a CF_2 absorption spectrum which was reported in tabular form at 0.5 nm intervals. CF_2 was produced by the photolysis of C_2F_4 and C_3F_6, and quantified by assuming quantum yields of 2.0 and 1.0, respectively. The results for the two gases agreed within the error limits of 15%. We used a 1 m monochromator to check the characteristics of our excimer laser line, and found a center position of 248.44 nm and a full width at half maximum of 0.264 nm. We then used this profile and an interpolation on the points of ref. [13] to derive an effective absorption cross section of 1.0×10^{-17} cm^2. Since both the width and position of the laser line are close to the slit width and wavelength reported in ref. [13], the uncertainty in this cross section is unlikely to be significantly larger than that quoted above.

To compute the infrared line strength, the ratio of peak absorption to the product of concentration and path length (the column density, nl), is required. Since in the UV absorption we have the product of CF_2 concentration, cross section and path length, we need only measure the ratio of column densities through the CF_2 flow along the paths traversed by IR and UV laser beams. Ideally, this would be done by measuring CF_2 absorption along both paths using the same technique. However, it was not practical to introduce the UV beam into our multipass cell, and the CF_2 IR absorption was too weak for a single pass measurement. Instead, we measured the absorption by a methane infrared line using the tunable diode laser beam following both the IR and UV paths, while maintaining identical flow conditions except with CH_4 replacing CF_2HCl. The column density ratio obtained was 19 with a 15% error estimate. The difference between this and the geometric value of 22.6 expected from dividing 32 IR passes by $\sqrt{2}$ for the 45° UV path is presumed to be due to the changing concentration profile of the gas emerging from the oven and mixing with the purge flows. Additional differences in column density between CH_4 and CF_2 due to the reactivity of the latter are expected to be small.

The infrared line strength can then be obtained from

$$S = 2.13\,\Delta\nu_{IR}\sigma_{UV}\frac{\alpha_{IR}/\alpha_{UV}}{nl_{IR}/nl_{UV}}. \qquad (1)$$

In this equation, $\Delta\nu_{IR}$ is the observed half width at half maximum of the infrared line. At the low pressure used, it is composed of the Doppler width of the absorption line and a contribution from the jitter width of the diode laser line. If the latter is small, the lineshape remains Gaussian, the factor of 2.13 is correct, and the observed linewidth is corrected for a finite laser linewidth by $\Delta\nu_{IR} = (\Delta\nu_D^2 + \Delta\nu_L^2)^{1/2}$, where $\Delta\nu_D$ is the Doppler linewidth. Using N_2O lines, we determined the laser linewidth to be about $(8\pm3)\times10^{-4}$ cm^{-1} (substantial variation in this value was a characteristic of the particular laser diode used).

The precise value of the Doppler width depends on the temperature of the CF_2. Since it is formed in an oven source, it cannot be assumed to be at room temperature. The signal to noise ratio in the small CF_2 absorptions was insufficient for an accurate direct measurement of the Doppler width. Instead, we analyzed the relative intensities of several nearby lines, using the intensities and positions predicted by an asymmetric rotor computer program [14] with molecular constants based on earlier diode laser spectroscopy of CF_2 [15]. Temperatures obtained from selected pairs of lines varied by more than 50 K, but all pairs indicated a temperature close to room temperature. We chose a temperature of 360 K as being representative of the flow conditions used in the line strength measurements, resulting in a Doppler width of 1.2×10^{-3} cm^{-1}, and a value for $\Delta\nu_{IR}$ of $(1.4\pm0.2)\times10^{-3}$ cm^{-1}.

Substituting all the above values into eq. (1) results in a line strength of $(1.4\pm0.4)\times10^{-20}$ cm^{-1} (molecule/cm^{-2})$^{-1}$. The uncertainty estimate is for one standard deviation. It reflects the error limits

discussed above and an estimate of 15% for $\Delta\nu_{IR}$ based on errors in measuring both the laser linewidth and the CF_2 temperature.

4. Discussion

To convert to a band strength, we divide the measured line strength by the fraction of the intensity in a single line [14],

$$\frac{f_{JK} g_J g_I \, e^{-E(J,K)/kT}}{Q_{NS} Q_R} . \quad (2)$$

In this expression, f_{JK}, the fraction of intensity in the given line compared to all lines with the same lower state, is given by the asymmetric rotor program [14] to be 0.41185. The degeneracy g_J is $2J+1$, while the nuclear spin weight g_I can be either 3 for eo ↔ oe transitions or 1 for ee ↔ oo and is 3 for this $21_{0,21}$–$20_{1,20}$ line [16]. The rotational energy of the lower state $E(J, K)$ is 160.06 cm^{-1}, and a temperature of 360 K is again assumed. The nuclear spin partition function Q_{NS} is $(2I_1+1)(2I_2+1)$, or 4 for two spin-1/2 atoms. The rotational partition function Q_R is given by Q_r/σ, where the symmetry number σ is 2 and Q_r is expressed in terms of the three rotational constants [16],

$$Q_r = 1.02718(T^3/ABC)^{1/2} . \quad (3)$$

Substituting all the above factors into eq. (2) and dividing it into the measured line strength, we obtain a band strength of $(1.1\pm0.4)\times10^{-17}$ cm^{-1} (molecule/cm^{-2})$^{-1}$ for the ν_1 band.

Recently, a measurement of this band strength has been reported which used tunable diode laser detection of both CF_2 and HCl following infrared multiphoton dissociation of CF_2HCl [17,18]. Their final value [18] of $(1.5\pm0.4)\times10^{-17}$ cm^{-1} (molecule/cm^{-2})$^{-1}$ agrees with the present value to within experimental error. The observations of Sugawara et al. [19] in a laser photolysis experiment can also be analyzed to produce a band strength estimate. To do so we must taken into account the fact that the line they observed at 1251.455 cm^{-1} was in fact an overlapped set of lines including the $36_{6,31}$–$36_{5,32}$, $40_{2,39}$–$40_{1,40}$, $21_{9,13}$–$22_{8,14}$ and $21_{9,12}$–$22_{8,15}$ transitions. We must also make assumptions about the length of the focal volume of their photolysis laser and the overlap between its cross section and that of their diode laser beam. Agreement with our value can indeed be obtained with plausible values of these parameters, so this observation serves as an order of magnitude check.

The experimental values are in good agreement with a theoretical prediction [20] of $(1.7\pm0.5)\times10^{-17}$ cm^{-1} (molecule/cm^{-2})$^{-1}$ made by transfer of atomic polar tensors. A recent ab initio calculation [21] used a variety of basis sets. The largest gave a value of 4.2×10^{-17} cm^{-1} (molecule/cm^{-2})$^{-1}$, while the (triple-zeta) set which gave the best agreement with the observed vibrational frequencies gave 6.7×10^{-17}.

Although the line observed here is a strong line of the ν_1 band, it is by no means the best line for sensitive measurement of CF_2 concentrations. Recently published Fourier transform spectra of both the ν_1 and ν_3 bands [22] show that substantially stronger lines can be found in the ν_3 band. Given the line strengths reported here and in ref. [18], the Fourier transform spectra allow the accurate determination of other line strengths. In particular, we can determine the ratio of the two band strengths. We integrated selected lines in each band and compared them to the intensities predicted by the asymmetric rotor computer code [14]. We found a ratio of 2.4 ± 0.8, with the ν_3 asymmetric stretch centered at 1114 cm^{-1} being the stronger. The theoretical prediction of ref. [20] for this ratio is 1.7, while that of ref. [21] is 7.7 for the largest basis set and 3.9 for the triple-zeta set. Again, the transfer-of-parameters method comes closest to matching the experimental value.

Acknowledgement

Helpful advice and technical assistance from M. Zahniser, D. Worsnop, S. Anderson, A. Freedman, and S. Coy, and from A.H. Maki of the National Institute of Science and Technology, are gratefully acknowledged. Research sponsored by the Air Force Office of Scientific Research (AFSC), under Contract F49620-87-C-0052.

References

[1] P.J. Hargis and M.J. Kushner, Appl. Phys. Letters 40 (1982) 779.

[2] S. Pang and S.R.J. Brueck, Mater. Res. Symp. Proc. 17 (1983) 161.

[3] K. Ninomiya, K. Suzuki, S. Nishimatsu and O. Okada, J. Vacuum Sci. Technol. A 4 (1986) 1971.

[4] J.W. Thoman Jr., K. Suzuki, S.H. Kable and J.I. Steinfeld, J. Appl. Phys. 60 (1986) 2775.

[5] Y. Matsumi, S. Toyoda, T. Hayashi, M. Miyamura, H. Yoshikawa and S. Komiya, J. Appl. Phys. 60 (1986) 4102.

[6] J.P. Booth, G. Hancock and N.D. Perry, Appl. Phys. Letters 50 (1987) 318.

[7] J.P. Booth, G. Hancock and N.D. Perry, Mater. Res. Soc. Symp. Proc. 117 (1988) 47.

[8] R. d'Agostino, F. Cramarossa, S. De Benedictis and G. Ferraro, J. Appl. Phys. 52 (1981) 1259.

[9] D. Field, A.J. Hydes and D.F. Klemperer, Vacuum 34 (1984) 563.

[10] I.C. Plumb and K.R. Ryan, Plasma Chem. Plasma Processes 6 (1986) 205.

[11] D.R. Herriot, H. Kogelnik and R. Kompfner, Appl. Opt. 3 (1964) 523.

[12] G. Guelachvili and K.N. Rao, Handbook of infrared standards (Academic Press, Orlando, (1986).

[13] S. Sharpe, B. Hartnett, H.S. Sethi and D.S. Sethi, J. Photochem. 38 (1987) 1.

[14] S. Carter and L.O. Halonen, Program ASYMVIB, Spectrochim. Acta 41A (9) (1985), software survey section.

[15] P.B. Davies, W. Lewis-Bevan and D.K. Russell, J. Chem. Phys. 75 (1981) 5602.

[16] G. Herzberg, Infrared and Raman spectra of polyatomic molecules (Van Nostrand Reinhold, New York, 1945).

[17] J.J. Orlando, J. Reid and D.R. Smith, Chem. Phys. Letters 141 (1987) 423.

[18] J.J. Orlando, J. Reid and D.R. Smith, Chem. Phys. Letters 147 (1988) 300.

[19] K. Sugawara, T. Nakanaga, H. Takeo and C. Matsumura, Chem. Phys. Letters 130 (1986) 560.

[20] J.H. Newton and W.B. Person, J. Chem. Phys. 68 (1978) 2799.

[21] Y. Yamaguchi, M.J. Frisch, T.J. Lee, H.F. Schaefer III and J.S. Binkley, Theoret. Chim. Acta 69 (1986) 337.

[22] J.B. Burkholder, C.J. Howard and P.A. Hamilton, J. Mol. Spectry. 127 (1988) 362.

APPENDIX C

Radical and molecular product concentration measurements in CF_4 and CH_4 radio frequency plasmas by infrared tunable diode laser absorption

J. Wormhoudt
Center for Chemical and Environmental Physics, Aerodyne Research, Inc., Billerica, Massachusetts 01821

(Received 22 August 1989; accepted 2 October 1989)

Infrared tunable diode laser absorption studies of radicals and stable molecules formed in radio frequency (rf) plasmas are being carried out in a laboratory reactor which allows a long absorption path. In this paper we report studies of CF_4 and CH_4 rf plasmas. We report absolute concentration measurements as functions of total pressure and rf power for CF_2 and C_2F_6 in CF_4 plasmas and for CH_3 and C_2H_2 in CH_4 plasmas.

I. INTRODUCTION

Tunable diode laser infrared absorption spectroscopy has been shown to be useful in the study of process plasmas, including chlorine etching plasmas[1-3] and silane deposition plasmas.[4-7] Diode lasers have also been used to study hydrocarbon species in organometallic chemical vapor deposition[8] and hot-filament diamond deposition.[9] However, there have been no applications to the hydrocarbon plasmas used to deposit diamond and hard carbon films. There have also been no applications to molecular concentration determination in the fluorocarbon plasmas widely used in semiconductor etching, although a number of laser-induced fluorescence[10-18] and electronic emission[19,20] studies have provided relative concentration profile information. Chemical kinetics modeling studies of CF_4[21] and CH_4[22] plasmas have identified several important molecular species. Measurements of absolute concentrations of these molecules are important in evaluating the chemical kinetic and electron collision mechanisms involved in these predictions. Here we present our first observations on a laboratory plasma reactor which allows a long absorption path.

II. EXPERIMENTAL

Figure 1 is a schematic drawing of the long path plasma apparatus. The active volume is contained inside a 1 m long Teflon inner liner with a 15 cm inner diameter. The electrodes which surround it are copper half-tubes, with water cooling provided by one line of copper tubing set into the electrode surface in a loop near the outer edge. They are separated from the stainless steel vacuum wall by an outer quartz dielectric tube.

The feed gas, together with any carrier or additive gases, enters the tube through a ring injector just before the upstream end of the electrodes. Argon purge gas is introduced behind each mirror, and small flows are also put into each of the cross ports which are used for visual observation and emission spectroscopy. With a 14 ℓ/s mechanical pump and 7 cm diameter pumping line, pressures in the 0.1–1.0 Torr range are achieved with total flows in the 15–400 sccm range. These translate into gas velocities of from 6 to 150 cm/s, or residence times in the active region of from 17 to 0.7 s. We conclude from studies in which the residence time was varied while the pressure remained constant that the plasmas studied have reached a steady state, with their composition not strongly affected by residence time.

The mirrors used for multipass infrared absorption have 15 cm diameters and are separated by approximately 2 m. They form an off-axis resonator,[23] in which the laser beam enters and exits through the same central hole in the downstream mirror, and forms a spot pattern on both mirrors which can be circular or which can be flattened into an ellipse (as we now use it) whose major axis is still almost the full 15 cm but with a minor axis of a little over 1 cm. For CF_4 studies, mirrors with a nominal 183 cm radius of curvature were used with a spacing resulting in 38 passes, while for CH_4 224 cm mirrors were used with 48 passes.

The 13.56 MHz rf power is taken from an RF Plasma Products supply with 1000 W capability. Powers reported are the values read from the digital meter on the supply. If all the power went into the plasma, power densities up to 0.1 W/cm^3 would be achieved, within the range of values used in commercial etching and deposition reactors. The fraction actually dissipated in the plasma is difficult for us to measure or estimate, but it is very likely to be less than half.

III. RESULTS AND DISCUSSION FOR CF_4 PLASMAS

Most observations were made in the 1090–1120 cm^{-1} spectral region. This ν_3 band region contains some of the strongest vibrational/rotational lines of the CF_2 radical. At the upper end of this range they are overlapped by strong sharp features of the C_2F_6 molecule, while at the lower end C_2F_6 features are not detectable. Thus, we were able to take spectra from which we could deduce concentrations of both molecules, or spectra in which we were confident that the CF_2 lines were free from interferences. Finally, some measurements of CF_4 dissociation were made in the weak band at around 1060 cm^{-1}, while others were made in the fundamental band in the 620–625 cm^{-1} region.

The strengths of the CF_4 and C_2F_6 spectral features used were simply measured directly using a cell of known path length and known pressures of these permanent gases. There have been two experimental measurements of CF_2 infrared line strengths, both in the neighboring ν_1 band centered at 1222 cm^{-1} which in the plasma would be overlapped by a strong CF_4 band with a center frequency of 1281 cm^{-1}. An analysis[24] of Fourier transform infrared (FTIR) spectra of both the ν_1 band and the stronger ν_3 band used in this work has yielded a ratio of their strengths. Use of the ν_1 strength as well as the ratio reported in Ref. 24 results in a ν_3 band strength of $(2.6 \pm 1.3) \times 10^{-17}$ cm^{-1} (molecule/cm^2)$^{-1}$

 0734-2101/90/031722-04$01.00

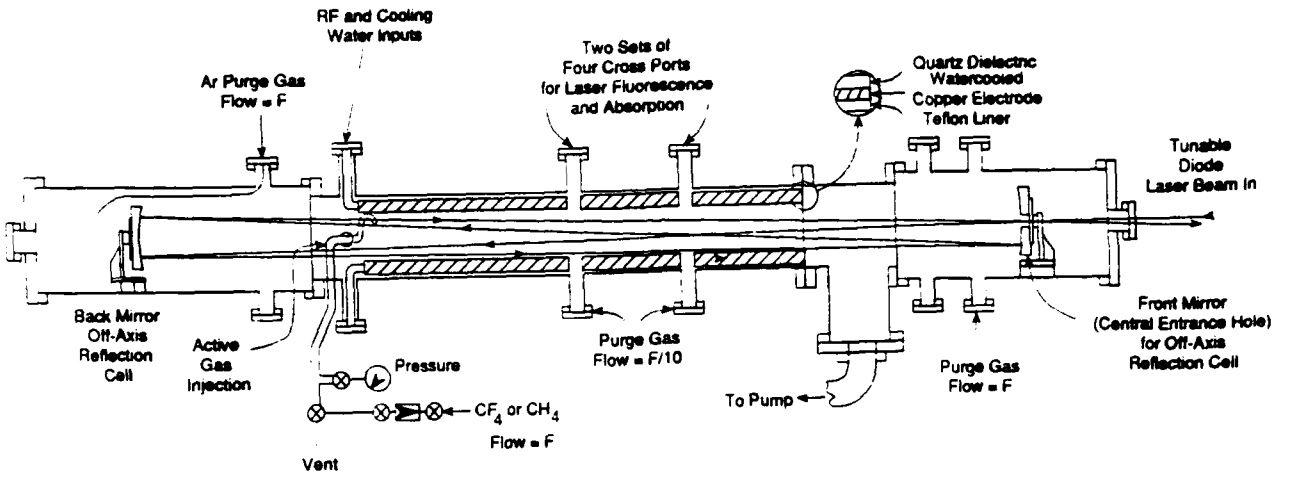

FIG. 1. Cross-sectional view of long path absorption plasma apparatus.

used in the present analysis. Individual line strengths were derived using the formulas given in Ref. 24, using line assignments and lower state energy levels given by two asymmetric rotor codes[25,26] and molecular constants from the FTIR study.[27] Gas temperatures are obtained from relative intensities of CF_2 rotational lines.

A. Concentration variation with rf power

Figure 2 gives an example of the absolute concentration data obtained from analysis of infrared absorption features. Although the qualitative behavior of higher radical concentrations at higher powers is reasonable, the straight-line growth of CF_2 as the applied rf power is increased is simply due to a particular balance of production and destruction rates. During the first few months of operation we observed a negative curvature with increasing power, as well as higher CF_2 concentrations by up to an order of magnitude. We suspect that the Teflon liner was initially a stronger source of fluorocarbon molecules. At higher concentrations, second-order recombination reactions begin to dominate over first-order production, and the increase in CF_2 with power becomes less than linear.

The behavior of the decomposition product C_2F_6 is seen to be in sharp contrast to CF_2 trends, being essentially constant and probably slightly decreasing with increasing power. We observed that the fraction of CF_4 dissociated increased with increasing power, so the fraction converted into C_2F_6 is clearly decreasing with increasing power. In this case, then, the balance between production and destruction has different results, with C_2F_6 possibly more vulnerable to electron-impact fragmentation than is CF_2. C_2F_6 appears to be an intermediate which reaches a steady-state concentration which happens to have a roughly constant value even as the CF_4 concentration is decreasing and the concentrations of other decomposition and recombination products are increasing.

B. Concentration variation with total pressure

Figure 3 shows absolute CF_2 and C_2F_6 number densities as a function of total pressure, for a constant mixing ratio. Features of the CF_2 curve include a sharp increase with decreasing pressure below 0.15 Torr, and an essentially constant behavior at higher pressures. The C_2F_6 concentration mirrors this behavior to a lesser extent, but may show a peak

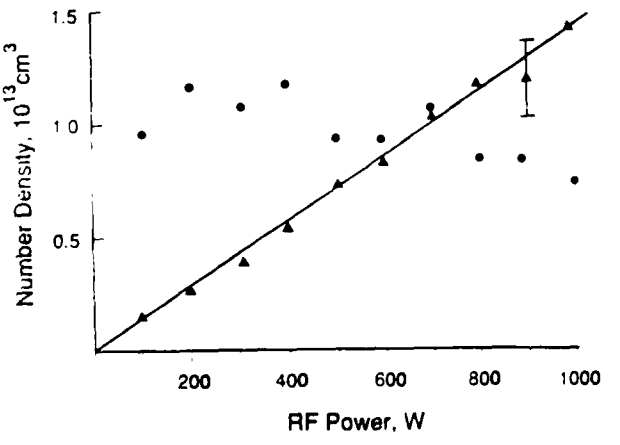

FIG. 2. CF_2 (▲) and C_2F_6 (■) number densities as functions of rf power, with reactor total pressure of 0.10 Torr and mixing fraction, $[CF_4]/[CF_4 + Ar]$, of 0.4.

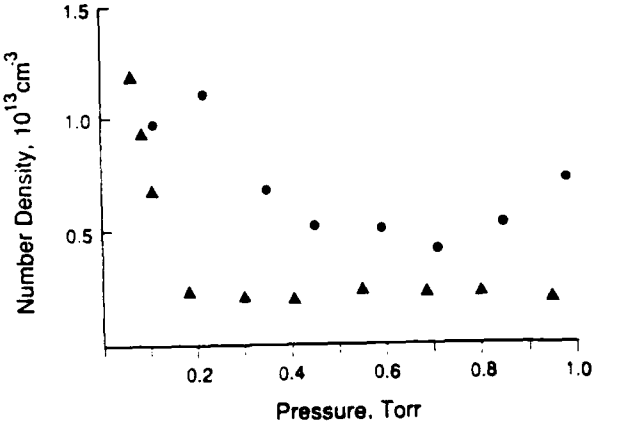

FIG. 3. CF_2 (▲) and C_2F_6 (■) number densities as functions of reactor total pressures, with rf power of 500 W and mixing fraction, $[CF_4]/[CF_4 + Ar]$, of 0.4.

at 0.2 Torr and may also be increasing as the pressure increases to 1.0 Torr.

This behavior could be explained in terms of bulk gas-phase chemistry. Higher pressures could favor gas-phase recombination reactions, shifting the steady state away from CF_2 and towards larger molecules. Of course, at even lower pressures the CF_2 concentration would eventually decrease with decreasing pressure. However, the surface source in our system might not decrease linearly with pressure, if higher ion energies produced more desorption per ion as the total (and ion) densities decreased. Still, we expect a peak in CF_2 concentration at some total pressure below 0.05 Torr. The possibilities that C_2F_6 peaks above this, and that it increases as the pressure goes past 1 Torr, are both consistent with it being a product of radical recombination and reaction whose rates are faster at higher total pressures.

On the other hand, these bulk gas considerations may not be the major mechanism behind the observed variations with pressure. Our visual observations looking down the tube are of increasing spatial nonuniformity with higher pressure, with the glow (and presumably the source of radicals) moving towards the electrodes. This explanation is related to the analysis of the recently published laser induced fluorescence study of CF_2 profiles in a parallel-plate reactor.[18] These results were interpreted in terms of a chemical diffusion length for CF_2 reaction, primarily with fluorine atoms. We expect that the source region is moving away from the laser spot pattern as the total pressure is raised, and that the chemical diffusion length is, if anything, decreasing as well, and that both effects may be contributing to the decrease in CF_2 column density observed.

On the other hand, C_2F_6 is a stable molecule, and if, at higher pressures, there is indeed a widening volume in the center of the tube with low electron, ion, and radical concentrations, C_2F_6 should have no trouble filling the tube uniformly at pressures of 1 Torr and below. Therefore, the lower C_2F_6 concentrations observed at higher pressures in Fig. 3 should still reflect a change in the gas phase chemistry averaged over the reactor volume.

IV. RESULTS AND DISCUSSION FOR CH_4 PLASMAS

Molecular species observed to date in CH_4 plasmas include the methyl radical, CH_3, and acetylene, C_2H_2. C_2H_2 was observed in the 745 cm^{-1} region, while CH_3 was observed on the $Q_6(6)$ and $Q_8(8)$ transitions at 607.02 and 608.30 cm^{-1}. As above for CF_4 and C_2F_6, relevant C_2H_2 line strengths are easily obtained from *in situ* measurements using known amounts of calibration acetylene, while the CH_3 band strength is taken from Ref. 28. We assumed a temperature of 500 K, higher than the temperatures measured for CF_4 plasmas. The transitions used were not strongly sensitive to temperature.

Figure 4 shows an example of CH_3 number density variation with rf power. It will be noted, first, that the methyl radical concentration is up to two orders of magnitude smaller than the CF_2 concentration in an otherwise similar CF_4 plasma. It is also seen that its concentration rapidly plateaus at a limiting steady state value. Both observations are consistent with concentrations determined by recombination chemistry, since the CH_3 radical is much more self-reactive than the CF_2 radical.

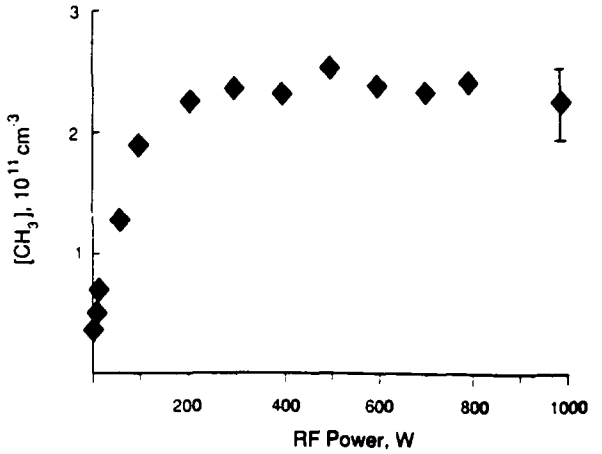

FIG. 4. CH_3 number density measured using the $Q_6(6)$ line, as a function of rf power, with reactor total pressure of 0.15 Torr and mixing fraction, $[CH_4]/[CH_4 + Ar]$, of 0.75.

Figure 5 shows the CH_3 radical concentration variation with total pressure. Once again, the absolute number density decreases as the total pressure (and the CH_4 number density) increases. The decrease is more gradual when compared to the steep drop in CF_2 concentration between 0.1 and 0.2 Torr. We can speculate that due to the high reactivity of CH_3, any region where the balance between production and destruction changes to produce a dramatic increase in number density must occur at lower pressures than for CF_2. Finally, Fig. 6 shows C_2H_2 number densities over the same total pressure range. Although C_2H_2 is present in much larger concentrations than the radicals we have studied, it still is under 10% of the input methane. Studies of the CH_4 dissociation fraction remain to be done. In addition, we expect to make observations of several other chemical species in these plasmas, and to investigate spectroscopic methods of temperature measurement.

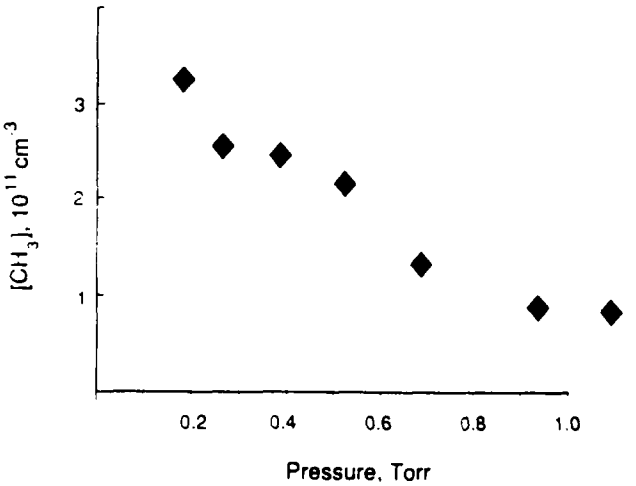

FIG. 5. CH_3 number density measured using the $Q_8(8)$ line, as a function of reactor total pressure, with rf power of 300 W and mixing fraction, $[CH_4]/[CH_4 + Ar]$, of 0.65.

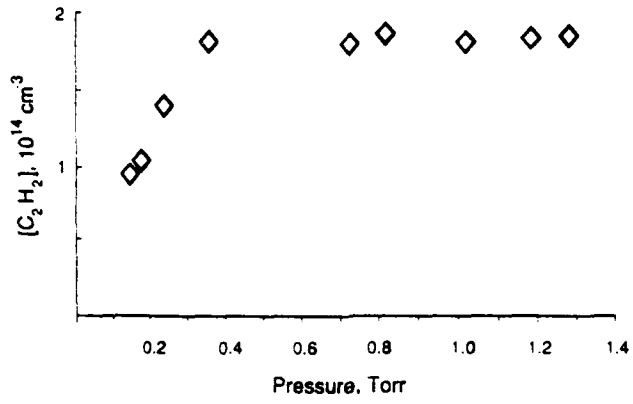

FIG. 6. C_2H_2 number density measured using the $2\nu_4^2 - \nu_5^1 R(6)$ line, as a function of reactor total pressure, with rf power of 500 W and mixing fraction, $[CH_4]/[CH_4 + H_2]$, of 0.5.

V. CONCLUSIONS

Infrared tunable diode laser absorption spectroscopy is a very useful diagnostic of rf plasmas, capable of detection of a wide variety of the radicals and stable molecules found in the CF_4 and CH_4 systems. Although our long path system resulted in strong absorption levels, allowing us to use simple direct detection using a slow laser scan rate and a simple detection system, standard techniques for high sensitivity detection would allow measurements of all the species measured to be made over the 10 cm paths typical of plasma processing equipment.

With the exception of CF_2 laser induced fluorescence (LIF) observations of Ref. 16, these are the first reported absolute concentration measurements of any of these species in any rf plasma system. We plan additional studies to gain a clearer picture of conditions in our apparatus. Our observations to date suggest that the reactor wall plays a large role in determining molecular concentrations in CF_4 plasmas. There is a strong possibility that both polymer deposition from the CF_4 feed gas and fluorocarbons emitted by the Teflon liner are contributors. The wall source decreased with continued operation, as monitored by CF_2 production in a pure argon plasma. The concentrations reported here were obtained when a pure argon plasma initially produced no observable CF_2 or C_2F_6. A second, more tentative conclusion, based on the observation that absolute concentrations of CF_2 and C_2F_6 are much smaller than the fraction of CF_4 dissociated, is that gas phase decomposition and recombination chemistry carries CF_4 fragments into a wide variety of fluorocarbon chemical species. In our less extensive CH_4 studies, wall effects were not observed, and while C_2H_2 is clearly a major decomposition product, there may well be other important species as well.

ACKNOWLEDGMENTS

W. Goodwin constructed and operated the apparatus. M. Zahniser, D. Worsnop, and S. Coy provided helpful advice and technical assistance. Research sponsored by the Air Force Office of Scientific Research (AFSC), under Contract No. F49620-87-C-0052.

[1] J. Wormhoudt, A. C. Stanton, A. D. Richards, and H. H. Sawin, J. Appl. Phys. **61**, 142 (1987).
[2] A. D. Richards, B. E. Thompson, K. D. Allen, and H. H. Sawin, J. Appl. Phys. **62**, 792 (1987).
[3] A. D. Richards and H. H. Sawin, J. Appl. Phys. **62**, 799 (1987).
[4] C. A. DeJoseph, Jr., P. D. Haaland, and A. Garscadden, IEEE Trans. Plasma Sci. **14**, 165 (1986).
[5] P. Chollet, G. Guelachvili, M. Morillon-Chapey, P. Gressier, and J. Schmitt, J. Opt. Soc. Am. B **3**, 687 (1986).
[6] P. B. Davies, N. A. Isaacs, S. A. Johnson, and D. K. Russel, J. Chem. Phys. **83**, 2060 (1985).
[7] N. Itabashi, K. Kato, N. Nishiwaki, T. Goto, C. Yamada, and E. Hirota, Jpn. J. Appl. Phys. **27**, L1565 (1988).
[8] J. E. Butler, N. Bottka, R. S. Sillmon, and D. K. Gaskill, J. Cryst. Growth **77**, 163 (1986).
[9] F. G. Celii, P. E. Pherson, H. Wang, and J. E. Butler, Appl. Phys. Lett. **52**, 2043 (1988).
[10] P. J. Hargis and M. J. Kushner, Appl. Phys. Lett. **40**, 779 (1982).
[11] S. Pang and S. R. J. Brueck, Mater. Res. Symp. Proc. **17**, 161 (1983).
[12] K. Ninomiya, K. Suzuki, S. Nishimatsu, and O. Okada, J. Vac. Sci. Technol. A **4**, 1971 (1986).
[13] J. W. Thoman, Jr., K. Suzuki, S. H. Kable, and J. I. Steinfeld, J. Appl. Phys. **60**, 2772 (1986).
[14] Y. Matsumi, S. Toyoda, T. Hayashi, M. Miyamura, H. Yoshikawa, and S. Komiya, J. Appl. Phys. **60**, 4102 (1986).
[15] J. P. Booth, G. Hancock, and N. D. Perry, Appl. Phys. Lett. **50**, 318 (1987).
[16] J. P. Booth, G. Hancock, N. D. Perry, and M. J. Toogood, Mater. Res. Soc. Symp. **117**, 47 (1988).
[17] S. G. Hansen, G. Luckman, and S. D. Colson, Appl. Phys. Lett. **53**, 1588 (1988).
[18] M. Kitamura, H. Akiya, and T. Urisu, J. Vac. Sci. Technol. B **7**, 14 (1989).
[19] R. d'Agostino, F. Cramarossa, S. DeBenedictis, and G. Ferraro, J. Appl. Phys. **52**, 1259 (1981).
[20] D. Field, A. J. Hydes, and D. F. Klemperer, Vacuum **34**, 563 (1984).
[21] I. C. Plumb and K. R. Ryan, Plasma Chem. Plasma Process. **6**, 205 (1986).
[22] L. E. Kline, W. D. Partlow, and W. E. Bies, J. Appl. Phys. **65**, 70 (1989).
[23] D. R. Herriot, H. Kogelnik, and R. Kompfner, Appl. Opt. **3**, 523 (1964).
[24] J. Wormhoudt, K. E. McCurdy, and J. B. Burkholder, Chem. Phys. Lett. **158**, 480 (1989).
[25] S. Carter and L. O. Halonen, Program ASYMVIB, Spectrochim. Acta Part A **41**, 1 (1985).
[26] A. H. Maki, National Institute of Science and Technology, Program ASYMBD7 (private communication).
[27] J. B. Burkholder, C. J. Howard, and P. A. Hamilton, J. Mol. Spectrosc. **127**, 362 (1988).
[28] J. Wormhoudt and K. E. McCurdy, Chem. Phys. Lett. **156**, 47 (1989).

APPENDIX D

ARI-RR-733

Radical and Molecular Product Concentration Measurements in CF_4 RF Plasmas by Infrared Tunable Diode Laser Absorption

Prepared by:

J. Wormhoudt

Center for Chemical and Environmental Physics
Aerodyne Research, Inc.
45 Manning Road
Billerica, MA 01821

Prepared for:

SPIE Symposium on Microelectronic Integrated Processing
SPIE Proceedings Volume 1185
Conference on Dry Processing for Submicrometer Lithography
Santa Clara, CA
October 8-13 1989

September 1989

Radical and molecular product concentration measurements in CF_4 RF plasmas by infrared tunable diode laser absorption

J. Wormhoudt

Center for Chemical and Environmental Physics, Aerodyne Research, Inc., Billerica, Massachusetts 01821

ABSTRACT

Absolute concentration measurements of radicals and stable molecules formed in radio frequency plasmas were performed by infrared tunable diode laser absorption in a laboratory reactor which allows a long absorption path. In this paper we report studies of CF_4 RF plasmas. We report CF_2, CF_4, and C_2F_6 concentrations in CF_4 plasmas as functions of total pressure, RF power, and oxygen addition.

1. INTRODUCTION

The sensitivity, wide applicability, and quantitative capability of tunable diode laser infrared absorption spectroscopy have been shown to be useful in the study of process plasmas, including chlorine etching plasmas[1-3] and silane deposition plasmas.[4-7] Diode lasers have also been used to study hydrocarbon species in organometallic chemical vapor deposition[8] and hot-filament diamond deposition.[9] However, there have been no applications to molecular concentration determination in the fluorocarbon plasmas widely used in semiconductor etching, although a number of laser-induced fluorescence[10-18] and electronic emission[19,20] studies have provided relative concentration profile information. Chemical kinetics modeling studies of CF_4 plasmas have identified several important molecular species.[21] Measurements of absolute concentrations of these molecules are important in evaluating the chemical kinetic and electron collision mechanisms involved in these predictions. Here we present our first observations on a laboratory plasma reactor which allows a long absorption path.

2. EXPERIMENTAL

Figure 1 is a schematic drawing of the long path plasma apparatus. The active volume is contained inside a 1 m long Teflon inner liner with a 15 cm inner diameter. The electrodes which surround it are copper half-tubes, with water cooling provided by one line of copper tubing set into the electrode surface in a loop near the outer edge. They are separated from the stainless steel vacuum wall by an outer quartz dielectric tube.

The feed gas, together with any carrier or additive gases, enters the tube through a ring injector just before the upstream end of the electrodes. Argon purge gas is introduced behind each mirror, and small flows are also put into each of the cross ports which are used for visual observation and emission spectroscopy. With a 30 cfm mechanical pump and 7 cm diameter pumping line, pressures in the 0.1 to 1.0 Torr range are achieved with total flows in the 15 to 400 sccm range. These translate into gas velocities of from 6 to 150 cm/s, or residence times in the active region of from 17 to 0.7 seconds. We conclude from studies in which the residence time was varied while the pressure remained constant that the

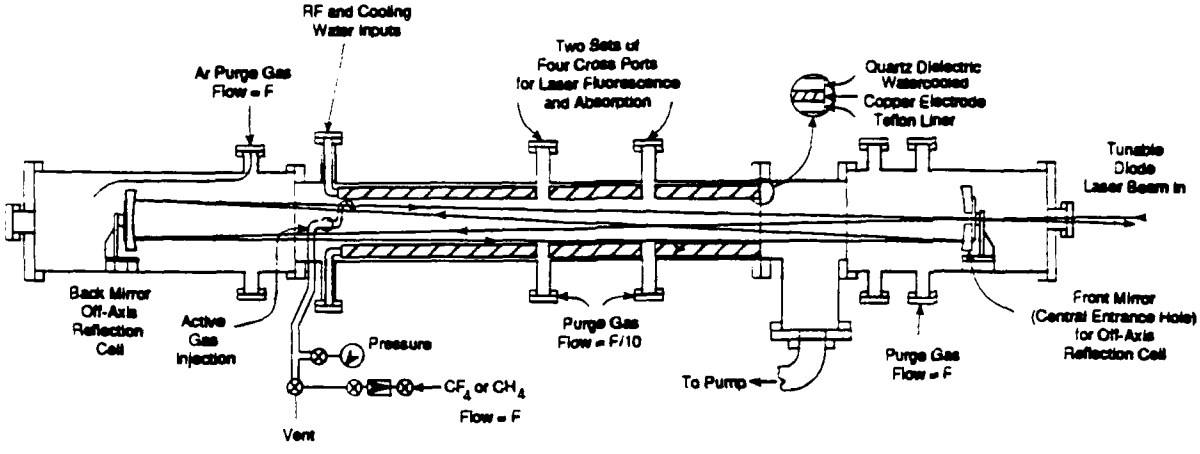

Figure 1. Cross sectional view of long path absorption plasma apparatus.

plasmas studied have reached a steady state, with their composition not strongly affected by residence time.

The mirrors used for multi-pass infrared absorption have 15 cm diameters and are separated by approximately 2 meters. They form an off-axis resonator,[22] in which the laser beam enters and exits through the same central hole in the downstream mirror, and forms a spot pattern on both mirrors which can be circular or which can be flattened into an ellipse (as we now use it) whose major axis is still almost the full 15 cm but with a minor axis of a little over 1 cm. Mirrors with a nominal 183 cm radius of curvature were used with a spacing resulting in 38 passes.

The 13.56 MHz RF power is taken from an RF Plasma Products supply with 1000 W capability. Powers reported are the values read from the digital meter on the supply. If all the power went into the plasma, power densities up to 0.1 W/cm^3 would be achieved, within the range of values used in commercial etching and deposition reactors. The fraction actually dissipated in the plasma is difficult for us to measure or estimate, but it is very likely to be less than half.

3. RESULTS AND DISCUSSION

Figure 2 is a schematic showing the absorption band positions of several molecules expected to be important in CF_4 plasmas, in the region of C-F stretching vibrations. Hatching indicates the presence in the literature of experimentally determined line positions. Solid regions are where an experimental high resolution spectrum is available, providing the information on line intensities and weak lines which facilitates identification of the absorber. For stable gases like CF_4 and C_2F_6, this information is of course available simply by filling the cell and repeating the diode scan. In unshaded regions, only predicted line positions (of varying accuracy) are available.

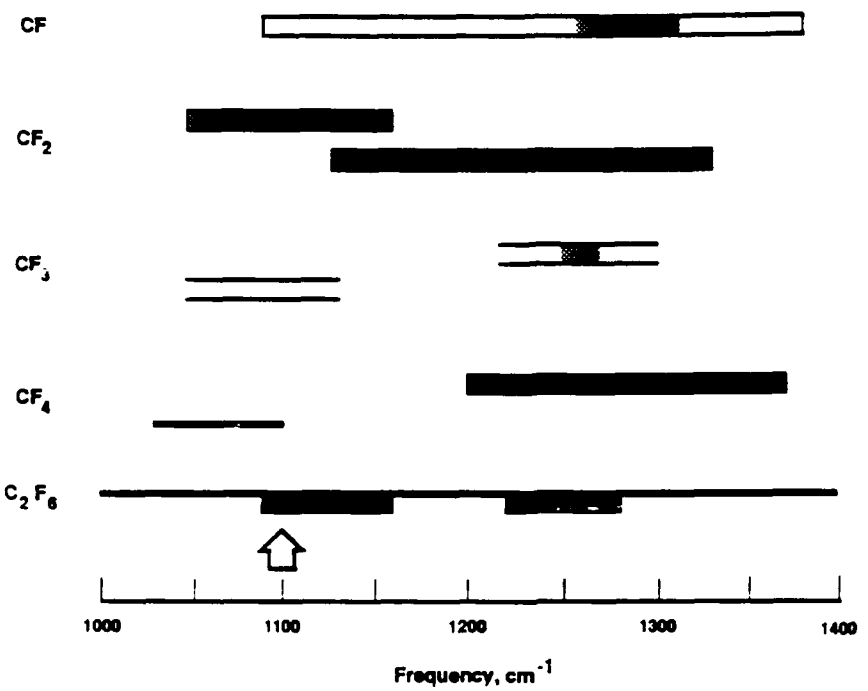

Figure 2. Infrared absorption band positions of CF_x molecules (see text for key).

Most observations were made in the 1090-1120 cm^{-1} spectral region, indicated by the arrow in the figure. This ν_3 band region contains some of the strongest vibrational/rotational lines of the CF_2 radical. At the upper end of this range they are overlapped by strong sharp features of the C_2F_6 molecule, while at the lower end C_2F_6 features are not detectable. Thus, we were able to take spectra from which we could deduce concentrations of both molecules, or spectra in which we were confident that the CF_2 lines were free from interferences. Figure 3 shows an example plasma absorption spectrum, matched up against a recent laboratory spectrum taken using a high resolution spectrometer.[23] Some measurements of CF_4 dissociation were made in the weak band at around 1060 cm^{-1}, while others were made in the fundamental band in the 620-625 cm^{-1} region.

The strengths of the CF_4 and C_2F_6 spectral features used were simply measured directly using a cell of known path length and known pressures of these permanent gases. The strength of the CF_2 ν_3 band used here involves some uncertainty. There have been two experimental measurements of CF_2 infrared line strengths, both in the neighboring ν_1 band centered at 1222 cm^{-1} which in the plasma would be overlapped by a strong CF_4 band with a center frequency of 1281 cm^{-1}. An analysis[24] of FTIR spectra of both the ν_1 band and the stronger ν_3 band centered around 1110 cm^{-1} has yielded a ratio of their strengths. Use of the ν_1 strength as well as the ratio reported in Ref. 26 results in a ν_3 band strength of $(2.6 \pm 1.3) \times 10^{-17}$ cm^{-1} $(molecule/cm^2)^{-1}$ used in the present analysis. (Ab initio calculations have indicated higher values,[24] with very recent calculations[25] being as high 6.3×10^{-17}, raising the possibility that CF_2 concentrations reported here are high by more than a factor of two.) Individual line strengths were derived using the formulas given in Ref. 24, using line assignments and lower state energy levels given by two asymmetric rotor codes[27,28] and molecular constants from the FTIR study.[23] Gas temperatures are obtained from relative intensities of CF_2 rotational lines, as described below.

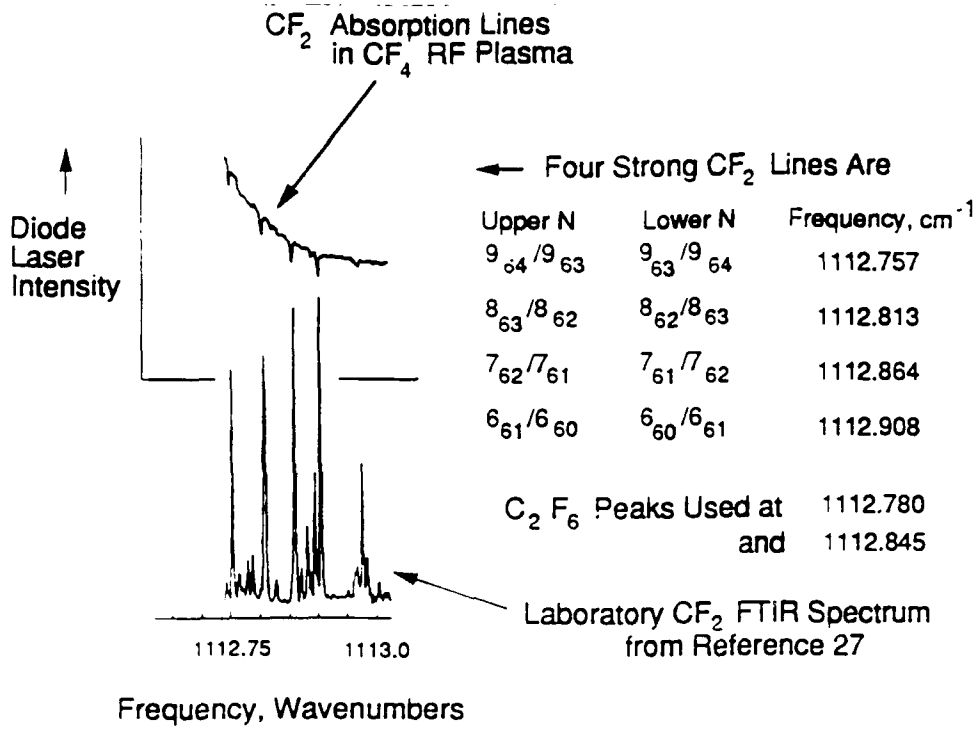

Figure 3. Example plasma reactor direct absorption spectrum (upper trace) with laboratory reference spectrum (lower trace).

3.1 Product concentration variation with RF power

Figure 4 gives an example of the absolute concentration data obtained from analysis of infrared absorption features. Although the qualitative behavior of higher radical concentrations at higher powers is reasonable, the straight-line growth of CF_2 as the applied RF power is increased is simply due to a particular balance of production and destruction rates. During the first few months of operation we observed a negative curvature with increasing power, as well as higher CF_2 concentrations by up to an order of magnitude. We suspect that the Teflon liner was initially a stronger source of fluorocarbon molecules. At higher concentrations, second-order recombination reactions begin to dominate over first-order production, and the increase in CF_2 with power becomes less than linear.

The behavior of the decomposition product C_2F_6 is seen to be in sharp contrast to the CF_2 trend, being essentially constant and probably slightly decreasing with increasing power. As shown below, we observed that the fraction of CF_4 dissociated increased with increasing power, so the fraction converted into C_2F_6 is clearly decreasing with increasing power. In this case, then, the balance between production and destruction has different results, with C_2F_6 possibly more

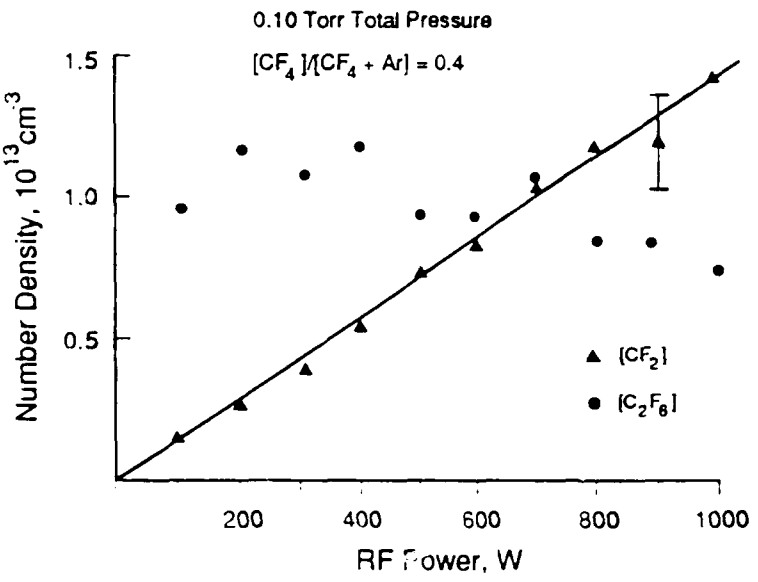

Figure 4. CF_2 and C_2F_6 number densities as functions of RF power, with reactor total pressure of 0.10 Torr and mixing fraction, $[CF_4]/[CF_4 + Ar]$, of 0.4.

vulnerable to electron-impact fragmentation than is CF_2. C_2F_6 appears to be an intermediate which reaches a steady-state concentration which happens to have a roughly constant value even as the CF_4 concentration is decreasing and the concentrations of other decomposition and recombination products are increasing.

3.2 Comparison to model predictions

To date, published model predictions have compared to observations of Smolinsky and Flamm,[29] who used a small discharge tube and a very high power density. They made mass spectrometric observations of several of the stable decomposition products downstream of the discharge. A prediction of the most recent published model, that of Plumb and Ryan,[21] is shown in Figure 5, along with the data points

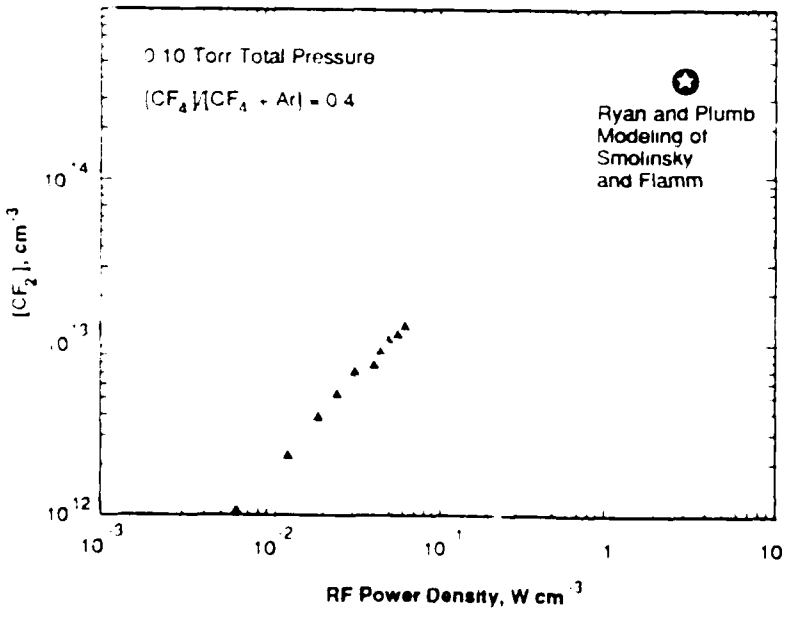

Figure 5. CF_2 concentration data of Figure 4 replotted against power density, assuming half of power deposited in plasma, compared with prediction of Ref. 21.

of Figure 4 replotted against power density on a log-log scale (with the assumption that half the RF power is deposited in the plasma). In addition to the large difference in power density, two other differences make direct comparison inappropriate. The prediction is for a higher pressure (0.5 Torr compared to our observation at 0.1 Torr - in our system, higher pressures give lower concentrations, as discussed below) and is for pure CF_4 rather than for a CF_4/Ar mix. As discussed above, with lower pressure and dilution inhibiting radical recombination, there is every reason to expect the high power (and high concentration) value to lie below the extrapolation of our low power curve, as it does. Preliminary modeling appropriate to conditions in our system[30] produced similar values to those observed for both CF_2 and C_2F_6 concentrations, but predicted much smaller CF_4 dissociation fractions than the observed levels we will present below. These predictions are very sensitive to assumptions about the role of the walls in determining concentrations, assumptions which are difficult to make with a high degree of confidence. At present, strong conclusions cannot be drawn from either the factor of two agreement in product concentrations or the order of magnitude disagreement in decomposition fraction.

3.3 Observations of CF_2 concentration with oxygen fraction

Molecular oxygen is a standard additive to CF_4 etching plasmas, being known to substantially increase the etch rate.[31] Oxygen atoms are known to react readily with CF_2 to form COF which eventually forms the stable species COF_2 and CO_2.[32] Comparing the predictions of Ryan and Plumb for a pure CF_2 plasma (at 0.5 Torr) of a CF_2 steady state number density of around 4×10^{14} cm^{-3} to those of Plumb and Ryan[33] for a 75% CF_4/25% O_2 plasma in which the CF_2 number density has dropped to 2×10^{13} cm^{-3} after about a 50 msec residence time and is continuing to drop, we expect oxygen addition to have a substantial effect.

The effect observed in Figure 6 is somewhat less dramatic, involving a drop of about a factor of six at the 20% oxygen level. In this set of observations the flows of CF_4 and Ar were fixed, with a $CF_4/(CF_4 + Ar)$ ratio of 0.4, while the O_2 fraction of the total flow was increased. The emission data[34] given in the right side of Figure 6 show a slightly larger fractional drop. Once again, this experiment was done in a small alumina tube with a high power density (as high as 4 W/cm^{-3}) with a pressure of 1 Torr.

3.4 Product concentration variations with total pressure

Figure 7 shows absolute CF_2 and C_2F_6 number densities as a function of total pressure, for a constant mixing ratio. Features of the CF_2 curve include a sharp increase with decreasing pressure below 0.15 Torr, and an essentially constant behavior at higher pressures. The C_2F_6 concentration mirrors this behavior to a lesser extent, but may show a peak at 0.2 Torr and may also be increasing as the pressure increases to 1.0 Torr.

This behavior could be explained in terms of bulk gas-phase chemistry. One could argue that higher pressures favor gas-phase recombination reactions, shifting the steady state away from CF_2 and towards larger molecules. Of course, at even lower pressures the CF_2 concentration would eventually decrease with decreasing pressure. However, the surface source in our system might not decrease linearly with pressure, if higher ion energies produced more desorption per ion as

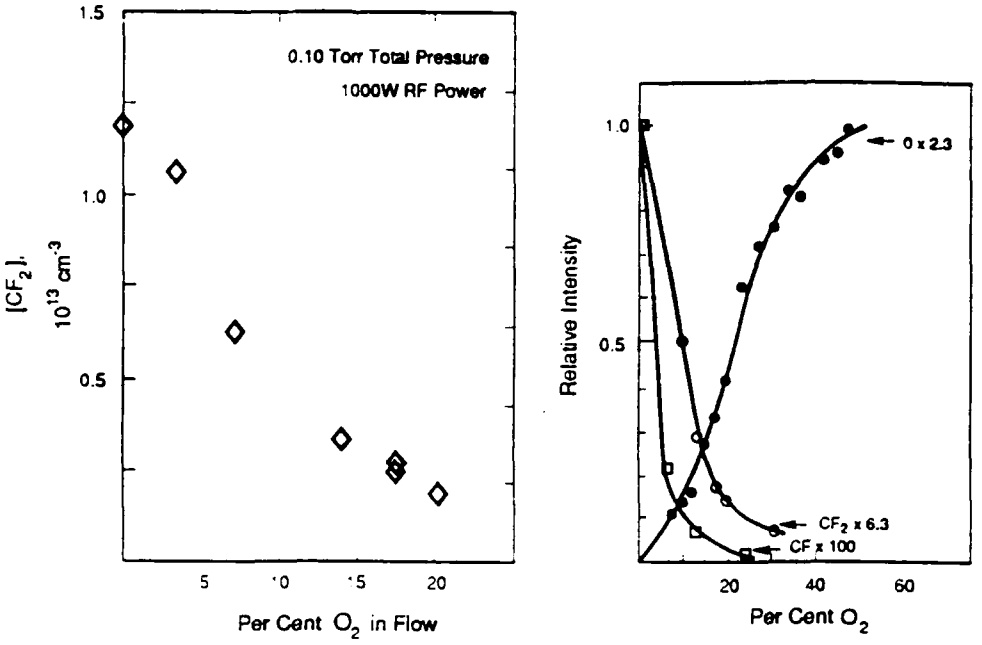

Figure 6. Long path plasma reactor measurements of CF_2 concentration with oxygen percentage in total flow (left), and radical concentrations measured by emission spectroscopy, at higher pressure and power density.[34]

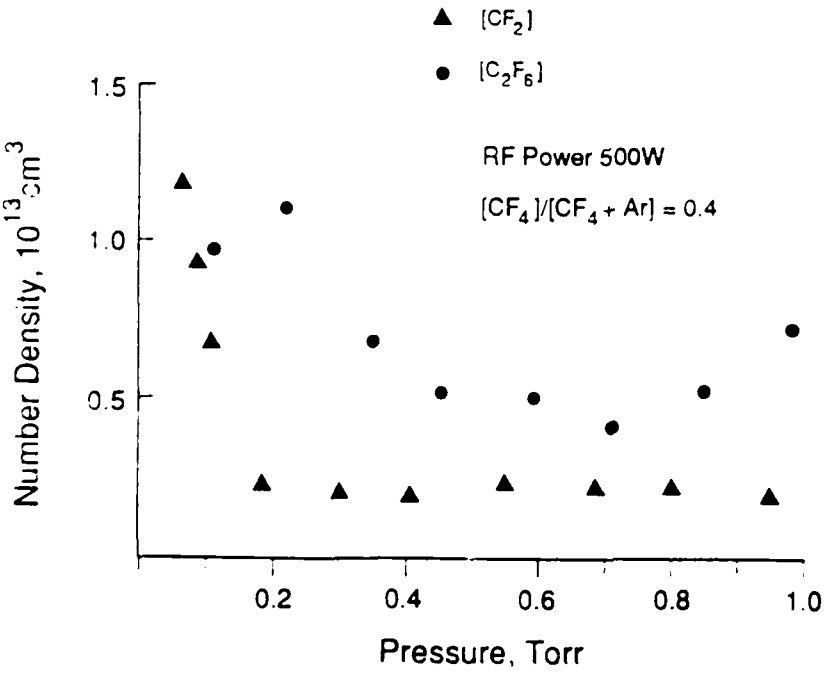

Figure 7. CF_2 and C_2F_6 number densities as functions of reactor total pressure, with RF power of 500 W and mixing fraction, $[CF_4]/[CF_4 + Ar]$, of 0.4.

the total (and ion) densities decreased. Still, we expect a peak in CF_2 concentration at some total pressure below 0.05 Torr. The possibilities that C_2F_6 peaks above this, and that it increases as the pressure goes past 1 Torr, are both consistent with it being a product of radical recombination and reaction whose rates are faster at higher total pressures.

However, these bulk gas considerations may not be the major mechanism behind the observed variations with pressure. Our visual observations looking down the axis of the tube are of increasing spatial nonuniformity with higher pressure, with the glow (and presumably the source of radicals) moving towards the electrodes. This observation is similar to those of a recently published laser induced fluorescence study of CF_2 profiles in a parallel-plate reactor.[18] These results were interpreted in terms of a chemical diffusion length for CF_2 reaction, primarily with fluorine atoms. We expect that the source region is moving away from the laser spot pattern as the total pressure is raised, and that the chemical diffusion length is, if anything, decreasing as well, and that both effects may be contributing to the decrease in CF_2 column density observed.

On the other hand, C_2F_6 is a stable molecule, and if, at higher pressures, there is indeed a widening volume in the center of the tube with low electron, ion, and radical concentrations, C_2F_6 should have no trouble filling the tube uniformly at pressures of 1 Torr and below. Therefore, the lower C_2F_6 concentrations observed at higher pressures in Figure 7 should still reflect a change in the gas phase chemistry averaged over the reactor volume.

3.5 Temperature measurements of CF_4 plasmas

We have already noted above that the observed CF_2 concentrations are a small fraction of the input CF_4. The temperature enters into the determination of these concentrations, both in converting the observed pressure into a density, and a accounting for the changing strengths in vibration-rotation lines. Neither of these corrections are large compared to other uncertainties, such as that in the band strength. The question of what fraction of the CF_4 actually dissociated goes into CF_2, as addressed by a CF_4 absorption experiment, depends more critically on knowledge of the temperature of the gas when the discharge is on. Without this knowledge a change in the total gas density or in the rotational population of the absorbing CF_4 level would be mistaken for a change in the CF_4 partial pressure.

Rotational degrees of freedom are expected to be in equilibrium with translation in these plasmas, so a search was undertaken for CF_2 lines with sufficiently differing lower state energies that a rotational temperature could be measured. The intensity of individual rotational lines is governed by their line strength and a temperature dependent Boltzmann factor. If the observed peak optical depth is divided by the line strength S (in arbitrary units), then the slope of the plotted quantity in Figure 8 against lower state energy, $\ln(od/S)$, is $-1/RT$. As can be seen from the scatter in the low energy points, a temperature determination would not be possible without the two small lines with lower state energies of 1715.8 and 1692.3 cm^{-1}, which appear at 1091.65 and 1091.835 cm^{-1}, respectively. The temperature given in the example, 425 K, is close to the 500 K reported in Ref. 34 at 1 Torr and a much higher power density, as determined by optical

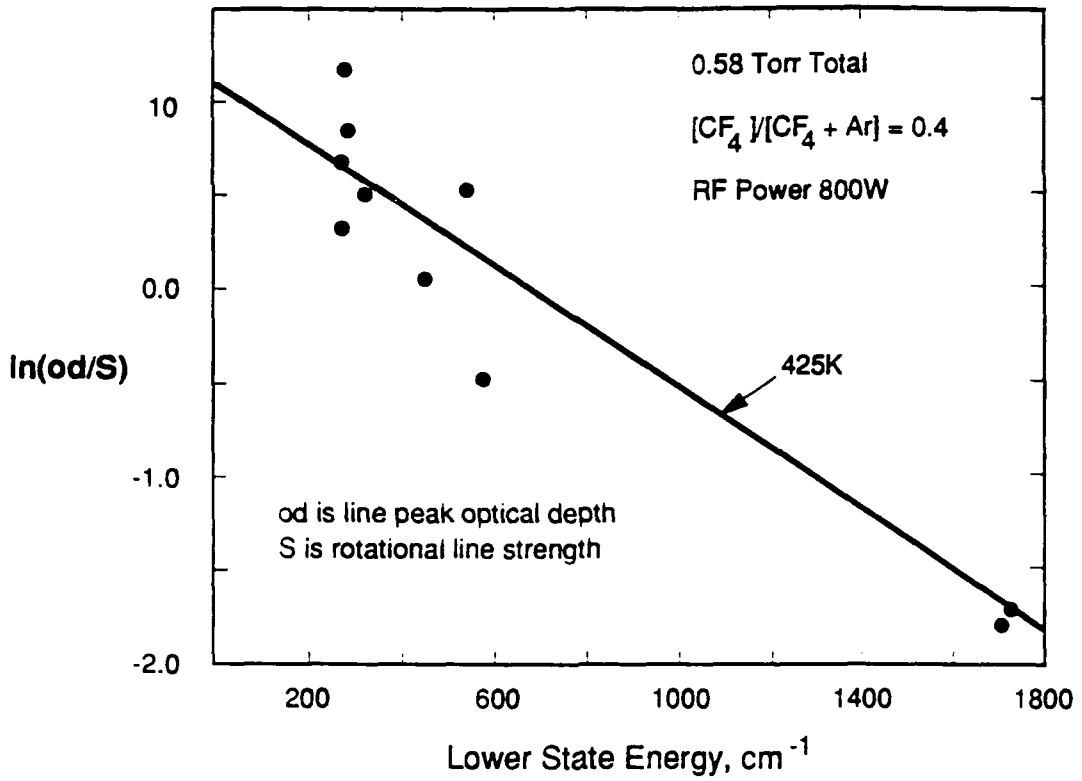

Figure 8. Example of rotational temperature determination.

emission from CO and N_2. Remarkably, observations like those in Figure 8 made at powers from 100 to 1000 W yielded no significant variation in the derived temperature. On the other hand, measurements at a total pressure of 0.10 Torr yielded a somewhat higher temperature, 465 K with a standard deviation of about 50 K.

We observed essential independence of bulk plasma temperature with applied power in our earlier chlorine atom work,[1] and ascribed it to the generation of larger concentrations of electronically and vibrationally excited molecules at higher powers. These excited species are much better conductors of heat to the walls than molecules with only rotational and translational energy, and as their concentration increases the heat flux to the apparatus increases roughly proportionally to the input power while the temperature can remain almost constant. It is certainly plausible that the same thing is going on in these CF_4 plasmas.

One other point of comparison is the laser induced fluorescence experiment of Hancock and co-workers, in which LIF of the CF molecule yielded a rotational temperature.[15] They were observing a commercial parallel plate plasma etching reactor with a volume of about 1200 cm^3, with applied 13.56 MHz power in the range of 50 to 200 W, giving power densities at the upper end of our range. Their pressure of 0.05 Torr is somewhat below our lowest value, while their residence time of about 0.1 s is two orders of magnitude shorter than ours at the same

pressure. Whether these differences affect the heat transfer and temperature is not easy to guess, but their observations do differ from ours, being lower and showing more dependence on applied power (ranging from 324 ± 15 K at 50 W to 443 ± 30 K at 200 W).

On the other hand, both our observations and the other data for CF_4 discharges agree on the qualitative point that discharge temperatures are fairly low, in the 300 to 500 K range, and therefore affect the density by less than a factor of two, while our chlorine plasma measurements[1] yielded temperatures as high as 800 K (not surprising in light of the lower thermal conductivity of chlorine).

3.6 Observations of CF_4 dissociation fraction

With the ability to approximately correct for temperature changes in analyzing CF_4 absorption observations, we can be confident that a large change in CF_4 absorption will in fact be due in part to CF_4 dissociation. One other correction should be noted, one due to the fact that the CF_4 is introduced slightly upstream of the discharge region. In the analysis leading to the data presented here, we assumed that if all CF_4 were immediately dissociated in the discharge, a peak absorption of 0.08 of the discharge-off value would still be observed.

Figure 9 shows the results of CF_4 dissociation measurements as a function of RF power. It can be seen that except for low powers, the fraction dissociated is always quite large. This particular set of measurements was made in a spectral

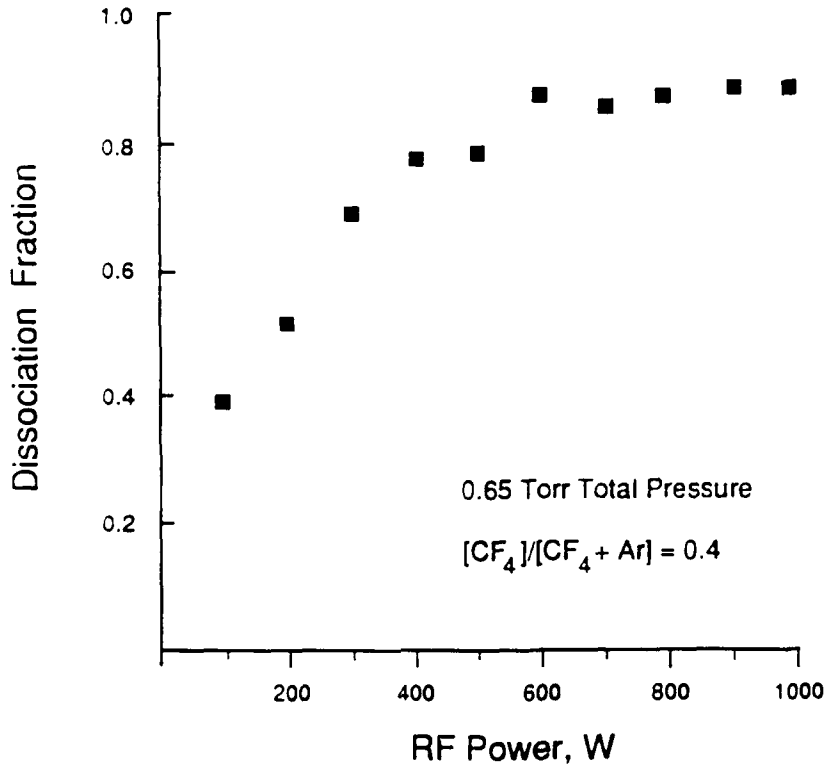

Figure 9. Fraction of CF_4 dissociated as a function of applied RF power, measured by CF_4 infrared line peak absorption.

region near 1062.5 cm^{-1}. The diode laser scan of an N_2O reference gas spectrum was not extensive enough to allow an exact identification of the lines, so the spectral location is known only from the monochromator setting, which has a typical error of less than 2 cm^{-1}. This spectral position is near the center of the $\nu_2 + \nu_4$ combination band of CF_4. Therefore, we expect the lines involved to be associated with low rotational quantum numbers (J), meaning their line strengths decrease when the plasma temperature goes up. An analysis assuming that J = 15 was used to produce Figure 9. Assuming J = 0, which results in the smallest dissociation fraction, does not significantly lower the high power points. A similar correction would result if the widths of the absorption lines increased as RF power was applied, but no systematic change was observed. Similar dissociation fractions were observed using high J lines in the CF_4 ν_4 fundamental band near 605 cm^{-1}.

4. CONCLUSIONS

Infrared tunable diode laser absorption spectroscopy is a very useful diagnostic of RF plasmas, capable of detection of a wide variety of the radicals and stable molecules found in CF_4 plasma systems. Although our long path system resulted in strong absorption levels, allowing us to use direct detection using a slow laser scan rate and a simple detection system, standard techniques for high sensitivity detection would allow measurement of all the species measured to be made over the 10 cm paths typical of plasma processing equipment.

With the exception of CF_2 LIF observations of Ref. 16, these are the first reported absolute concentration measurements of any of these species in any RF plasma system. We plan additional studies to gain a clearer picture of conditions in our apparatus. Our observations to date suggest that the reactor wall plays a large role in determining molecular concentrations in CF_4 plasmas. There is a strong possibility that both polymer deposition from the CF_4 feed gas and fluorocarbons emitted by the Teflon liner are contributors. The wall source decreased with continued operation, as monitored by CF_2 production in a pure argon plasma. The concentrations reported here were obtained when a pure argon plasma initially produced no observable CF_2 or C_2F_6. A second, more tentative conclusion, based on the observation that absolute concentrations of CF_2 and C_2F_6 are much smaller than the fraction of CF_4 dissociated, is that gas phase decomposition and recombination chemistry carries CF_4 fragments into a wide variety of fluorocarbon chemical species.

5. ACKNOWLEDGEMENTS

W. Goodwin constructed and operated the apparatus. M. Zahniser, D. Worsnop, and S. Coy provided helpful advice and technical assistance. Helpful contributions to the analysis by I.C. Plumb and R.C. Woods are gratefully acknowledged. Research sponsored by the Air Force Office of Scientific Research (AFSC), under Contract No. F49620-87-C-0052.

6. REFERENCES

1. J. Wormhoudt, A. C. Stanton, A. D. Richards and H. H. Sawin, J. Appl. Phys. 61, 142 (1987).

2. A. D. Richards, B.E. Thompson, K.D. Allen and H.H. Sawin, J. Appl. Phys. 62, 792 (1987).
3. A. D. Richards and H. H. Sawin, J. Appl. Phys. 62, 799 (1987).
4. C.A. DeJoseph, Jr., P.D. Haaland and A. Garscadden, IEEE Trans. Plasma Science PS-14, 165 (1986).
5. P. Chollet, G. Guelachvili, M. Morillon-Chapey, P. Gressier and J. Schmitt, J. Opt. Soc. Am. B 3, 687 (1986).
6. P.B. Davies, N.A. Isaacs, S.A. Johnson and D.K. Russell, J. Chem. Phys. 83, 2060 (1985).
7. N. Itabashi, K. Kato, N. Nishiwaki, T. Goto, C. Yamada and E. Hirota, Jpn. J. Appl. Phys. 27, L1565 (1988).
8. J.E. Butler, N. Bottka, R.S. Sillmon and D.K. Gaskill, J. Cryst. Growth 77, 163 (1986).
9. F.G. Celii, P.E. Pehrsson, H. Wang and J.E. Butler, Appl. Phys. Lett. 52, 2043 (1988).
10. P.J. Hargis and M.J. Kushner, Appl. Phys. Lett. 40, 779 (1982).
11. S. Pang and S.R.J. Brueck, Mater. Res. Symp. Proc. 17, 161 (1983).
12. K. Ninomiya, K. Suzuki, S. Nishimatsu and O. Okada, J. Vac. Sci. Technol. A 4 1971 (1986).
13. J.W. Thoman, Jr., K. Suzuki, S.H. Kable and J.I. Steinfeld, J. Appl. Phys. 60, 2772 (1986).
14. Y. Matsumi, S. Toyoda, T. Hayashi, M. Miyamura, H. Yoshikawa and S. Komiya, J. Appl. Phys. 60, 4102 (1986).
15. J.P. Booth, G. Hancock and N.D. Perry, Appl. Phys. Lett. 50, 318 (1987).
16. J.P. Booth, G. Hancock, N.D. Perry and M.J. Toogood, Mater. Res. Soc. Symp. 117, 47 (1988).
17. S.G. Hansen, G. Luckman and S.D. Colson, Appl. Phys. Lett. 53, 1588 (1988).
18. M. Kitamura, H. Akiya, and T. Urisu, J. Vac. Sci. Technol. B 7, 14 (1989).
19. R. d'Agostino, F. Cramarossa, S. DeBenedictis and G. Ferraro, J. Appl. Phys. 52, 1259 (1981).
20. D. Field, A.J. Hydes and D.F. Klemperer, Vacuum 34, 563 (1984).
21. K.R. Ryan and I.C. Plumb, Plasma Chem. Plasma Process. 6, 231 (1986).
22. D.R. Herriot, H. Kogelnik and R. Kompfner, Appl. Opt. 3, 523 (1964).
23. J.B. Burkholder, C.J. Howard and P.A. Hamilton, J. Mol. Spectry. 127, 362 (1988).
24. J.H. Newton and W.B. Person, J. Chem. Phys. 68, 2799 (1978).
25. K.A. Peterson and R.C. Woods, private communication.
26. J. Wormhoudt, K.E. McCurdy and J.B. Burkholder, Chem. Phys. Lett. 158, 480 (1989).
27. S. Carter and L.O. Halonen, Program ASYMVIB, Spectrochim. Acta 41A (9) (1985), software survey section.
28. A.H. Maki, National Institute of Science and Technology, Program ASYMBD7, private communication.
29. G. Smolinsky and D.L. Flamm, J. Appl. Phys. 50, 4982 (1979).
30. I.C. Plumb, private communication.
31. C.J. Mogab, A.C. Adams and D.L. Flamm, J. appl. Phys. 49, 3796 (1978).
32. K.R. Ryan and I.C. Plumb, Plasma Chem. Plasma Process. 4, 271 (1984).
33. I.C. Plumb and K.R. Ryan, Plasma Chem. Plasma Process. 6, 205 (1986).
34. R. d'Agostino, F. Cramarossa, S. DeBenedictis and G. Ferraro, J. Appl. Phys. 52, 1259 (1981).

APPENDIX E

presented at 1989 Fall Meeting of the Materials Research Society, to be published in Proceedings of MRS Symposium on Characterization of Plasma-Enhanced CVD Processes, Ed. D. E. Ibbotson, G. Lucovsky, and D. W. Hess

RADICAL AND MOLECULAR PRODUCT CONCENTRATION MEASUREMENTS IN CH_4 RF PLASMAS BY INFRARED TUNABLE DIODE LASER ABSORPTION

J. Wormhoudt
Center for Chemical and Environmental Physics, Aerodyne Research, Inc., Billerica, Massachusetts 01821

ABSTRACT

Infrared tunable diode laser absorption studies of radicals and stable molecules formed in radio frequency plasmas are being carried out in a laboratory reactor which allows a long absorption path. In this paper we describe studies of CH_4 RF plasmas. We report absolute concentration measurements as functions of total pressure and RF power for CH_3 and C_2H_2 in CH_4 plasmas, as well as measurements of the CH_4 rotational temperature and dissociation fraction.

INTRODUCTION

Tunable diode laser infrared absorption spectroscopy has been shown to be useful in the study of process plasmas, including chlorine etching plasmas[1-3] and silane deposition plasmas.[4-7] Diode lasers have also been used to study hydrocarbon species in organometallic chemical vapor deposition[8] and hot-filament diamond deposition.[9] However, there have been no applications to the hydrocarbon plasmas used to deposit diamond and hard carbon films.[10-13] Electronic emission can be used to provide several kinds of information on electronically excited species, including their spatial distributions and rotational and vibrational temperatures.[14-16] Recently, mass spectrometric sampling has been used to measure concentrations of two important radical species.[17-18] However, infrared absorption is both quantitative and nonintrusive, and as such has advantages over emission and sampling techniques for the study of realistic reactor systems. Chemical kinetics modeling studies of CH_4[19-21] plasmas have identified several important molecular species. Measurements of absolute concentrations of these molecules are important in evaluating the chemical kinetic and electron collision mechanisms involved in these predictions. Here we present our first observations on a laboratory plasma reactor which allows a long absorption path.

EXPERIMENTAL

Figure 1 is a schematic drawing of the long path plasma apparatus. The active volume is contained inside a 1 m long Teflon inner liner with a 15 cm inner diameter. The electrodes which surround it are copper half-tubes, with water cooling provided by one line of copper tubing set into the electrode surface in a loop near the outer edge. They are separated from the stainless steel vacuum wall by an outer quartz dielectric tube.

The feed gas, together with any carrier or additive gases, enters the tube through a ring injector just before the upstream end of the electrodes. Argon purge gas is introduced behind each mirror, and small flows are also put into each of the cross ports which are used for visual observation and

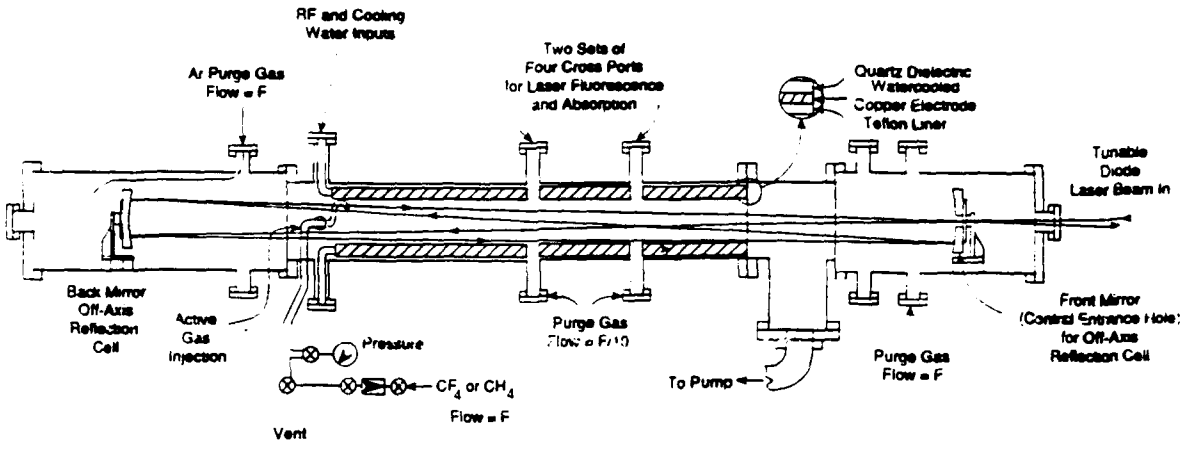

Figure 1. Cross sectional view of long path absorption plasma apparatus.

emission spectroscopy. With a 30 cfm mechanical pump and 7 cm diameter pumping line, pressures in the 0.1 to 1.0 Torr range are achieved with total flows in the 15 to 400 sccm range. These translate into gas velocities of from 6 to 150 cm/s, or residence times in the active region of from 17 to 0.7 seconds. We conclude from studies in which the residence time was varied while the pressure remained constant that the plasmas studied have reached a steady state, with their composition not strongly affected by residence time.

The mirrors used for multi-pass infrared absorption have 15 cm diameters and are separated by approximately 2 meters. They form an off-axis resonator,[22] in which the laser beam enters and exits through the same central hole in the downstream mirror, and forms a spot pattern on both mirrors which can be circular or which can be flattened into an ellipse (as we now use it) whose major axis is still almost the full 15 cm but with a minor axis of a little over 1 cm. For CH_4 studies, mirrors with a nominal 224 cm radius of curvature were used with a spacing resulting in 48 passes.

The 13.56 MHz RF power is taken from an RF Plasma Products supply with 1000 W capability. Powers reported are the values read from the digital meter on the supply. If all the power went into the plasma, power densities up to 0.1 W/cm^3 would be achieved, within the range of values used in commercial etching and deposition reactors. The fraction actually dissipated in the plasma is difficult for us to measure or estimate, but it is very likely to be less than half.

RESULTS AND DISCUSSION

Molecular species observed to date in CH_4 plasmas include the methyl radical, CH_3, and acetylene, C_2H_2. C_2H_2 was observed in the 745 cm^{-1} and 1275 cm^{-1} regions, while CH_3 was observed on the $Q_6(6)$ and $Q_8(8)$ transitions at 607.02 and 608.30 cm^{-1}. Relevant C_2H_2 line strengths are easily obtained from in situ measurements using known amounts of calibration acetylene, while the CH_3 band strength is taken from Ref. 23.

Plasma temperatures were obtained using the ratio of CH_4 line intensities. The lines used were set of lines with high rotational energies (high J) at 1273.7822, 1273.7843 and 1273.7859 cm^{-1}, and a low-J ^{13}C line at 1274.0176 cm^{-1}. As an example of the variation of plasma temperature with applied power we quote observations for a total pressure

of 0.12 Torr and a CH_4 fraction in the tube of 0.63 of the total of CH_4 and Ar purge gas. The plasma temperature rises to about 325 K with only 50 W applied power, and continues to rise in a roughly linear fashion to arrive at about 400 K in the region of 1000 W of applied power.

Figure 2 shows an example of CH_3 number density variation with RF power. The methyl radical concentration is more than four orders of magnitude smaller than the CH_4 concentration. In addition, its concentration rapidly plateaus at a limiting steady state value. Both observations are consistent with concentrations determined by recombination chemistry, and indeed the CH_3 radical is known to be highly self-reactive.

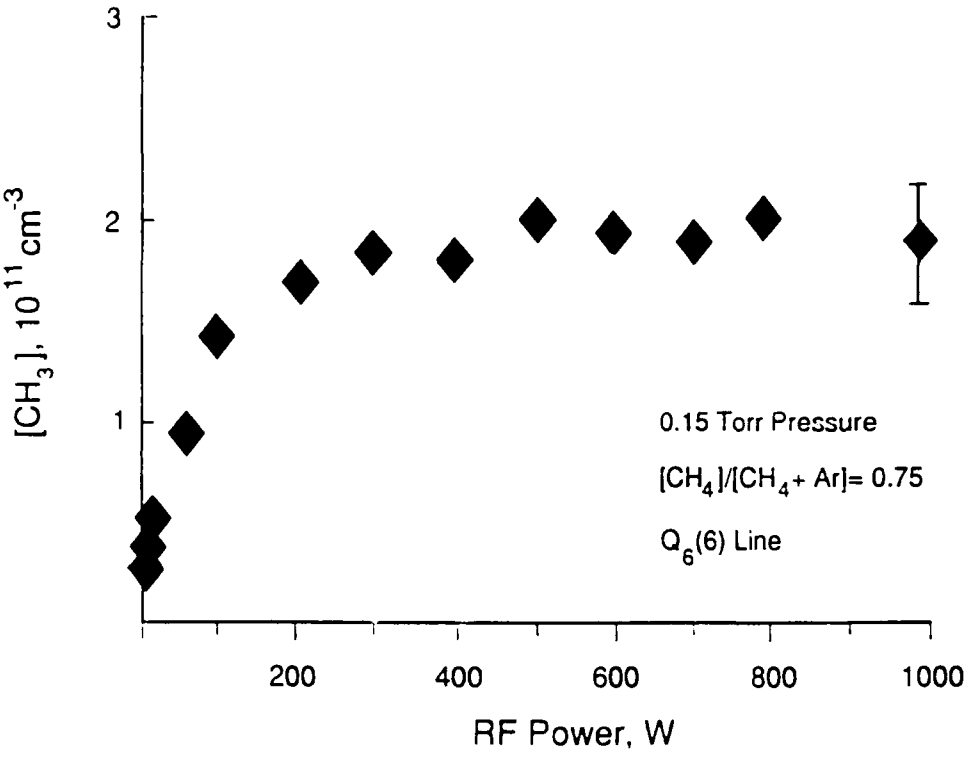

Figure 2. CH_3 number density measured using the $Q_6(6)$ line, as a function of RF power, with reactor total presusre of 0.15 Torr and mixing fraction, $[CH_4]/[CH_4 + Ar]$, of 0.75.

Figure 3 shows the CH_3 radical concentration variation with total pressure. The absolute number density decreases as the total pressure (and the CH_4 number density) increases. We can speculate that due to the high reactivity of CH_3, any region where the balance between production and destruction changes to produce a substantial increase in number density must occur at lower pressures than those studied. Figure 4 shows C_2H_2 number densities over the same total pressure range. Although C_2H_2 is present in much larger concentrations than the radicals we have studied, it still is under 10 percent of the input methane.

Figure 5 shows a set of measurements of the CH_4 dissociation fraction, measured using the same ^{13}C line used in the temperature measurement described above. The observed peak optical depths must be corrected to values which are representative of the CH_4 concentration in the active plasma region by subtracting out the optical depth appropriate to a small region between the ring injector and the electrodes, where it is assumed

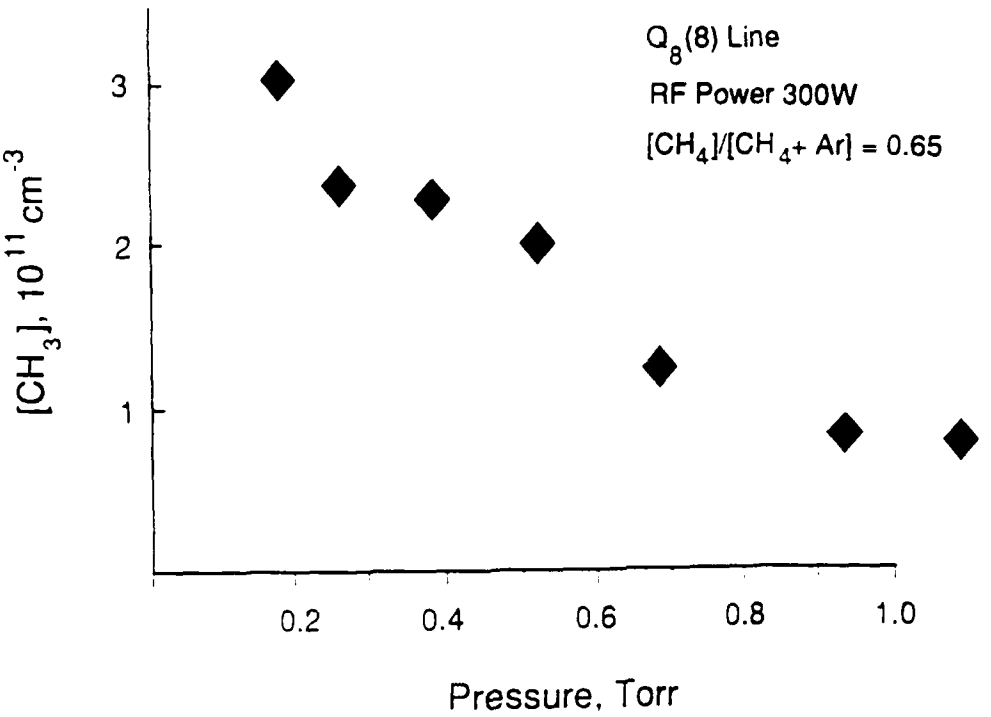

Figure 3. CH_3 number density measured using the $Q_8(8)$ line, as a function of reactor total pressure, with RF power of 300 W and mixing fraction, $[CH_4]/[CH_4 + Ar]$, of 0.65.

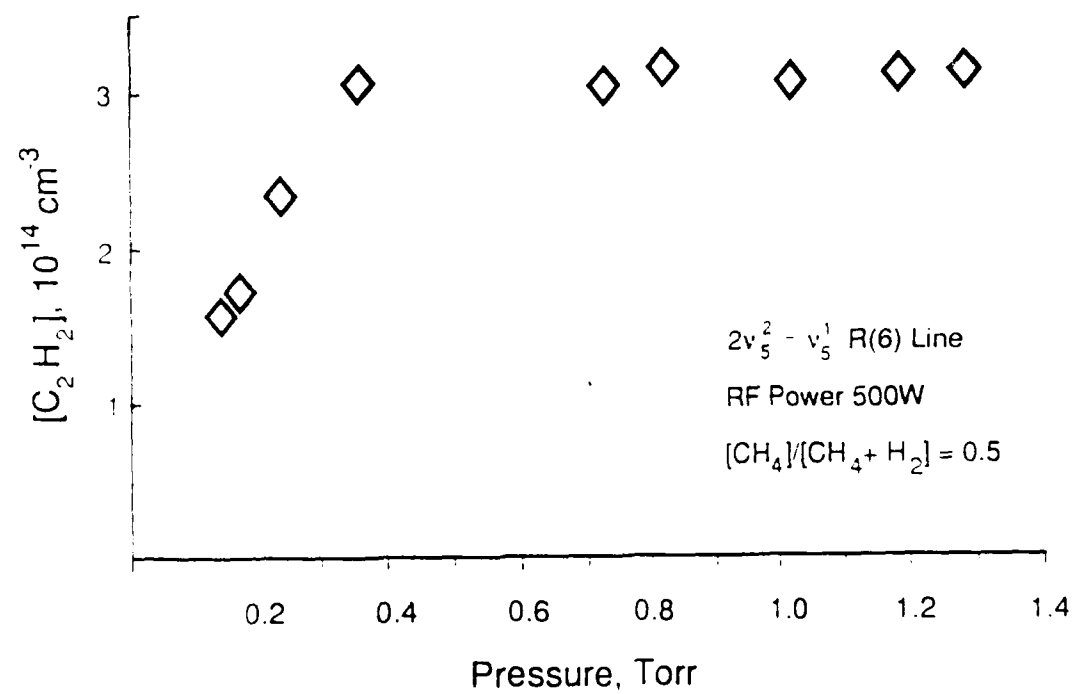

Figure 4. C_2H_2 number density measured using the $2\nu_5^2-\nu_5^1$ R(6) line, as a function of reactor total pressure, with RF power of 500 W and mixing fraction, $[CH_4]/[CH_4 + H_2]$, of 0.5.

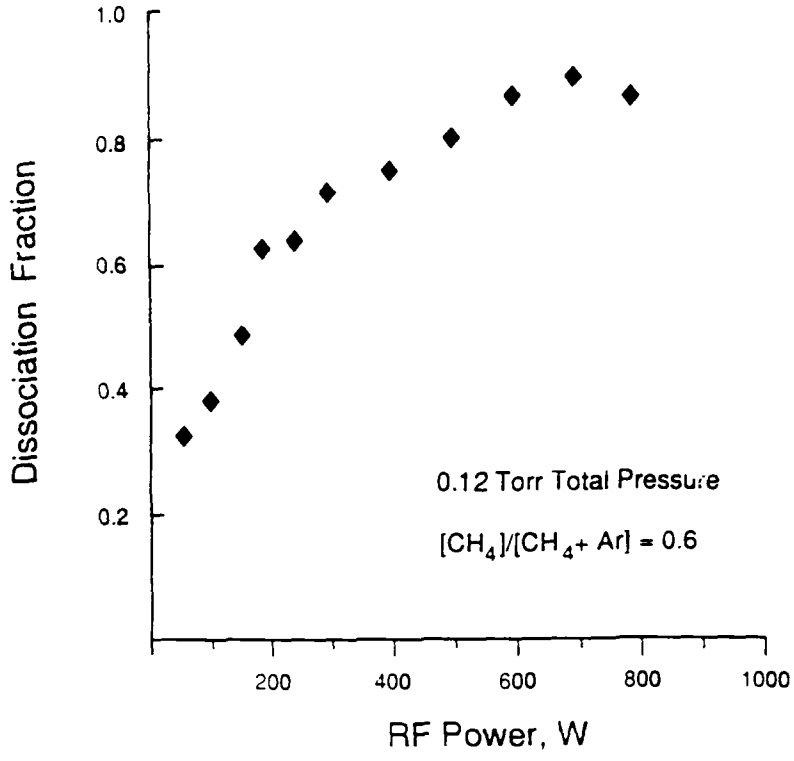

Figure 5. Fraction of CH_4 dissociated as a function of applied RF power.

that no dissociation occurs. This region is estimated to be about 5 cm long, compared to an effective single pass absorption length (calculated from the tabulated line strength, the observed line width and discharge-off optical depth, and an average CH_4 concentration in the tube) of about 125 cm.

The fraction of CH_4 which remains is related to the ratio of these corrected optical depths. However, before it is subtracted from one to yield a dissociation fraction, this ratio is corrected by multiplying it by the ratio of discharge-on and discharge-off temperatures to correct for the change in density, and by the ratio of Boltzmann factors (discharge-off to discharge-on) to correct for the change in line strength as the gas is heated (if a change in line width had been observed, a correction for this would also have been included). In this way, the observed column densities are converted into a fraction of the total CH_4 which is dissociated, which represents an average over the line of sight down the tube. It can be seen that except at very low powers the majority of the CH_4 has been dissociated, and that the dissociation fraction approaches 0.9 at high powers.

CONCLUSIONS

Infrared tunable diode laser absorption spectroscopy is a very useful diagnostic of RF plasmas, capable of detection of a wide variety of the radicals and stable molecules found in the CH_4 system. Although our long path system resulted in strong absorption levels, allowing us to use

direct detection using a slow laser scan rate and a simple detection system, standard techniques for high sensitivity detection would allow measurements of all the species measured to be made over the 10 cm paths typical of plasma processing equipment. A high degree of CH_4 dissociation is observed, with only a small fraction going into the steady-state concentration of the reactive CH_3 radical. While C_2H_2 is clearly a major decomposition product, there may well be other important species as well.

ACKNOWLEDGEMENTS

W. Goodwin constructed and operated the apparatus. M. Zahniser, D. Worsnop, and S. Coy provided helpful advice and technical assistance. Research sponsored by the Air Force Office of Scientific Research (AFSC), under Contract No. F49620-87-C-0052.

REFERENCES

1. J. Wormhoudt, A. C. Stanton, A. D. Richards and H. H. Sawin, J. Appl. Phys. 61, 142 (1987).
2. A. D. Richards, B.E. Thompson, K.D. Allen and H.H. Sawin, J. Appl. Phys. 62, 792 (1987).
3. A. D. Richards and H. H. Sawin, J. Appl. Phys. 62, 799 (1987).
4. C.A. DeJoseph, Jr., P.D. Haaland and A. Garscadden, IEEE Trans. Plasma Science PS-14, 165 (1986).
5. P. Chollet, G. Guelachvili, M. Morillon-Chapey, P. Gressier and J. Schmitt, J. Opt. Soc. Am. B 3, 687 (1986).
6. P.B. Davies, N.A. Isaacs, S.A. Johnson and D.K. Russell, J. Chem. Phys. 83, 2060 (1985).
7. N. Itabashi, K. Kato, N. Nishiwaki, T. Goto, C. Yamada and E. Hirota, Jpn. J. Appl. Phys. 27, L1565 (1988).
8. J.E. Butler, N. Bottka, R.S. Sillmon and D.K. Gaskill, J. Cryst. Growth 77, 163 (1986).
9. F.G. Celii, P.E. Pehrsson, H. Wang and J.E. Butler, Appl. Phys. Lett. 52, 2043 (1988).
10. D.E. Meyer, N.J. Ianno, J.A. Woollam, A.B. Swartzlander and A.J. Nelson, J. Mater. Res. 3, 1397 (1988).
11. G. Amaratunga, A. Putnis, K. Clay and W. Milne, Appl. Phys. Lett. 55, 634 (1989).
12. J.W. Zou, K. Reichelt, K. Schmidt and B. Dischler, J. Appl. Phys. 65, 3914 (1989).
13. J.M. Mackowski, R. Pignard, N. Vedovotto, P. Robert and A. Donnadieu,
14. J.A. Mucha, D.L. Flamm and D.E. Ibbotson, J. Appl. Phys. 65, 3448 (1989).
15. J. Wagner, C.H. Wild, A. Bubenzer and P. Koidl in Plasma Processing, edited by J.W. Coburn, R.A. Gottscho and D.W. Hess (Mater. Res. Soc. Proc. 68, Pittsburgh, PA 1986) pp. 205-210.
16. T. Kokubo, F. Tochikubo and T. Makabe, J. Phys. D: Appl. Phys. 22, 1281 (1989).
17. H. Toyoda, H. Kojima and H. Sugai, Appl. Phys. Lett. 54, 1507 (1989).
18. H. Kojima, H. Toyoda and H. Sugai, Appl. Phys. Lett. 55, 1292 (1989).
19. L.E. Kline, W.D. Partlow, and W.E. Bies, J. Appl. Phys. 65, 70 (1989).
20. W.D. Partlow and L.E. Kline in Plasma Processing, edited by J.W. Coburn, R.A. Gottscho and D.W. Hess (Mater. Res. Soc. Proc. 68, Pittsburgh, PA 1986) pp. 309-319.
21. K. Tachibana, M. Nishida, H. Harima and Y. Urano, J. Phys. D: Appl. Phys. 17, 1727 (1984).
22. D.R. Herriot, H. Kogelnik and R. Kompfner, Appl. Opt. 3, 523 (1964).
23. J. Wormhoudt and K.E. McCurdy, Chem. Phys. Lett., 156 47 (1989).

APPENDIX F

ARI RR-786

ADVANCED COMPOUND SEMICONDUCTOR DEPOSITION DIAGNOSTIC DEVELOPMENT USING TUNABLE INFRARED DIODE LASER ABSORPTION IN A LONG PATH PLASMA REACTOR

Prepared by

J. Wormhoudt
Center for Chemical and Environmental Physics
Aerodyne Research, Inc.
45 Manning Road
Billerica, MA 01821

Prepared for

Proceedings of the Symposium
on Plasma Processing
177th Meeting of the Electrochemical Society
Montreal, Quebec
May 6-11, 1990

June 1990

ADVANCED COMPOUND SEMICONDUCTOR DEPOSITION DIAGNOSTIC DEVELOPMENT USING TUNABLE INFRARED DIODE LASER ABSORPTION IN A LONG PATH PLASMA REACTOR

J. Wormhoudt
Aerodyne Research, Inc., Billerica, MA 01821

ABSTRACT

Infrared tunable diode laser absorption studies of radicals and stable molecules formed in radio frequency plasmas are being carried out in a laboratory reactor which allows a long absorption path. In this paper we report measurements of the CH_4 rotational temperature and dissociation fraction in methane plasmas, as well as absolute concentration measurements of C_2H_4 in both methane plasmas and plasmas including organoarsine compounds.

INTRODUCTION

Tunable diode laser infrared absorption spectroscopy has been shown to be useful in the study of mechanisms in process plasmas including chlorine etching plasmas(1-3) and silane deposition plasmas (4-8). Diode lasers have also been used to study hydrocarbon species in hot-filament diamond deposition (9) and organometallic chemical vapor deposition (10,11). In this latter work, however, no decomposition products of trimethylarsenic were observed, although CH_3 radicals formed from other organometallic compounds were seen.

In the present work, a long path plasma reactor has been used to generate easily detectable amounts of a wide variety of radical species. Recent work has focused on absolute species concentration and temperature measurements in methane plasmas. These systems have their own intrinsic interest, due to their applications in diamond and hard carbon deposition as well as gallium arsenide etching. In addition, they contain the hydrocarbon species also important in MOCVD. We have also begun measurements of hydrocarbon species formed from the decomposition of organoarsine compounds, and we also plan observations of arsenic hydride species, which may play a key role in suppressing carbon incorporation in MOCVD (12-16).

EXPERIMENTAL

Figure 1 is a schematic drawing of the long path plasma apparatus. The active volume is contained inside a 1 m long Teflon inner liner with a 15 cm inner diameter. The electrodes which surround it are

copper half-tubes, with water cooling provided by one line of copper tubing set into the electrode surface in a loop near the outer edge. They are separated from the stainless steel vacuum wall by an outer quartz dielectric tube.

The feed gas, together with any carrier or additive gases, enters the tube through a ring injector just before the upstream end of the electrodes. Argon purge gas is introduced behind each mirror, and small flows are also put into each of the cross ports which are used for visual observation and emission spectroscopy. With a 30 cfm mechanical pump and 7 cm diameter pumping line, pressures in the 0.1 to 1.0 Torr range are achieved with total flows in the 15 to 400 sccm range. These translate into gas velocities of from 6 to 150 cm/s, or residence times in the active region of from 17 to 0.7 seconds. We conclude from studies in which the residence time was varied while the pressure remained constant that the plasmas studied have reached a steady state, with their composition not strongly affected by residence time.

The mirrors used for multi-pass infrared absorption have 15 cm diameters and are separated by approximately 2 meters. They form an off-axis resonator (17), in which the laser beam enters and exits through the same central hole in the downstream mirror, and forms a spot pattern on both mirrors which can be circular or which can be flattened into an ellipse (as we now use it) whose major axis is still almost the full 15 cm but with a minor axis of a little over 1 cm. For these studies, mirrors with a nominal 224 cm radius of curvature were used with a spacing resulting in 48 passes.

The 13.56 MHz RF power is taken from an RF Plasma Products supply with 1000 W capability. Powers reported are the values read from the digital meter on the supply. If all the power went into the plasma, power densities up to 0.1 W/cm^3 would be achieved, within the range of values used in commercial etching and deposition reactors. The fraction actually dissipated in the plasma is difficult for us to measure or estimate, but it is very likely to be less than half.

RESULTS AND DISCUSSION

C_2H_2 and CH_3 Observations-Molecular species observations in CH_4 plasmas already reported (18,19) include those of the methyl radical, CH_3, and acetylene, C_2H_2. C_2H_2 was observed in the 745 cm^{-1} and 1275 cm^{-1} regions, while CH_3 was observed on the $Q_6(6)$ and $Q_8(8)$ transitions at 607.02 and 608.30 cm^{-1}. Relevant C_2H_2 line strengths are easily obtained from in situ measurements using known amounts of calibration acetylene, while the CH_3 band strength was taken from Ref. 20.

C_2H_2 was seen to be a major decomposition product, while the more reactive CH_3 radical was present in much smaller concentrations. For

example, at 500 W RF power, C_2H_2 mole fractions of input CH_4 varied from 0.06 at a total pressure of 0.2 Torr to 0.02 at 1.0 Torr (CH_4 and carrier gas each making up about half the flow). Under the same conditions, CH_3 mole fractions of CH_4 varied from 8×10^{-5} to 4×10^{-6}.

These observations raised at least two questions which can now be given tentative answers based on additional results presented here. First, does C_2H_2 account for the majority of dissociated CH_4 which would imply a low (order of 0.12) fractional dissociation, or are these more dissociation product species not yet detected?

The second question concerns the drop in fractions of both C_2H_2 and CH_3 with increasing pressure. It is observed that at low pressures the glow discharge fills the flow tube, while at higher pressures (approaching 1 Torr) the center of the tube is darker and the glow is concentrated near the electrodes. Does this smaller volume of glow (in which most of the electron impact dissociation occurs) result in lower average dissociation of CH_4 at higher pressures, and is this in turn the reason for lower fractions of dissociation products? Or, does the plasma chemistry change with total pressure, changing the distribution of products?

CH_4 Dissociation and Temperature Observations-Both of these questions call for a measurement of the CH_4 dissociation fraction. However, this in turn requires an accurate knowledge of the plasma temperature, since an observed decrease in adsorption line intensity can be due to dissociation or simply to a change in density due to gas heating, or a combination of both effects. We were fortunate to find a region of the CH_4 absorption spectrum (shown in Figure 2) which provided both concentration and temperature information in a single diode scan. The strong line on the right hand side is seen to have a low energy ground state and to decrease in intensity both due to dissociation and heating, while the intensities of the lines on the left remain almost unchanged as dissociation is almost counterbalanced by increases in relative intensity due to gas heating.

Plasma temperatures were obtained using the ratio of CH_4 line intensities. The lines used were the set of lines with high rotational energies (high J) at 1273.7822, 1273.7843 and 1273.7859 cm^{-1}, and the low-J ^{13}C line at 1274.0176 cm^{-1}. As an example of the variation of plasma temperature with applied power we show in Figure 3 observations for a total pressure of 0.12 Torr and a CH_4 fraction in the tube of 0.63 of the total of CH_4 and Ar purge gas. The plasma temperature rises to about 325 K with only 50 W applied power, and continues to rise in a roughly linear fashion to arrive at about 400 K in the region of 1000 W of applied power.

Figure 4 shows a set of measurements of the CH_4 dissociation fraction, measured using the same ^{13}C line used in the temperature measurement described above. The observed peak optical depths must be

corrected to values which are representative of the CH_4 concentration in the active plasma region by subtracting out the optical depth appropriate to a small region between the ring injector and the electrodes, where it is assumed that no dissociation occurs. This region is estimated to be about 5 cm long, compared to an effective single pass absorption length (calculated from the tabulated line strength, the observed line width and discharge-off optical depth, and an average CH_4 concentration in the tube) of about 125 cm.

The fraction of CH_4 which remains is related to the ratio of these corrected optical depths. However, before it is subtracted from one to yield a dissociation fraction, this ratio is corrected by multiplying it by the ratio of discharge-on and discharge-off temperatures to correct for the change in density, and by the ratio of Boltzmann factors (discharge-off to discharge-on) to correct for the change in line strength as the gas is heated (if a change in line width had been observed, a correction for this would also have been included). In this way, the observed column densities are converted into a fraction of the total CH_4 which is dissociated, which represents an average over the line of sight down the tube. It can be seen that except at very low powers the majority of the CH_4 has been dissociated, and that the dissociation fraction approaches 0.9 at high powers.

We can also see in Figure 2 that additional absorption lines appear when the discharge is on. These turn out to be C_2H_2 lines. We found no information on this band in the spectroscopic literature, but simply identified it, and quantified the line strengths at room temperature, by taking spectra of a static sample of C_2H_2 in the flow tube. The fact that we do not know lower state energies and hence temperature dependences for these lines introduces an uncertainty into absolute concentration measurements made using them. However, since the temperature rise in the plasma is small, we expect the error to be small, most likely much less than a factor of two. In fact, the C_2H_2 concentrations shown in Figure 5, obtained assuming no significant change in line strength, agree with previously published (19) observations using known lines, when those observations are corrected from an assumed temperature to the observed temperatures reported here.

<u>AsH_x Species in Organoarsine Decomposition</u>-From its inception in 1986, our research program has had as its ultimate goal the development and demonstration of laser diagnostics to support deposition mechanism studies for compound semiconductors, with gallium arsenide chosen as being representative and having the largest base of phenomenological observations and modeling studies with which our investigations could connect. We chose as a particular focus a hypothesis connecting suppression of carbon incorporation into the growing film with the action of AsH_x radicals in carrying reactive hydrogen to the surface. Considering that the MOCVD of GaAs from arsine and trimethyl gallium, most of the gallium is thought to arrive at the surface with at least one CH_3 group still attached, it is in one sense remarkable

21. J.R. Anacona, P.B. Davies and S.A. Johnson, Mol. Phys. 56, 989 (1985).
22. T. Sheng, B. Pihlstrom, Z. Yu and G.J. Collins, Appl. Phys. Lett. 55, 2411 (1989).
23. B. Pihlstrom, T. Sheng, Z. Yu and G.J. Collins, to appear in Materials Research Society Symposium Proceedings Vol. 165, Characterization of Plasma-Enhanced CVD Processes, ed. D.E. Ibbotson, G. Lucovsky and D.W. Hess.
24. T.R. Omstead, D.G. Coronell and K.F. Jensen, abstracts of Fourth Biennial Workshop on Organometallic Vapor Phase Epitaxy, Monterey, CA, October 8-11, 1989, The Minerals, Metals and Materials Soceity, Warrendale, PA.
25. J. Wormhoudt, to appear in Proc. SPIE 1185, (1990).

ACKNOWLEDGEMENTS

W. Goodwin constructed and operated the apparatus. M. Zahniser, D. Worsnop, and S. Coy provided helpful advice and technical assistance. This research was sponsored by the Air Force Office of Scientific Research (AFSC), under Contract No. F49620-87-C-0052.

REFERENCES

1. J. Wormhoudt, A. C. Stanton, A. D. Richards and H. H. Sawin, J. Appl. Phys. 61, 142 (1987).
2. A. D. Richards, B.E. Thompson, K.D. Allen and H.H. Sawin, J. Appl. Phys. 62, 792 (1987).
3. A. D. Richards and H. H. Sawin, J. Appl. Phys. 62, 799 (1987).
4. C.A. DeJoseph, Jr., P.D. Haaland and A. Garscadden, IEEE Trans. Plasma Science PS-14, 165 (1986).
5. P. Chollet, G. Guelachvili, M. Morillon-Chapey, P. Gressier and J. Schmitt, J. Opt. Soc. Am. B 3, 687 (1986).
6. P.B. Davies, N.A. Isaacs, S.A. Johnson and D.K. Russell, J. Chem. Phys. 83, 2060 (1985).
7. N. Itabashi, K. Kato, N. Nishiwaki, T. Goto, C. Yamada and E. Hirota, Jpn. J. Appl. Phys. 227, L1565 (1988).
8. N. Itabashi, N. Nishiwaki, M. Magane, T. Goto, A. Matsuda, C. Yamada and E. Hirota, Jpn. J. Appl. Phys. 1, 29, 585 (1990).
9. F.G. Celii, P.E. Pehrsson, H. Wang and J.E. Butler, Appl. Phys. Lett. 52, 2043 (1988).
10. J.E. Butler, N. Bottka, R.S. Sillmon and D.K. Gaskill, J. Cryst. Growth 77, 163 (1986).
11. D.K. Gaskill, V. Kolubayev, N. Bottka, R.S. Sillmon and J.E. Butler, J. Crystal Growth 93, 127 (1988).
12. T.F. Kuech, G.J. Scilla and F. Cardone, J. Crystal Growth 93, 550 (1988).
13. R.M. Lum, J.K. Lingert, D.W. Kisker, S.M. Abys, and F.A. Stevie, J Crystal Growth 93, 120 (1988).
14. C.A. Larsen, N.I. Buchan, S.H. Li and G.B. Stringfellow, J. Crystal Growth 93, 15 (1988).
15. D.M. Speckman and J.P. Wendt, J. Crystal Growth 93, 29 (1988).
16. T.F. Kuech, M.A. Tischler, P.J. Wang, G. Scilla, R. Potemski, and F. Cardone, Appl. Phys. Lett. 53, 1317 (1988).
17. D.R. Herriot, H. Kogelnik and R. Kompfner, Appl. Opt. 3, 523 (1964).
18. J. Wormhoudt, J. Vac. Sci. Technol. A 8, 1722 (1990).
19. J. Wormhoudt, to appear in Materials Research Society Symposium Proceedings Vol. 165, Characterization of Plasma-Enhanced CVD Processes, ed. D.E. Ibbotson, G. Lucovsky and D.W. Hess.
20. J. Wormhoudt and K.E. McCurdy, Chem. Phys. Lett., 156 47 (1989).

and improvement of our detection sensitivity using computer averaging of laser scans.

C_2H_4 in TMAs and CH_4 Decomposition-On the other hand, our observations in the 1076-1078 cm^{-1} region did show a set of absorption lines whose appearance was associated with the plasma decomposition of TMAs. We soon determined that the same lines appeared upon decomposition of CH_4, and that they were due to C_2H_4. Estimates of C_2H_4 concentrations based on room temperature line strengths (again, no line identifications were available) gave the result that in both CH_4 and TMAs systems the conversion to C_2H_4 was substantial, with perhaps on the order of half the input carbon being converted.

With this observation and the CH_4 dissociation study reported above, we can return to the questions we posed at the beginning of this discussion. We now know that the fractional dissociation of CH_4 is high, and its conversion fraction into C_2H_4 is large. We have not made a systematic study of CH_4 dissociation fraction as a function of total pressure. However, our more extensive observations of CF_4 precisely overlay each other. At higher pressures, our observations (25) are that the CF_4 dissociation decreases somewhat, but only by 10 or 20 per cent from 0.1 to 1.0 Torr. If this is true for CH_4 as well, this is clearly not the reason for a drop in CH_3 fraction by a factor of 20. We conclude that a major reason for the drop in fractions of particular dissociation products is that higher pressures facilitate chemical reactions which shift the molecular species distributions to larger and less reactive molecules.

CONCLUSIONS

Infrared tunable diode laser absorption spectroscopy is a very useful diagnostic of RF plasmas, capable of detection of a wide variety of the radicals and stable molecules found in the CH_4 system. Although our long path system resulted in strong absorption levels, allowing us to use simple direct detection using a slow laser scan rate and a simple detection system, standard techniques for high sensitivity detection would allow measurements of all the species measured to be made over the 10 cm paths typical of plasma processing equipment. A high degree of CH_4 dissociation is observed, with only a small fraction going into the steady-state concentration of the reactive CH_3 radical. While C_2H_4 and C_2H_2 are clearly major decomposition products, there may well be other important species as well.

that only a tiny fraction of the incoming carbon is in fact incorporated. Even a tiny fraction, however, has tremendous effects on the electrical properties of the film.

An understanding of carbon incorporation mechanisms has become even more important as the industry has moved away from arsine as the arsenic source to organoarsine compounds which are safer but which themselves carry carbon to the growth surface. It is observed that compounds such as trimethylarsenic (TMAs) which have no As-H bonds give rise to very high levels of carbon incorporation, while compounds which could directly dissociate to AsH or AsH_2 radicals give much lower carbon. The above hypothesis is now regularly invoked in explaining these observations (12-16).

Clearly, measurements of absolute AsH, AsH_2, and AsH_3 concentrations in organoarsine decomposition systems would add much to our understanding. AsH_2 has never been observed by direct infrared absorption, although one infrared band position is known through analysis of its electronic spectra. The AsH radical has received one preliminary study using tunable diode lasers (21). It will be the first AsH_x radical we attempt to observe. However, the observation we report here is a search of a region of containing known AsH_3 lines, in a plasma containing TMAs.

Determination of AsH_3 concentrations is a useful preliminary to looking for AsH, since the AsH band overlaps an AsH_3 band. In addition, recent investigations into afterglow decomposition of organometallics including TMAs in a deposition chamber (22,23) and into microwave plasma generation of AsH_3 from TMAs (24) have reported AsH_3 as a decomposition product. We noted that, using present thermodynamic data for arsenic containing species, the only energetically favored gas phase reactions which can lead to AsH_3 are those which add hydrogen atoms to AsH_x radicals, and that these three-body recombination reactions will be extremely slow at the reduced pressures of plasma discharges. Therefore, our observations of decomposition of a 2/1 mixture of Ar and TMAs at a total pressure of 0.44 Torr and an input RF power of 400 W were made under conditions in which AsH_3 observation would have been surprising.

In the event, we observed no AsH_3, down to a sensitivity level conservatively estimated to be 10^{11} cm^{-3}. In other words, the fraction of TMAs converted into AsH_3 under these conditions is much less than 10^{-4}. This is not necessarily in conflict with observations of AsH_3 formation in other plasma sources (22-24), since plasma sputtering of hyrogenated arsenic films in those systems could give rise to AsH_x species which are unable to form in gas phase reactions. We intend further observations, including tertiarybutylarsine as the arsenic-containing species (one which is capable of direct dissociation into AsH_2), as well as use of hydrogen as a carrier gas,

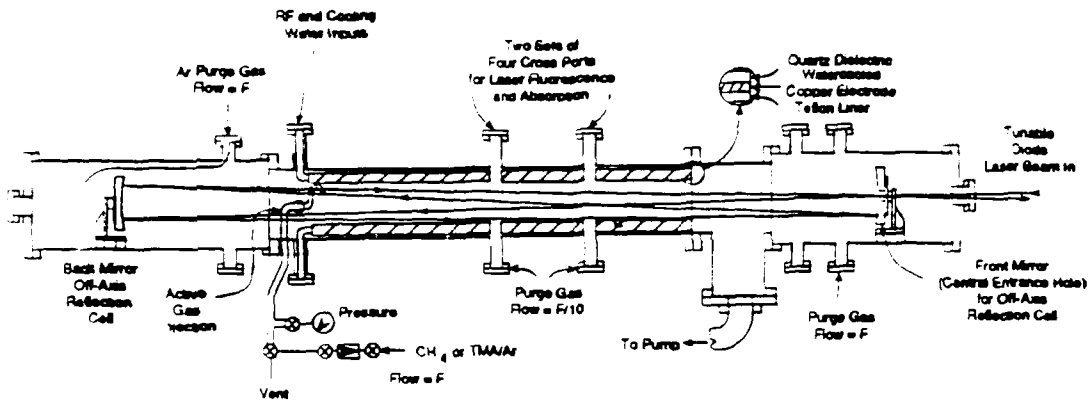

Figure 1. Cross-section of Long Path Absorption Plasma Apparatus.

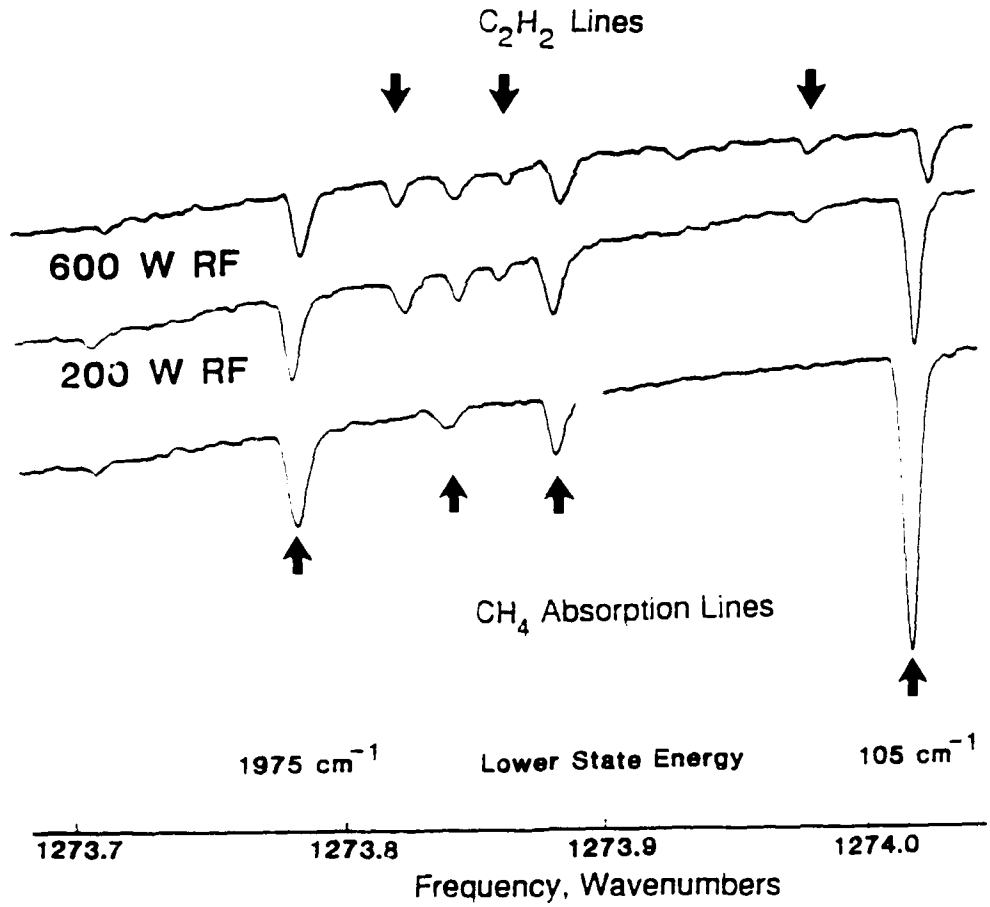

Figure 2. Infrared Spectral Region Used in CH_4 Dissociation Fraction and Temperature Measurement (Lower Trace, Plasma Off, Upper Traces, Plasma On).

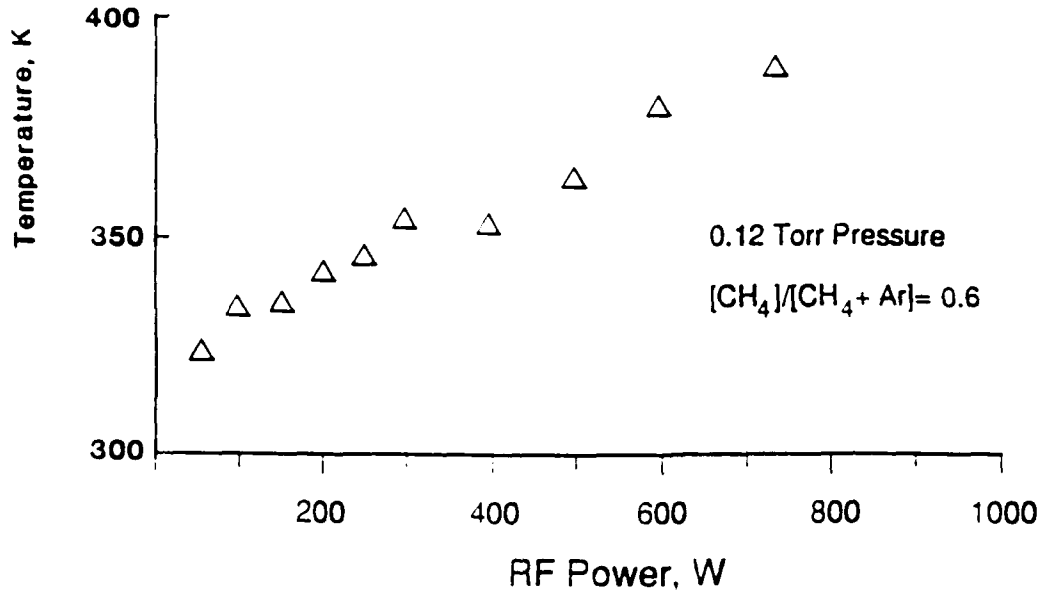

Figure 3. Methane Plasma Temperature Obtained from CH_4 Rotational Line Intensities.

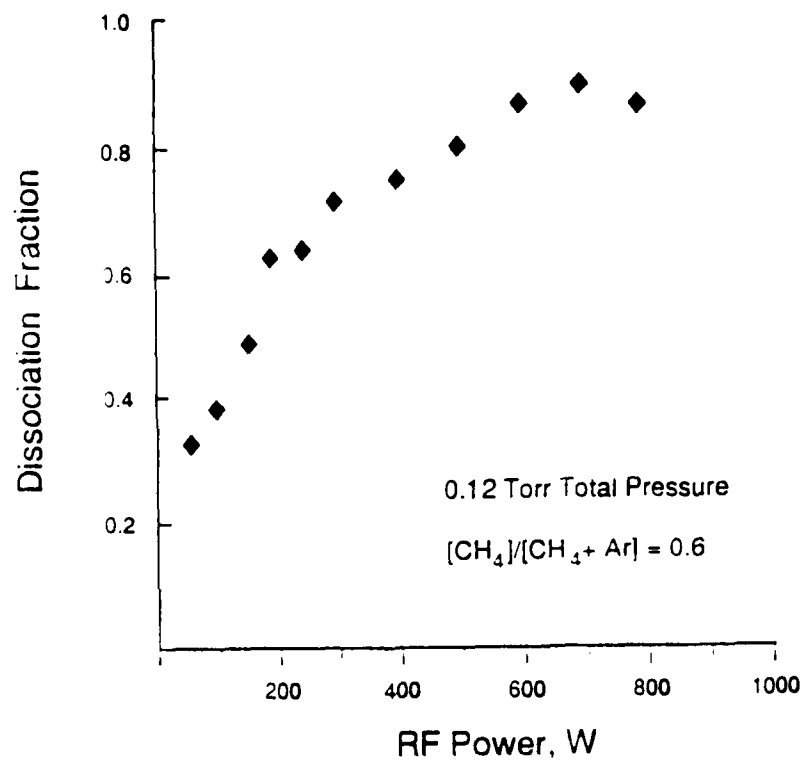

Figure 4. CH_4 Dissociation Fraction Measured by Infrared Absorption Line Intensities.

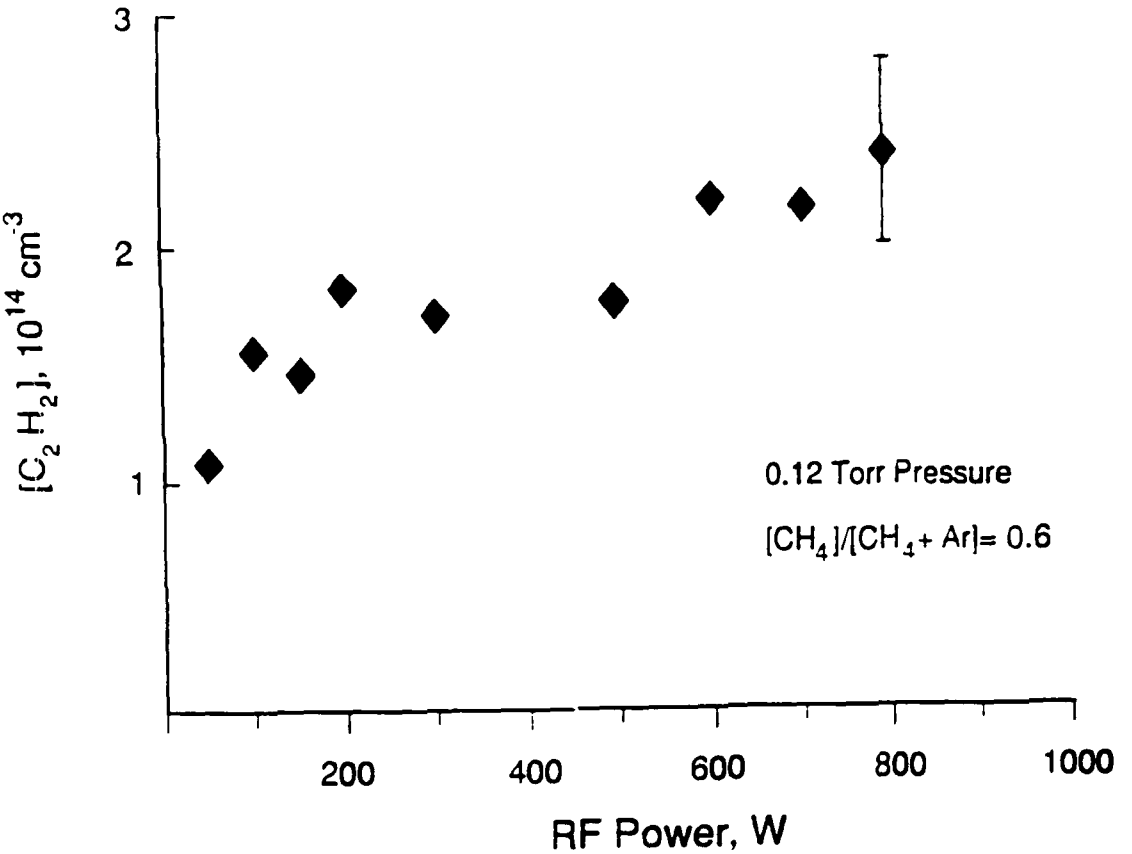

Figure 5. C_2H_2 Concentrations Obtained from Absorption Lines in Figure 2.